UNPACKING THE SOIL WATER CHARACTERISTIC CURVE: MEASUREMENT TECHNIQUES, PROPERTY-TRANSFER PREDICTIONS, AND IMPLICATIONS FOR DAYCENT MODEL SIMULATIONS

by

ELIZABETH O'BRIEN MCNAMEE

A thesis submitted in partial fulfillment of the requirements for the degree of

Masters of Science
(Soil Science and Agroecology)

at the

UNIVERSITY OF WISCONSIN-MADISON
2016

Approved by:

_____

Dr. Bill Bland
Professor, Department of Soil Science

Date: _____

ABSTRACT

The soil water characteristic curve (SWCC) relates soil volumetric water content, θ, to soil matric potential, ψ, and is used to estimate soil hydraulic parameters such as field capacity (FC) and hydraulic conductivity that are critical inputs to environmental models. Quantifying the SWCC is time consuming and expensive, and property-transfer models are one approach to estimating the SWCC from more easily obtained soil properties. The objectives of this research were *1)* to investigate the differences between laboratory and *in situ* measurements of the SWCC on a well-structured silt loam soil, *2)* examine the ability of property-transfer models to predict the SWCC, and *3)* evaluate the effect of different FC estimations taken from various SWCC measurement approaches on the nitrous oxide (N_2O) emissions predicted by DayCent, a widely used process-based, biogeochemical ecosystem model. Measurements were conducted in three systems: the corn phases of a corn-soy rotation (CS2) and a corn followed by three years of alfalfa rotation (CS4), and a rotationally grazed pasture (CS6) at the Wisconsin Integrated Cropping Systems Trial (WICST) in southern Wisconsin, USA. Laboratory measurements reported greater θ for a given ψ than *in situ* measurements, and differences in θ were greatest at ψ near zero. We believe that these differences arose because of hysteresis and air entrapment, as field soils never reached the water contents experienced in the laboratory. The CNEAP property-transfer model, which does not account for soil structure, predicted greater θ at a given ψ than the Nimmo (1997) property-transfer model,

which accounts for soil structure. The Nimmo model showed closest agreement with the laboratory measured SWCC, suggesting it is important to incorporate soil structure into property-transfer predictions of the SWCC in this well-aggregated silt loam soil. When FC was defined as the θ at ψ=33 kPa, laboratory-derived FC estimates ranged from 28 to 32% and *in situ* derived FC estimates ranged from 23-24% across the treatments. Using FC estimates derived from *in situ* SWCC (23, 24%) led to underestimations of θ at 15 cm by the DayCent model compared to observed θ. Laboratory derived FC estimates (28, 32%) resulted in slightly better θ predictions by DayCent, however differences were not striking. DayCent simulated cumulative N_2O emissions over the growing season were 1.5-2.3x greater when a laboratory-derived FC was input to DayCent rather then an *in situ* derived FC, but all simulated N_2O emissions were of the same order of magnitude of previously measured N_2O emissions at WICST. These results suggest that how SWCC are determined and the hydraulic parameters that are estimated from SWCC can significantly influence modeled processes that depend on soil water status, highlighting the importance of the fundamental SWCC relationship and questioning the validity of assumptions surrounding the classic paradigm of field capacity.

ACKNOWLEDGEMENTS

An overwhelming thank you goes to Bill Bland, who has been thoughtful, patient, accessible, and always willing to ponder a problem with me. Bill taught me many things over the course of my degree, from the technical to the abstract, and I am very grateful.

Thank you to my committee members: Matt Ruark, who provided excellent feedback; Francisco Arriaga, who answered my many questions, thought about soil water processes with me at length, and helped me construct tools and instruments in the lab; Nick Balster, who provided big-picture perspective and helped me to develop as a public speaker.

Special thanks goes to several students and researchers that graciously gave their time: Clay Vanderleest lent his expansive instrumentation knowledge; Mingwei Yuan discussed results and was a wonderful sounding board of ideas; Melanie Stock was always willing to talk soil physics and processes; Gregg Sanford provided project design feedback; Alex Butz and James Tesmer answered many calls from the field and assisted with whatever problems arose; Jimmy Sustachek helped with sampling; Dr. Sarah Collier played a large role in shaping this project and contributed the laboratory data to the analysis; Richard Gaillard generously ran the model simulations and answered any modeling questions. Thank you to the researchers and administrators involved in the Dairy CAP grant by which this work was funded.

Friends and family that have supported and encouraged me, thank you. A final thanks and dedication to my father, Jamie McNamee, who died in November 2015. He was my greatest advocate and biggest challenger, always inspiring me with his unquenchable excitement, enthusiasm, and delight in the joys of every day.

Age quod agis.

TABLE OF CONTENTS

LIST OF TABLES AND FIGURES

INTRODUCTION

Soil hydraulic parameters, such as soil volumetric water content, matric potential, and unsaturated hydraulic conductivity, are necessary to quantify water flow and mass transport through the soil (Kosugi et al., 2002). The relationships between these hydraulic parameters becomes especially important in model simulations, where many processes (e.g. chemical transport to groundwater, greenhouse gas emissions, and plant water uptake) are dependent on soil water dynamics. The estimation of soil hydraulic parameters must be accurate, and as climate models simulating important drivers of change on our planet continue to develop, it is critical that these inputs and relationships are correct.

This research focused on the soil water characteristic curve (SWCC), a fundamental soil hydraulic relationship that informs ecosystem models. Measurement and estimation approaches for the SWCC were reviewed, with particular attention to the inclusion of soil structural properties and pore space in SWCC property-transfer models. Measurements of the SWCC were conducted on a well-aggregated, silt loam, prairie-derived soil in south-central Wisconsin and compared to SWCC predictions. Finally, the different hydraulic parameter estimates from measured and predicted SWCC were used in the biogeochemical model DayCent to test how these approximations influence model outputs.

LITERATURE REVIEW

The Soil Water Characteristic Curve (SWCC)

The soil water characteristic curve (SWCC) relates soil matric potential ψ to volumetric water content θ. Matric potential is the result of capillary and adsorptive forces of the soil on the water present binding to the water and lowering its potential energy (Hillel, 2004). Matric potential is expressed here in units of force per unit area, kilopascals (kPa). Matric potential is always negative in unsaturated material, approaching zero as the soil becomes more saturated. The terms matric "suction" or "tension" are the positive equivalents of matric "potential" (i.e. the absolute values) (Hillel, 1998). Matric "suction" will be used here to convey matric potential in order to avoid using a negative sign, which makes graphing on log scales impossible.

At matric suctions equal to zero, θ is equal to the saturated water content θ_s. While saturation implies that all of the pore space in the soil is filled with water, it is rare that θ_s is equal to the porosity Φ, due to entrapped air in the soil (Kosugi et al., 2002). The θ may also stay at θ_s for values of ψ slightly greater than zero. The ψ at which the initial decrease in θ from θ_s occurs is the air-entry suction ψ_{ae} (Kosugi et al., 2002). At this point, also known as the threshold of desaturation, enough suction to empty the largest pore is applied, and the water in that pore is replaced by air (Hillel, 1998). The air-entry value is typically small in coarse textured or well-aggregated soils with large pores, as the larger pores will drain under smaller suctions, and is typically larger in finer textured or

poorly aggregated soils, where greater suctions are required to drain the smaller pores (Hillel, 1998).

As matric suction increases, the pores in the soil matrix are drained of water. Large pores empty first, as the capillary and adsorptive forces in these pores are less than in smaller pores. In the dry (high) matric suction range, θ decreases asymptotically approaching the residual water content θ_r. Historically, θ_r was used because measurement techniques could not measure these low water contents, so the models assumed θ approached a specific value (Kosugi et al., 2002). Today, the significance of θ_r is debated; some argue that θ_r is the wetness left in smaller soil pores that don't have a continuous network (Hillel, 1998), while others state that theoretically θ goes to zero as ψ approaches infinity, and in practice θ_r is just a fitting parameter in SWCC models (Kosugi et al., 2002). The θ is sometimes represented as effective saturation S_e:

$$S_e = \frac{(\theta - \theta_r)}{(\theta_s - \theta_r)}$$

Desorption and sorption, or drying and wetting, are the two ways to create a continuous curve between ψ and θ. Typically these curves will be different for the same soil; the equilibrium θ will generally be larger in a drying curve then a wetting curve for a given ψ. This phenomenon is known as hysteresis: the equilibrium water content at a given matric suction is dependent on the previous process (sorption or desorption) (Hillel, 1998).

Measuring the Soil Water Characteristic Curve

Measurement methods

The SWCC is constructed from paired soil matric suction and water content measurements over a wide range of matric suctions (typically 0 kPa to plant wilting point, 1500 kPa). Measuring the SWCC is difficult, as no lab or field instruments cover the full plant available water suction range accurately. Typically, laboratory measurements of θ and ψ are collected in pairs after a known suction has been applied to a soil sample and the sample θ reaches a static equilibrium (Dane and Hopmans, 2002). "Equilibrium" is commonly determined as the point at which θ remains constant. In reality, θ could stop decreasing for reasons other than reaching equilibrium, such as a very low hydraulic conductivity or confined soil pores preventing water loss. The applied equilibrium concept is a potential source of error in the incremental SWCC measurement techniques.

Common laboratory techniques for measuring the SWCC include the hanging water column/suction plate method, pressure plate extractor, the dew point method, and the evaporation method, (Dane and Hopmans, 2002; Schelle et al., 2013). These methods are precise at different matric suction ranges and are chosen based on available time, resources, and study intent. In the low suction range, the SWCC is predominately influenced by the soil structure, so undisturbed samples are typically used in measurements that cover the wet end of the SWCC (Dane and Hopmans, 2002). At larger suctions, the SWCC is believed

to be influenced by soil texture and not structure, hence disturbed soil samples are commonly used (Schelle et al., 2013).

In the hanging water column method, undisturbed saturated samples are placed on a porous plate, the pores of which are filled with water that is in hydraulic contact with bulk water. A known negative pressure is applied through a hanging water column to the sample (via the porous plate), causing water to flow out of the sample until equilibrium is reached (Dane and Hopmans, 2002). Suctions of 0-85 kPa can be measured. The volumetric water content of the sample is determined by weighing before and after oven drying, multiplying the gravimetric water content by the soil bulk density, and dividing by the density of water (usually assumed to be 1 g cm^{-3}). Sample equilibrium can take a long period of time (1-3 weeks), and only one sample can be run at a time per hanging water column. This one-sample problem is avoided with the use of a suction table, which operates on the same basic principles (Dane and Hopmans, 2002).

Another technique that is precise in the wet end of the SWCC is the evaporation method. Undisturbed soil samples are saturated, installed with two tensiometers, and weighed regularly as soil water evaporates from the top surface of the sample (Schindler et al., 2010b). Water content is calculated at the end of the analysis period by oven drying the sample and converting gravimetric water content to volumetric water content. This results in many retention measurements. The HYPROP (UMS, Munich, Germany) is a commercial device that uses the evaporation method to determine the SWCC, and was used in this

research. Applying the extended evaporation method to the HYPROP method, suctions from 0 to 100-300 kPa can be measured (Schindler et al., 2010b; a).

With a pressure plate extractor, soil samples (usually disturbed) are packed in 1-cm high rings, saturated, and drained while in contact with a porous plate. A known air pressure is applied to the samples and they are drained to equilibrium. The samples are then weighed to determine θ, replaced on the extractor, and a larger pressure is applied. This process is repeated for the desired amount of SWCC points. Pressure plates can measure suctions 0 to 500-1500 kPa, depending on the ability to apply that much pressure, and measurements become less precise in the drier range. Errors arise from poor contact between the samples and the porous plate as the samples dry (Dane and Hopmans, 2002). This limited area of contact greatly slows water outflow from the sample, causing apparent equilibrium before it has occurred.

The dew point method measures very high matric suctions. In a sealed chamber, the liquid water in a soil sample is equilibrated with the vapor water in the air above the sample (Scanlon et al., 2002). The dew point of the air and the sample temperature are measured and used to calculate relative humidity, which is used to calculate total potential using the Kelvin equation (Schelle et al., 2013). Water content is determined gravimetrically with oven drying and converted to volumetric water content with a field measured bulk density. In this research, the dew point method is employed with the WP4C PotentiaMeter (Decagon Devices, Inc., Pullman, WA). The WP4C provides precise measurements from

approximately 5,000-316,000 kPa. The precision is approximately 0.5 kPa, so for error to be less then 10%, samples need to be drier then 500 kPa (Decagon Devices, Inc., 2015).

Field, or *in situ*, techniques for measuring the SWCC are a combination of matric suction measurements and soil water content measurements made side by side. Matric suction is commonly measured with a tensiometer, which measures suctions from 0-80 kPa. Water content is frequently measured by time domain reflectometry (TDR) or frequency domain reflectometry (FDR) probes.

Comparisons of measurement methods

Many studies have compared laboratory and field measurements of the SWCC to one another (for example, Basile et al., 2003; Schelle et al., 2013; Schindler et al., 2015). Schelle et al. (2013) compared the four laboratory measurements described above for eight different soil types with a wide variation in texture. The authors found that the suction table data and HYPROP data had comparable SWCC in the wet-moderate suction range, while the pressure plate tended to over-estimate water contents. In the moderate moisture range there was good agreement among replicates when using the HYPROP, and a wide range in equilibrium water contents among suction table samples, speaking to the consistency of the HYPROP results. However, the HYPROP replicates diverged towards saturation, likely because the heterogeneous soil structure was not captured by the 250-cm^3 sample size (Schelle et al., 2013).

The authors also observed a hysteretic effect when using disturbed

samples in the WP4C that were dried or wet-up over time. This effect was most pronounced in the finer textured soils (Schelle et al., 2013). HYPROP and WP4C data are often used in conjunction to determine the entire SWCC curve. The drying-curve WP4C data were a better continuation of the HYPROP measured end of the curve then the wetting-curve WP4C data. However, the wetting-curve is easier to measure, and if WP4C measurements are used with HYPROP data for soils where hysteresis is still prominent in the dry end of the SWCC, the inconsistencies or connection between the two ends of the curve may be more pronounced (Schelle et al., 2013).

Basile et al. (2003) compared field measurements and laboratory (evaporation method) measurements. From suctions of 0-10 kPa, the evaporation method SWCC had higher θ then the *in situ* curve, and the two curves converged as suction increased. The authors argued that the difference between laboratory and field measurements could largely be explained by hysteresis and trapped air; each curve was a different hysteretic branch, and if differences in experimental conditions were minimized, laboratory and field curves looked more similar (Basile et al., 2003).

Prediction and Estimation of the Soil Water Characteristic Curve

As described above, the SWCC is notoriously difficult and time consuming to measure. In order to reduce these difficulties, a number of different models have been developed to predict or estimate the SWCC from available water

retention data or more-easily measured soil properties. These SWCC estimates or predictions are frequently employed in simulation models of landscape scale processes. Some of these SWCC models are completely empirical, most are parametric, and some have a physical or theoretical basis. The most prominent models are described below.

Parametric and empirical models

Historically, the SWCC has been described using empirically-based parametric models (Haverkamp et al., 2002). Equations for the curve are fit to volumetric water content and matric suction data (Leong and Rahardjo, 1997). The components of the SWCC described above (θ_s, ψ_{ae}, θ_r) may be included in these functions as physically based parameters, along with dimensionless parameters that are determined empirically (Kosugi et al., 2002).

Common examples of such equations are Gardner (1958) and Brooks and Corey (1964). Brooks and Corey (1964)is one of the most widely adopted early models:

$$S_e(\psi) = (\psi/\psi_{ae})^{\lambda} \qquad \text{for } \psi < \psi_{ae}$$

$$S_e = 1 \qquad \text{for } \psi \geq \psi_{ae}$$

This power function relates θ to ψ for $\psi<\psi_{ae}$ using a dimensionless parameter λ that reflects the pore size distribution index, and the air entry suction ψ_{ae}(Kosugi et al., 2002). The $\psi<\psi_{ae}$ limitation results in a discontinuity at the air entry value, which provides challenges when used in numerical modeling (Assouline and Or, 2013).

The van Genuchten (1980) is perhaps the most widely used empirically based parametric model today:

$$\theta(\psi) = \theta_r + \frac{\theta_s - \theta_r}{[1 + (-\alpha\psi)^n]^m}$$

The sigmoidal expression uses three empirical parameters (α, n, and m) determined using least squares fitting procedures to soil θ and ψ data. The θ_s and θ_r may also be fitted or set. Although van Genuchten (1980) does not explicitly have the air entry suction included in the model like Brooks and Corey (1964) does, the inverse of α is proportional to the air entry suction (Kosugi et al., 2002). In many adoptions of the model the number of parameters is reduced by assuming that m = 1-(1/n). This model has been shown to be a good fit for many soil types, especially near saturation, but is less accurate at dry water contents. The advantage of van Genuchten (1980) near saturation increased its popularity among modelers (Assouline and Or, 2013).

Extensive lab and field measurements are required to create a SWCC using empirical methods. This can be time and resource intensive, and the extrapolations of these equations to specific soil types can be unrealistic (Haverkamp et al., 2002).

Models relating particle size distribution to pore sizes and the SWCC

The continuous SWCC is difficult to measure, and this has increased efforts to develop models that relate easily measured soil properties to the SWCC. These models are known as property-transfer models (not to be confused with

pedotransfer functions which will be addressed shortly), and soil texture, particle size distribution (PSD), and bulk density data are the most frequently used soil properties.

Many physically based models adopt the shape similarity hypothesis that the cumulative PSD and the SWCC have the same fundamental shape (Haverkamp et al., 2002), a theory supported by the analysis of Haverkamp et al. (1988) of 600 soils in the GRIZZLY soil database. This highlights the important role of soil texture in determining the shape of the SWCC. The role of soil structure in determining the SWCC is estimated with dry bulk density in early models. In many models, particle size is related to a local pore size through the particle radius and assumptions regarding pore and particle shape, such as cylindrical pores and spherical particles (Haverkamp et al., 2002). Pores are then related to matric suction through the equation of capillarity ($R = C_c/\psi$ where typically C_c=130 μm-kPa and R is the pore radius) (Nimmo et al., 2007).

The Arya and Paris (1981) model and the Haverkamp and Parlange (1986) model are two popular physically-based SWCC prediction strategies. The Arya-Paris model uses cumulative PSD and bulk density data to estimate the SWCC. The cumulative PSD is divided into class fractions with an average particle size and weight. Soil particles are assumed to be spherical, pores are assumed to be cylindrical, and the bulk density (and therefore porosity) of the soil is applied to all particle size fractions uniformly. The authors derive a nonlinear relationship between mean pore radius R of a particle size fraction i and mean

particle diameter *D*:

$$R_i = \frac{1}{2} D_i \left[\frac{2e{n_i}^{1-\alpha}}{3} \right]^{0.5}$$

where e is the void ratio (ratio of porosity to volume of solids), n is the number of particles, and α is an empirical parameter intended to correct for the tortuosity of soil pores. This parameter was determined experimentally and a value of 1.38 is commonly adopted. The mean pore radius R_i is then related to matric suction through the capillarity equation. Corresponding θ for each particle size class are calculated from the cumulative pore volume, assuming that pore volumes are filled with water and accumulated beginning with the smallest particle size fraction. The resulting θ and ψ data to predict the SWCC is discrete and limited by the number of particle size classes that were used to determine the PSD (Arya and Paris, 1981).

Haverkamp et al. (2002) outline four problems, assumptions, or inconsistencies inherent in the Arya-Paris model. First, saturated water content is equal to the total porosity, a condition that is rarely observed in the field, and occurs because the model does not account for air entrapment in the soil. Therefore the Arya-Paris model tends to overestimate θ in the wet-end of the SWCC. In well-aggregated soils, the overestimation of θ may also be attributed to the inability of dry bulk density to capture the influence of structure on the SWCC. Secondly, the proposed average α=1.38 value is determined from a small number of soils, and is applied uniformly to all particle size fractions. Research suggests that α should vary with particle size fraction, and it has been found that

α varies not just based on soil type, but by water content as well. Additionally, hysteresis is not accounted for in the model. Lastly, the Arya-Paris model has an inherent compatibility problem. The assumption that the porosity of the soil is uniform across particle size fractions, or the constant partial porosity hypothesis, means that the cumulative pore fraction can be set equal to the cumulative distribution of particle weights, which the Arya-Paris model does. In order for this to be true, however, the pore radius R_i must be directly proportional to the particle diameter D_i. The Arya-Paris model does not use a linear relationship between R_i and D_i because of the inclusion of the tortuosity parameter α as an exponent (see above equation), violating this assumption (Haverkamp et al., 2002). The Arya-Paris model is therefore not completely sound from a theoretical basis.

The Haverkamp-Parlange (1986) model is similar to the Arya-Paris model in that it assumes shape similarity between cumulative PSD and the SWCC and uses dry bulk density to estimate structural contributions. However the Haverkamp-Parlange is a continuous function (instead of discrete points) that also accounts for hysteresis (Haverkamp et al., 2002). It is only reasonable for sandy soils and soils with weak structure (Assouline and Or, 2013), so it will not be elaborated on here.

Nimmo et al. (2007) improved upon Arya and Paris (1981) in a model the authors refer to as the continuous-function equivalent of the Arya-Paris model, or CNEAP:

$$\psi = \frac{C_c}{r}\left\{\frac{3}{2e}\left[\frac{m_0}{2\pi\rho_p}\frac{M(r)}{r^2}\right]^{\alpha-1}\right\}^{1/2}$$

$$\theta(\psi) = \Phi M_{cum}(R(\psi))$$

where *M(r)* is differentiated from the cumulative PSD $M_{cum}(r)$, m_0 is the standard mass (1 g, used for unit consistency), and ρ_p is the particle density. The authors adjusted Arya- Paris (1981) into the continuous function CNEAP to eliminate the interval-size dependence. The CNEAP and Arya-Paris (1981) models produce near identical results (Nimmo et al., 2007).

There are additional models that relate PSD to pore size and the SWCC that are based on different fundamental assumptions about particle-pore relationships (see Assouline and Or, 2013). These are not applied here, and therefore will not be elaborated on.

Models accounting for structure effects in the SWCC

The property-transfer models described above appear to account for the role of texture in the SWCC, but the role of structure is not fully captured. The Nimmo (1997) model attempts to remedy this issue by accounting for structural properties of the soil in the SWCC. Nimmo (1997) hypothesizes that volumetric water content is the sum of a textural component and a structural component, as is porosity. Porosity is therefor separated into textural porosity Φ_t and structural porosity Φ_s, where $\Phi_t + \Phi_s = \Phi$, the total porosity. Two distinct models are used to calculate each component, and the SWCC is predicted from the sum of the models (Nimmo, 1997). The Arya-Paris model is used to estimate the textural

water content component based on PSD with the porosity set to a texture-associated porosity of 0.3. The textural pore space is assumed to be random, or "non-structured", therefore Φ_t is set to 0.3 based on theory and observations of the porosity of randomly structured materials (Nimmo, 1997). The structural water content component is estimated using aggregate size distribution (ASD) data and the remaining (structural) porosity in a manner analogous to the textural component. These two components are summed across ψ for the total SWCC (Nimmo, 2002).

More specifically, the structural component of Nimmo (1997) is determined by relating aggregate size to pore size, pore size to capillary radius, and capillary radius to matric suction. The ASD data are fit to the lognormal distribution of Gardner (1956) to determine the geometric mean radius (GMR) and geometric standard deviation (GSD) of the soil aggregates. In relating aggregate size to pore size, the model applies the scaling of the relation of the pore radius to aggregate radius using the void ratio, but also incorporates a ratio β of pore body size to pore opening size, as the ψ at which a pore empties depends on the radius of the pore opening, not the pore body. Theory and observation suggest β=2.2 (Nimmo, 1997). Further, the author argues that aggregates fit together more tightly than soil particles because aggregates can be formed in place and are more malleable, therefore interaggregate pores are longer and perhaps narrower in soil with more uniformity (i.e. a well-aggregated soil). The GSD of the ASD is used as an index of aggregate size variability that

represents the tightness of fit of aggregates, where 0 indicates perfectly tight fitting and 1 indicates a random, loose fit between soil aggregates. Applying these adjustments and capillary theory relates aggregate radius r_{agg} to a matric pressure ψ by:

$$r_{agg}(\psi) = \frac{-C\beta}{\sigma\eta_s^{1/3}\psi}$$

where C= 0.13 mm kPa^{-1} (from capillary theory- for small contact angles and surface tensions 10% less then pure water), β is the ratio of pore body radius to pore opening radius, σ is the GSD in inverse natural log units, and η_s is the structural void ratio ($\Phi_s/(1-\Phi_s)$. This relationship assumes that interaggregate pores have a circular cross-section, when in fact because these pores are likely narrow, they may have a more elongated shape (Nimmo, 1997). The aggregate radius r_{agg} is normalized with the GMR and GSD and the result is a cumulative lognormal distribution function relating ψ to the structural water content (Nimmo, 2002):

$$\theta_s = \frac{\Phi_s}{\sqrt{2\pi}\log\sigma}\int_{-\infty}^{\log r_{agg}} \exp\left[\frac{-(\log r_{agg} - \log GMR)^2}{2(\log\sigma)^2}\right] d\log r_{agg}$$

It is important to note that ASD measurements are not well standardized (Dıaz-Zorita et al., 2002), so ASD data can be less reliable than particle size distribution data (Nimmo, 2002). However, Nimmo (2002) points out that the Nimmo model SWCC is less sensitive to GMR and GSD then other model inputs, suggesting that the effect of variable ASD measurement techniques has less weight on the resulting SWCC, at the very least.

As a result, the Nimmo model is most appropriate for well structured, well-aggregated soils, and it fits data in these cases better than the Arya-Paris model alone (Nimmo, 2002). In weakly structured, weakly aggregated soils, however, the structural component has less influence on soil water content, and so the Nimmo model is not as appropriate (Nimmo, 2002).

Pedotransfer Functions and Additional Models

Pedotransfer functions (PTFs) are empirical and statistical functions that relate simple soil properties to the SWCC. Properties typically used are bulk density or porosity, organic carbon content, soil texture, and penetration resistance. Many times the data used to calibrate PTFs is from a specific location, so extrapolation of these relationships to other locations can cause significant errors. PTFs can provide reasonable initial estimates for large scale analyses (Assouline and Or, 2013).

There are more models for the SWCC that fall outside the scope of this research analysis. They include fractals and percolation theory, accounting for angular pores, and applying pore scale statistics (Assouline and Or, 2013).

The Use of SWCC in Climate Models

Ecosystem and biogeochemical models are used to simulate flows of carbon, nutrients, and gas exchange in terrestrial systems. The CENTURY model operates on a monthly time step to simulate changes in soil organic matter, plant development, and nutrient availability due to alterations in land management

and climate. The DayCent model is the daily time step version of CENTURY, adjusted to a daily time step in order to more accurately simulate nitrogen gas emissions, which depend on nonlinear relationships in daily processes (Del Grosso et al., 2011). DayCent is used to estimate nitrous oxide (N_2O) emissions from agricultural systems for the Inventory of the U.S. Greenhouse Gas Emissions and Sinks that is compiled by the U.S. Environmental Protection Agency and reported to the United Nations in accordance with the Framework Convention on Climate Change (Del Grosso et al., 2011; U.S. Environmental Protection Agency, 2016). The accuracy of the N_2O emissions estimated by DayCent are therefore valuable from not only a scientific lens, but a policy perspective as well.

The land surface submodel used in DayCent simulates daily soil water dynamics and temperature fluxes in the soil (Parton et al., 1998). The user specifies the number and thickness of soil horizons and soil properties for each layer. The soil properties include texture, bulk density, wilting point, field capacity, the extent that water content can drop below wilting point, root fraction, organic matter fraction, saturated hydraulic conductivity, and pH (Del Grosso et al., 2011). It has been suggested that if time series soil water content data are available, field capacity and wilting point be estimated by maximum θ one to two days after rainfall and minimum θ during dry period, respectively (Del Grosso et al., 2011). Alternatively, it is suggested that these inputs be estimated from pedo-transfer SWCC functions, and the authors recommend Saxton and Rawls (2006) which uses soil texture and organic matter content data. DayCent

represents the saturated flow of water through the soil profile with unidirectional downward flow, where water fills a soil layer to saturation before moving into the next layer, and layers exceeding field capacity θ are drained to the layers below. Unsaturated flow is bidirectional using Darcy's law to compute the water flux between adjacent soil layers (Parton et al., 1998).

A nitrogen gas flux submodel is used in DayCent to simulate N_2O emissions. This submodel assumes that both nitrification and denitrification processes contribute to N_2O soil emissions, and emissions are calculated as a function of a number of soil properties, including water filled pore space (WFPS) and soil texture (Parton et al., 2001). The WFPS at a given time is determined from bulk density (ρ_b) and θ:

$$WFPS = \frac{\theta}{1 - (\rho_b / 2.65)}$$

where $1-(\rho_b/2.65)$ is equivalent to soil porosity Φ and 2.65 is the assumed particle density in g cm^{-3}. Hence, the WFPS is sensitive to bulk density inputs, as bulk density determines the pore space that is available to be filled with water. Further, the user-specified field capacity and wilting point parameters affect how WFPS is allocated over time. In the simulation of denitrification, when WFPS < 55%, no denitrification is assumed to occur, and when 55% < WFPS < 90% denitrification increases exponentially and levels off as WFPS approaches saturation (Parton et al., 2001). In the simulation of the nitrification model, the effect of WFPS is related to nitrification based on empirical data and changes depending on soil texture (Parton et al., 2001). Changes in θ, and therefore WFPS,

are regulated by the land surface submodel, which includes field capacity and bulk density inputs. In this analysis we explore the sensitivity of the DayCent model to field capacity and bulk density parameters through changes in simulated θ and N_2O emissions. As mentioned previously, soil hydraulic properties like the SWCC, which field capacity is estimated from, are difficult to measure and predict, and may result in different DayCent predictions depending on the method employed.

OBJECTIVES

The overall goal of this study was to assess alternative methods for estimating the SWCC in a prairie-derived, cultivated silt loam Wisconsin soil, and the implications of differences that arose in estimated SWCC for downstream applications of this fundamental descriptor of soil water behavior. Specific objectives included:

1) Investigate differences between laboratory and *in situ* measurements of the SWCC on a well-structured, silt loam soil.

2) Examine the ability of property-transfer models to predict the SWCC compared to measured (*in situ* and laboratory) data, with particular attention to the importance of accounting for soil structure. The CNEAP texture-based model (the updated version of Arya-Paris, 1981) and the Nimmo (1997) structure-texture model are used to investigate this difference.

3) Evaluate the effect of field capacity estimations from the methodological differences determining the SWCC (*in situ*, laboratory, and property-transfer models) on the output of ecosystem models like DayCent, which model greenhouse gas emissions to inform policy decisions.

MATERIALS AND METHODS

Site Description

The study was conducted at the Wisconsin Integrated Cropping Systems Trial (WICST) at the University of Wisconsin's Arlington Agricultural Research Station in Arlington, Wisconsin (43° 18' N, 89° 21' W) during the 2014 and 2015 growing seasons. The soil was a Plano silt loam (fine-silty, mixed, superactive, mesic Typic Argiudoll). The mean annual temperature at Arlington was 7.7°C and mean annual precipitation was 912 mm (1985-2015, National Weather Service). In 2015, mean annual temperature was 8.1° C and annual precipitation was 993 mm. Over the 2015 growing season (May-September), the average temperature was 18.5° C and precipitation was 527 mm (National Weather Service, 2016).

The WICST was a long-term trial established in 1990 to compare six different cropping systems: three forage-based and three cash-grain based. The trial was a randomized complete block design with four replicates. All phases of each system were present every year, plots were 0.3 ha in size, and operations were conducted with commercial farm-scale equipment. Since the establishment of WICST, management has changed as necessary to remain current with best management practices and technological advancements (Posner et al., 2008).

This study examined the soil water characteristic curve (SWCC) of three of the WICST systems: the cash-grain corn-soybean system (CS2), the conventional dairy forage system (CS4, corn followed by three years of alfalfa), and the rotationally grazed pasture system (CS6). These particular systems were chosen

in order to capture a range of agricultural practices common to Wisconsin dairy agroecosystems. Due to instrumentation costs, measurements were limited to the third replicate of WICST, and only the corn phase of CS2 and CS4 systems. Rotation CS2 was strip-tilled in the fall prior to corn (*Zea mays* L.), and soybeans [*Glycine max* (L.) Merr.] were planted using a no-till drill, while CS4 was chisel-plowed in the fall, prior to corn and prior to alfalfa seeding. The corn in both CS2 and CS4 received commercial fertilizer at the recommended rates, and in CS4 cattle manure slurry was applied in the fall prior to corn and first year alfalfa seeding. Weeds were chemically controlled in CS2 and CS4. Rotation CS6 was seeded with a mixture of red clover (*Trifolium pratense* L.) with a no-till drill, timothy (*Phleum pratense* L.), smooth bromegrass (*Bromus inermis* L.), and orchardgrass (*Dactylis glomerata* L.), and was rotationally grazed by six heifers per plot (Table 1).

SWCC Measurement

Volumetric Water Content

Soil volumetric water content (θ) was measured with CS616 frequency domain reflectometers (FDRs) in each plot (Campbell Scientific Inc., Logan, Utah). The CS616s were installed horizontally at 15, 25, 45, and 70 cm depths. To minimize field disturbance during the growing season, CS616s were installed at 45 and 70cm depths (one at each depth in CS4 and CS6, two at each depth in CS2) April 22-23 2015 prior to field operations. Three CS616 probes were installed at

15 and 25 cm depths June 24-30 after planting and side-dressing in order to avoid instrument damage from field machinery.

CS616 Reflectometer Calibration

The CS616 reflectometer outputs the period (in microseconds) of an electromagnetic pulse that is sent along its metal rods. The velocity of the electromagnetic pulse is dependent on the dielectric permittivity of the material (in this case soil, water, and air) surrounding the rods. Water has a higher dielectric permittivity than soil and air, which slows the electromagnetic pulse, and so a relationship between output period and θ can be constructed (Campbell Scientific, Inc., 2016). The output period is converted to θ using a calibration equation. The manufacturer's factory calibration equation is:

$$\theta = -0.0663 - 0.0063 * period + 0.0007 * period^2$$

Vaz et al. (2013) found that the factory-supplied calibration works well for a range of θ, 0-0.15 $m^3 m^{-3}$, but significantly overestimates θ greater than 0.15 $m^3 m^{-3}$. We also found this to be the case (Figure 1). Vaz et al. (2013) developed a CS616 probe calibration using seven mineral soils varying in texture. The authors conducted this calibration in the laboratory using containers packed with dry soil. Water was incrementally added to reach a target θ. Every time water was added the soil was thoroughly mixed, repacked to a similar bulk density, and measured for θ and the period using the CS616. The calibration that Vaz et al. (2013) suggested for mineral soils is:

$$\theta = -0.5783 + 0.1527\sqrt{period}$$

An on-site calibration of the CS616 probes was conducted in summer 2015. Sixteen probes were installed just north of the CS2 treatment, four probes at each of the four depths (15, 25, 45, and 70 cm) for calibration. Two pits were dug and two sets of probes were installed in the opposite sides of each pit, and then the pits were filled with soil. Bulk density samples (7.5 cm diameter x 7.5 cm height) were taken over the field season at each probe depth (three per depth per sample time, eight sample times in total). When taking samples, the soil was excavated to 3.75 cm above the measurement depth (e.g. 11.25 cm for a 15 cm deep measurement; 66.25 cm for a 70 cm deep measurement) and carefully sampled for bulk density. When excavating, an area approximately 80 x 40 cm was cleared to the proper depth in order to minimize compaction from sampling in the shallower depths. The gravimetric water content was determined by weighing samples before and after oven drying at 105°C for three days. This was multiplied by the bulk density over the density of water (assumed to be 1 g cm^{-3}) to arrive at the volumetric water content θ. This was considered the true water content. While bulk density samples were being taken, the set of CS616 probes closest to the sampling area were connected to a CR1000 datalogger (Campbell Scientific Inc., Logan, UT) and the probe period was recorded every ten minutes for approximately sixty minutes. Little to no variation was observed in the probe period during the sampling time. Period verses true water content was graphed in order to determine an *in situ* calibration curve for the moisture probes. Despite careful sampling timing over the season, only a limited range of θ was captured,

and therefore the field calibration curves do not have a large enough range in period to be confidently used to establish a calibration curve on their own (Figure 1).

While the field measured θ-period data could not be used to determine an entire new calibration curve, the data from 15 and 25 cm matched reasonably well with what is predicted using the Vaz et al. (2013) calibration (Figure 2) within the limited range that θ-period data was collected. This calibration was adopted for these depths. The field measured θ-period data from 45 and 70 cm depths were lower than the Vaz et al. (2013) calibration predicts. This could be due to the increased clay content and bulk density at these depths (Campbell Scientific, Inc., 2016), although the soils used by the authors for this calibration included those with clay contents as high as 30%, which is the extreme found at WICST. The same functional form as the Vaz et al. (2013) calibration ($\theta=a+b*\sqrt{period}$) was used for 45 and 70 cm depths, but the calibration curve was fitted (in MATLAB 2014b) using the field measured θ-period data from 45 and 70cm (Figure 3). None of the calibration equations were forced through a zero point because we wanted to avoid any uncertainty that accompanies assuming the period at which θ equals zero. Further, the range of periods measured in the field over the growing season was relatively small (26-34 μS at 45 cm; 32-36 μS at 70 cm) and close to the periods measured in the calibration data. The final calibrations used were:

$$15 + 25 \text{ cm:} \quad \theta = -0.5783 + 0.1527 * \sqrt{period}$$

$$45 + 70 \text{ cm}: \quad \theta = -0.4166 + 0.1171 * \sqrt{period}$$

Suction Measurements

Soil suction was measured using "Jet-fill" tensiometers (Model 2725ARL; Soil Moisture Equipment Corp., Goleta, CA). Tension was measured and recorded by pressure transducers, either Soil Moisture Equipment Corp. (Model 5301; Goleta, CA) or Omega Engineering Inc. (Model PX209-30VAC5V; Stamford, CT). An airtight seal between pressure transducers and tensiometers was assured by o-rings, Teflon thread tape, pipe sealant, and silicon sealant. Two tensiometers (one with each pressure transducer type) were installed at each of the 4 depths in each plot next to moisture probes.

At installation (June 26-July 2, 2015), a 2.25 cm diameter hole was augered so the midpoint of the tensiometer's porous cup would be at the 15, 25, 45, or 70 cm depth and perpendicular to the soil surface. The tensiometer body was connected to the porous cup, filled with degassed water, and placed upright in a bucket of water for approximately ten minutes to saturate the porous cup. Tensiometers were topped off with water, pumped with a hand-pump to remove bubbles from the pressure transducer connection, and the "Jet-fill" cap was attached. A slurry was made with water and soil removed from the augered hole. This was poured into the hole to ensure good contact between the soil and the tensiometer. The tensiometer was inserted and space around the tensiometer was backfilled and packed tightly to avoid preferential flow.

Tensiometer water level was checked frequently throughout the season

(minimum 2x/week). If the water level was low, tensiometers were refilled with de-gassed water and hand-pumped to remove bubbles. If there was only an air bubble at the top of the tensiometer body, the tensiometer was refilled using the "Jet-fill" top or hand-pumped. Times of tensiometer servicing were recorded in order to be removed from the final data.

All instruments (tensiometers and CS616s) were connected to a CR1000 datalogger and an AM16/32B multiplexer (Campbell Scientific, Inc., Logan, UT). Measurements were taken every 30 seconds and 20-minute averages were recorded July 2-October 14, 2015. Instruments were removed on October 14 before harvest.

In Situ Soil Water Characteristic Curves

In situ soil water characteristic curves (SWCC) were constructed using the θ and ψ data described above. A set of rules was used in order to systematically identify and summarize dry down periods from the continuous data. The θ and ψ measurements were graphed over time and dry down periods that occurred over the season were identified according to the following criteria:

1. Decrease in θ over time: initial identifications of dry downs were made from the θ data when θ begins to decrease. End point was when θ begins to increase.
2. Corresponding ψ measurements for the same time period were selected.
3. Dry down period began when θ decrease *and* ψ increase.
4. Daily θ and ψ values were represented by the average of 5:00-6:00 AM

(four data points).

5. If tensiometer readings were < -80 kPa the measurement was not included.

Dry down periods were identified at each depth, and approximately 6-7 dry down periods were found at the shallower depths. The amount of dry down periods measured decreased with depth as the range of water contents experienced decreased. These dry down periods were used to construct soil water characteristic curves for each depth and plot.

Laboratory SWCC

The wet end of the SWCC was measured in the laboratory with the evaporation method using a HYPROP device (UMS, Munich, Germany). The dry end of the SWCC was measured using the dewpoint method with the WP4C PotentiaMeter (Decagon Devices, Inc., Pullman, WA).

Soil sampling for laboratory measurements was conducted July 16-18, 2014. Samples were collected at two locations per plot, 10 and 30 meters from the edge of the plot either north or south of the WICST central access drive, and centered east to west. In the CS2 and CS4 corn phase samples were taken between rows. A coring device fitted with a slide hammer and inner sampling rings of 8.05 cm diameter and 5 cm height was used to collect samples centered at depths 15 and 45 cm in each location. Samples were carefully trimmed in the field to match sampling ring height, capped, and stored at 4° C until processing.

The SWCC were generated according to the HYPROP and WP4C

manufacturer recommended procedures (UMS, 2012; Pertassek et al., 2015; Decagon Devices, Inc., 2015). Samples were gradually saturated with tap water from the bottom over 16-20 hours. The height of any soil swelling that occurred was recorded for calculation of effective sample volume. Holes of a known volume were augered in the saturated sample to accommodate tensiometers. HYPROP components were filled with degassed water and the sample (in its sample ring) was loaded onto the HYPROP apparatus and placed on a scale. Samples were allowed to air dry with mass and suction measurements automatically recorded every 10 minutes for the duration of the dry down until tensiometers cavitated. Sample run times were typically 2-7 days.

After the HYPROP measurement, samples were detached from the HYPROP apparatus and the sampling ring was removed with care to make sure all the soil was retained. Samples were dried overnight in an oven at 105° C, cooled, and weighed. Bulk density was calculated from the oven dry weight and sample volume. Samples were then ground by hammer mill to pass a 2-mm sieve and stored at room temperature. Ten subsamples of approximately 4 g were taken from each sample, weighed in tins, and hydrated by the addition of an increasing number of droplets of distilled water, in order to reach approximately 2-20% gravimetric water content across the ten subsamples. Hydrated soil was thoroughly mixed, and tins were capped and sealed and allowed to equilibrate for 16-24 hours. Water potential was then measured on the subsamples using the WP4C. The weights of the subsamples were recorded following the WP4C

measurement, dried at 105° C for 16 hours, cooled in a dessicator, and re-weighed. Gravimetric water content was calculated from the wet and dry subsample weights and converted to volumetric water content using the entire sample bulk density. Dr. Sarah Collier (Postdoctoral Fellow at UW-Madison and DairyCAP Research Associate) and her team processed all samples between August 2014 and July 2015.

SWCC Model Inputs

Particle Size Distribution and Aggregate Size Distribution

Soil samples for particle size analysis (PSA) and dry-aggregate size distribution (DASD) were collected October 26-27, 2015, after harvest but before fall tillage and manure application. A truck mounted probe (Giddings Machine Company Inc., Windsor, CO) was used to collect three 7.5 cm diameter cores and three 2.5 cm diameter cores. Soil 5 cm above and below the four depths of interest (i.e. 5-20 cm for the 15 cm depth) was removed from each of the 2.5 cm diameter cores and combined in a composite sample for each depth to be used for PSA.

The PSA was conducted in the laboratory using the hydrometer method (described in Gee and Or, 2002; method of Day (1965) modified by Gee and Bauder (1986)). Two 40-50 g subsamples were analyzed for each depth. Hydrometer readings were taken at 40 seconds (3x) and 3, 10, 30, 60, 90, 120, 412, and 1440 minutes to construct a detailed particle size distribution. After the

hydrometer readings were taken, each sample was sieved through 1000, 500, 250, 106, and 53 um sieves, dried, and weighed in order to partition the sand fraction.

No standard method for DASD has been widely adopted; sampling method, sample preparation, sieve sizes, shaking device, and shaking time can all vary. After considering dry aggregate analysis method reviews (Dıaz-Zorita et al., 2002; Nimmo and Perkins, 2002; Larney, 2008), what was assumed to be the most practical and minimal-error-inducing approach was used. The 7.5 cm diameter cores were transported to the lab in the plastic tubes they were taken in. The plastic tubes were cut open and the soil 5 cm above and below the four depths of interest was carefully removed. The core-extracted soil was first divided along planes of weakness using the drop-shatter technique, and further broken down using gentle hand manipulation (Dıaz-Zorita et al., 2002). Samples were air dried until the change in weight was less than one percent over six hours. Two subsamples of approximately 300 g were taken from each sample. Size fractionation was determined using the Ro-Tap Test Sieve Shaker (W.S. Tyler, Mentor, OH) for 30 seconds with 8, 4, 2, 1, 0.5, and 0.25 mm sieves. Soil on each sieve was weighed and the DASD was determined. In some cases the sieves were loaded with more then 300 g of soil, and these samples were removed from the final analysis.

Wet aggregate size distribution (WASD) data from 2008 was available at the 5-20 cm depth (Jokela et al., 2011). The authors used the wet-sieving method

of Cambardella and Elliott (1993) with 4, 2, 1, 0.5, and 0.25 mm sieves, and sieved samples for ten minutes at 30 strokes/minute with 1-cm amplitude.

Bulk Density

Bulk density from several different sources and time periods is reported in this research. Due to the long-term nature of the WICST trial, taking multiple samples that were large enough to capture a representative volume was discouraged in the interest of minimizing system disturbance. Instead, bulk density values from previous years were used in combination with more recent sampling. The samples for HYPROP/WP4C analysis taken in 2014 (described above) were used for bulk density at 15 and 45 cm. As these samples were only taken at two depths, bulk density data from Sanford et al. (2012) were used to estimate 25 cm and 70 cm bulk densities. The authors made bulk density measurements in 2007 and 2008 using a 3.7 cm hammer core and a 5.4 cm hydraulic core, respectively, at 0-15, 15-30, 30-60, and 60-90 cm depths. The 2007 and 2008 measurements were very similar despite differing sample diameters, so the authors reported average values. The 15-30 cm and 60-90 cm measurements were used in this study to approximate the 25 and 70 cm depths. Sanford et al. (2012) assumed that no significant change in bulk density below 30 cm was likely to have occurred from the start of the WICST trials in 1989 to 2009 because these are well-structured, grassland soils that have been exposed to relatively light agricultural equipment. It seems reasonable to extend this assumption from 2009 to 2015, at least in the case of the 70 cm depth that is

approximated by this data. The last bulk density measurements used were collected by Jokela et al. (2011) at the same time samples for wet ASD analysis were taken. Bulk densities were hand sampled in late October 2008 after harvest at 5-15 cm depth using a 3.8 cm diameter core, with 16 cores taken per plot in a zig-zag pattern (Jokela et al., 2011). These bulk density data were used with the wet ASD data in the wet aggregate Nimmo model.

DayCent Model Simulations

The DayCent model was run for CS2 and CS4 from 1985-2015 under four field capacity scenarios and three bulk density scenarios for a total of twelve runs for each cropping system. The CS6 system was not simulated because DayCent runs for this system are not available (Richard Gaillard, personal communication). Bulk densities of 1.17, 1.26, 1.36 g cm^{-3} at 15 cm were tested, and these values were chosen to capture the range of bulk densities measured in the CS2 and CS4 systems at this depth. The field capacity values used in the simulations were estimated from *in situ* and laboratory water contents at 33 kPa, the matric suction commonly associated with field capacity in a fine textured soil (Hillel, 1998). In the *in situ* data, field capacities at 15 cm ranged from 23-24% θ across the CS2 and CS4 systems, and in the laboratory data field capacities ranged from 28-32% θ. Therefore, field capacities of 23, 24, 28, and 32% θ were input into the DayCent model for 15 cm. At 45 cm, a similar process was used, and field capacity inputs to DayCent were 23 and 26% (estimated from *in situ* data) and 32

and 34% (estimated from laboratory data). Bulk density was 1.33 g cm^{-3} at 45 cm. DayCent simulated θ in 2015 for each model run was compared to observed 15 cm θ using linear regression in SAS. Model simulations were evaluated using RMSE, correlation coefficient, and coefficient of determination.

Other DayCent model inputs included daily minimum and maximum air temperature and daily precipitation (UW Extension, 2016), vegetation cover (corn), and soil texture (National Cooperative Soil Survey, 1996). Average management practices were used in the model from 1985-2009, and precise management dates and operations (planting, fertilizer application, harvest, tillage) were input from 2010-2015. The simulated N_2O emissions from April through November 2015 were summed and cumulative emissions were reported for each treatment (CS2, CS4) and field capacity and bulk density model run. Simulated cumulative N_2O emissions were used as one way of assessing the importance of soil hydraulic parameters in model predictions. DayCent simulations and corresponding statistics were performed courtesy of Richard Gaillard (Research Assistant, USDA-ARS Dairy Forage Research Center).

RESULTS

Volumetric Water Content

Soil θ was similar across treatments at each depth, and the range in VWC experienced over the season decreased with depth (Figure 4). The 15 cm probes responded quickly to rainfall events with increases in θ, and the magnitude of θ response to precipitation decreased with depth. In CS6 the 15 and 25 cm probes had a lower θ over the season, and the magnitude of θ responses to rainfall was smaller than in the corn rotations. The CS2 45 cm probe measured approximately 4% lower θ throughout the season then CS4 and CS6.

Measured SWCC

In situ SWCCs

The *in situ* SWCCs developed from drying episodes showed few differences among the three treatments (Figures 5-8). Drying episode length ranged from 3-19 days. The variation in θ measurements over the tensiometer suction range was small. The θ at 15 cm decreased less then 5% from 0-80 kPa, and this decrease became smaller with depth. The dry-down periods at 15 and 25 cm (Figures 5-6) overlapped among treatments for the most part, although the 25 cm CS6 pasture treatment showed some events with θ approximately 2% less then the rest of the measurements. Rotations CS4 and CS6 45 cm depth SWCC were very similar, however the CS2 45 cm curve was shifted downwards to lower

θ (Figure 7) because of the lower θ measured over the season in this treatment at 45 cm. Fewer dry-down periods occurred within the tensiometer measurement range at the 70 cm depth in CS2 and CS4, and none occurred in CS6 (Figure 8). The CS2 and CS4 curves that were measured were relatively close to one another at this depth.

Dry-down periods from the same treatment and depth did not result in identical SWCCs (Figures 5-8), which could be explained in part by hysteresis (see discussion; Figure 9).

Comparison of Field and Laboratory SWCC

Two cores were taken at 15 and 45 cm in each treatment for HYPROP/WP4C analysis. The measurements showed small differences (maximum 2%) in θ between the two 15-cm HYPROP cores within treatments for a given ψ (Fig 10). At 45 cm, CS2 and CS4 HYPROP cores showed hardly any difference between cores, however the CS6 45-cm cores exhibited variation similar to that of the 15-cm cores.

The *in situ* θ observations were consistently lower for a given tension compared to the laboratory measured HYPROP/WP4C data, although the size of differences differed by depth. At 15 cm for suctions 10-80 kPa, the HYPROP data reported θ that were 5-10% greater then the *in situ* data (Figure 10). Differences between methods increased as suctions approached 0 kPa, and were as large as 15-20% near 1 kPa. This was also true at 45 cm (Figure 12) with the exception of

CS2, which had even greater differences in θ across measurement techniques due to the lower *in situ* θ measurements made by the moisture probes in that plot.

CNEAP and Nimmo Model Data Inputs

Particle size distribution

Measured particle size distributions (PSD) were similar across treatments (Figure 14). The higher clay content at 70 cm in all treatments and CS6 45 cm compared to other depths (27% vs 20%) was reflected in the separation of these curves from the others at the smallest particle size range. The measured PSD were in agreement with previous PSD measurements in the area as part of the National Cooperative Soil Survey (1996), and with the percent sand silt and clay measured in the WICST treatments in 2008 (Sanford et al., 2012).

Aggregate size distribution: GMR and GSD

The average geometric mean radius (GMR) and average geometric standard deviation (GSD) were calculated from the measured aggregate size distribution. With the dry-aggregate method, there appeared to be minimal differences in GMR among treatments at the same depth (Figures 15), and on average the dry GMR appeared to increase with depth within a treatment, with the exception of CS2-15 cm. The dry GSD was relatively similar across treatments and depths, with the exception of CS6-15cm (Figure 16). Wet aggregate GMR was smaller then dry aggregate GMR in all treatments at 15 cm,

and all wet GSD were smaller then dry GSD. The wet-aggregate data had a greater GMR in CS6 relative to CS2 and CS4, and a smaller GSD in CS6.

Bulk Density

Bulk density at 15 and 45 cm measured in three studies (including this one) yielded a range of values for CS4 and CS6 (Figure 17). Bulk densities measured by Sanford et al., (2012) were 1.38, 1.35, and 1.33 g cm^{-3} at 15-30 cm (used here for 25 cm) and 1.42, 1.40, and 1.40 g cm^{-3} at 60-90 cm (used here for 70 cm), for CS2, CS4, and CS6, respectively. In all cases the samples taken for subsequent HYPROP analysis (15 and 45 cm) gave the lowest estimates of all the different measurements across treatments. It is important to note that these measurements were all taken in the same Block 3 of WICST, but in different years, so the exact same plot was not necessarily measured at each sampling time. The HYPROP-related measurements were probably the most carefully sampled, taken by hand with the new HYPROP sample sleeves.

SWCC Model Predictions

Across all treatments and depths the CNEAP model had the highest θ for a given suction (Figures 10-13) compared to measurements and the Nimmo model. This ranged from 5 m^3 m^{-3} greater θ compared to the Nimmo model at very dry suctions, to 20 m^3 m^{-3} greater θ at 10 kPa. The CNEAP model and dry-aggregate Nimmo model had the same θ values at 0 kPa. The wet-aggregate Nimmo model

at 15 cm had a lower θ at saturation than the dry-aggregate Nimmo model in the CS4 and CS6 treatments.

The SWCC models differed from one another in overall shape. The CNEAP model was a sigmoidal curve. The Nimmo model appeared sigmoidal in shape from high suctions to 10 kPa when θ rapidly increased as suctions approached 0, resulting in an additional inflection point (when suction was graphed on a log scale). This secondary inflection point between 0-10 kPa in the 15-cm Nimmo model was more pronounced when the dry-aggregate data was used than when wet-aggregate data was used. The wet aggregate Nimmo model predicted greater θ then the dry-aggregate model until 0-1 kPa, when the dry aggregate model exceeded the wet.

The air entry matric potential, as estimated from the modeled curves, occured between 10-20 kPa in the CNEAP model and 0-0.1 kPa in the Nimmo model.

Sensitivity of SWCC Models to Inputs

CNEAP Tortuosity Parameter α

The tortuosity parameter α in the CNEAP model was varied to test model sensitivity to this empirical parameter (Figure 18). A smaller value of α shifted the curve laterally and a given θ corresponds to a lower suction. Large α values had the opposite effect.

Nimmo Model Bulk density

The range in bulk densities reported for a rotation plot at different sampling times and by different coring retrieval methods raised the question of the sensitivity of the Nimmo model to this parameter. The Nimmo model was tested using three representative bulk densities: low (1.17), medium (1.32) and high (1.48). All other model inputs were held constant (Figure 19).

The bulk density used in the Nimmo model had no influence on the textural component of the model because the porosity was fixed at 0.3. To remain consistent with this specification, the bulk density used in the textural component of the model was back-calculated from the porosity assuming a particle density of 2.65 g-cm^{-3} (BD = (1-Φ)* 2.65 g-cm^{-3}), and was 1.86 g-cm^{-3}. Therefore the textural component of the Nimmo model was the same across the bulk density range tested here (Figure 19).

The structural component of the Nimmo model, however, was sensitive to changes in bulk density when all other model inputs (GMR, GSD) remained constant. Bulk density was inversely proportional to the structural porosity, resulting in less structural pore space and a smaller θ at a given ψ as bulk density increased (Figure 19). This sensitivity was limited to the 0-10 kPa range, where the structural component was most influential, and resulted in 0.04-0.05 m^3 m^{-3} differences in θ at 0 kPa, with differences increasing towards saturation. Therefore this sensitivity analysis suggested that bulk density had an effect on

the SWCC predicted by the Nimmo model, however this effect was likely limited to predictions in the 0-10 kPa range.

Nimmo Model GMR, GSD, and Sieve sizes

Because measurement of aggregate size distribution is not standardized (Dıaz-Zorita et al., 2002), the influence of GMR and GSD on the Nimmo model was assessed. Three hypothetical aggregate size distributions were used to test extreme GMR values and varying GSD values and what they mean for the Nimmo model:

Case 1: ASD was highly skewed towards larger aggregates

Case 2: ASD was equally distributed across all size classes

Case 3: ASD was highly skewed towards smaller aggregates

Case 1 had the largest GMR (10.9 mm), followed by Case 2 (0.7 mm) and Case 3 (0.046 mm), and the GSD was the same in Cases 1 and 3 (0.145) and smaller then Case 2 GSD (0.187). To compare model sensitivity to GMR size with GSD held constant, we looked at the differences in the Nimmo model from Case 1 to Case 3 (Figure 20). With a larger GMR, the SWCC was shifted downwards to smaller θ for a given ψ, and the curve increased more rapidly in the very wet end (0-5 kPa). The model associates larger aggregates with larger interaggragate pores, and in Case 1 where the average aggregate was very large, most of the structural pore space was partitioned to the large pores associated with these large aggregates, while almost none of the pore space was partitioned to the pores between smaller aggregates.

The influence of GSD on the model was tested by varying from large GSD (Case 1: 2.24) to medium (Case 2: 0.187) to small (Case 3:0.009) GSD while GMR remained constant (0.7 mm) (Figure 21). The Nimmo model uses the GSD as an index of the tightness of fit of the aggregates to one another, or narrowness of pores (Nimmo, 1997). When GSD was small (Case 3), aggregates were tightly fit together, creating small, narrow pores between them that hold on to θ more tightly according to capillary theory, leading to larger θ at greater ψ then Cases 1 and 2 (Nimmo, 1997). When GSD was large (Case 1), it implied that the aggregates fit loosely together, creating larger pores that hold water only at low suctions, resulting in smaller θ at a given suction (Figure 21).

The 5-20 cm wet aggregate data (Jokela et al., 2011) provided the opportunity to compare the sensitivity of the Nimmo model to aggregate size distribution methods and sieve size classes. In addition to different overall analysis methods (i.e. wet versus dry), the dry aggregate analysis included an additional 8 mm sieve, while soil was pushed through an 8 mm diameter sieve mesh in the wet aggregate analysis.

It was difficult to tease apart if the discrepancies in the wet and dry Nimmo models were due to overall analysis differences, or if the additional sieve in the dry aggregate analysis played a role. In an attempt to isolate the causes, I explored the sensitivity of the Nimmo model to sieve sizes. An 8-mm diameter sieve size class was added to the wet-aggregate data and a negligible amount of soil (0.0001 g, less then 0.01% of the total sample weight) was attributed to that

size class, effectively saying the 8 mm sieve existed in the analysis but there were no aggregates >8 mm in diameter. Adding the 8 mm sieve to the analysis significantly altered the wet aggregate Nimmo model (Figure 22: referred to as "adjusted wet aggregate data") in each treatment, creating a SWCC that was closer to the dry aggregate Nimmo model. This alteration was likely due to the adjustments in GMR and GSD by adding an additional sieve size (Figure 23). In the adjusted data, GMR was lower then the original wet aggregate data GMR, and GSD was over three times greater. Therefore, the Nimmo model appeared to be sensitive to the number of sieve size classes through the effects the number of sieve classes have on GMR and GSD. This did not demonstrate, however, that the Nimmo model was not sensitive to the type of aggregate analysis that was used.

Comparisons of Measured and Modeled SWCCs

In all cases the CNEAP model predicted the highest water contents across the entire range of suctions, followed by the Nimmo model and the HYPROP/WP4C data (when available), and then the *in situ* data (Figures 10-13). Interestingly, at 15 cm the Nimmo model and HYPROP/WP4C data showed good agreement, particularly when the wet-aggregate Nimmo model was considered. The rapid increase in θ from 0-10 kPa in the Nimmo model was mimicked by the HYPROP/WP4C data. This increase was small in the *in situ* data, and did not occur in the CNEAP model.

In the drier end of the curve (~1500 kPa), the HYPROP/WP4C data and the Nimmo model corresponded closely with each other, more so then the HYPROP/WP4C and the CNEAP model did.

DayCent Simulations of θ and N_20 Emissions

The DayCent model was run with four different field capacities; two determined from *in situ* measurements (23 and 24%) and two determined from laboratory measurements (28 and 32%). Field capacity (FC) was defined as the θ at 33 kPa matric suction. Simulations with varying bulk density (BD) (1.17, 1.26, 1.36 g cm^{-3}), covering the range of field-measured bulk density, were also conducted for a total of twelve simulations for both CS2 and CS4 treatments (Table 2).

The DayCent-simulated 15 cm soil moisture consistently underestimated the observed soil moisture when *in situ* derived FC parameters (23 and 24%) were used, with the exception of DOY 260-262 (Figures 24-25 a, b). This was true across the three BD model runs and for CS2 and CS4. Model runs using the laboratory derived FC parameters (28 and 32%) showed closer approximations to observed θ in general, although from DOY 230 onward, the model run using FC=32% over predicted the θ by 3-5% θ on average (Figure 24-25 c, d).

Different statistics should be used when evaluating model performance (Del Grosso et al., 2011). Gribb et al., (2009) used RMSE values, calculated based on predicted vs. measured moisture contents, to evaluate the effect of various soil

hydraulic property estimates on moisture simulations conducted with the HYDRUS-1D model. Jarecki et al., (2008) used the correlation coefficient *r* when comparing DayCent predicted and observed soil water content, while Parton et al. (2001; 1998) used the coefficient of determination r^2. In this analysis, we examined these statistics as well as the slope of the observed vs. predicted regression line. Slope was examined in an attempt to quantify *how* differences in observed and predicted water content values vary, i.e. over or under prediction by DayCent.

The relationship between predicted and observed soil water content values varied more with FC then with BD (Figures 26-27). The RMSE (Table 3) was lowest in the most extreme case, FC = 32% and BD = 1.36 g cm^{-3}, for both treatments, indicating that these parameters resulted in simulations that minimized the differences in predicted and observed water content. However, the RMSE did not vary much across the model runs (0.038-0.046, Table 3), indicating that overall the DayCent simulations minimized differences between predicted and observed water contents to a similar degree.

The correlation coefficient *r* was greatest for FC = 32% and BD = 1.36 g cm^{-3} in both treatments (0.784 CS2; 0.801 CS4; Table 4), indicating that these parameters resulted in the best correlation between observed and predicted values. The remaining *r* values ranged between 0.582 and 0.780. Overall there was no overwhelmingly strong correlation between predicted and observed values. The same basic results from the correlation coefficient *r* remained true

when evaluated using the coefficient of determination r^2 (range of 0.339-0.642), as r^2 is the correlation coefficient squared (Table 5).

Previous studies found that the DayCent model predicts water filled pore space fairly well (e.g. r^2=0.64 Parton et al., 2001; r^2=0.58-0.86 Parton et al., 1998) over the growing season for a wide range of soil types. However, in a chisel plowed corn field on a silt loam soil, Jarecki et al. (2008) found the correlation between DayCent-simulated and observed soil water content to be weak (r=0.26). Our results showed correlation coefficients and coefficients of determination within these ranges found in the literature (Tables 4-5).

The slope of the linear regression of observed vs. simulated soil water content was significantly different from 1 (α=0.05) and the y-intercept was significantly different from 0 (α=0.05) in all model runs (Tables 6-7). Here, a slope of 1.0 and an intercept of 0 indicated that predicted and observed values closely followed one another across their full range on average, but this did not address scatter about the 1:1 line. A slope=1.0 but with an intercept different from zero suggested a systematic bias in the simulations. All of the CS2 model runs had slopes greater than 2.0, while some in the CS4 model runs were closer to 1.0. In examining the observed vs. simulated scatterplots, it appeared that the slopes were highly distorted by the few days that DayCent predicts very high soil water contents (e.g. Figures 26-27 a, b).

Overall, it appears that here DayCent under predicted the soil water content when FC is derived from *in situ* methods. Model predictions using FC

derived from laboratory methods showed slightly better correlations to observed data, however the comparative statistics (RMSE, *r*, r^2) did strongly favor one simulation over another.

The DayCent-simulated N_2O emissions increased as field capacity and bulk density increased in both treatments (Figure 28). Emissions were 1.5-2.3x greater when field capacity was 32% vs 23% (Figure 28). The increase in emissions with increasing BD was subtle across the lower field capacities and most pronounced when FC was 32% (Figure 28).

DISCUSSION

Measured SWCC

In-situ SWCCs across treatments and depths

Hysteresis explained the differences in SWCC between dry-down periods for the same treatment and depth (Figures 5-9). The range in θ for a given suction across dry-down periods was small (~1-3 m^3 m^{-3}). Hysteresis arises by multiple mechanisms: the ink bottle effect created from heterogeneity in the shape and size of interconnected pores, differences in soil water-soil particle contact angles depending on if wetting or drying is occurring, entrapped air in the soil, and swelling and shrinking of the soil that can alter porosity and pore size distribution (Or and Wraith, 2002). A combination of these mechanisms was likely occurring in the soil. Figure 9 exhibits the hysteretic behavior seen in the measurements by including the wetting periods between dry-down periods. When the curves are followed in chronological order, it appears that θ for a given suction depended on the previous moisture state of the soil.

Laboratory Measurements

One possible explanation for the inconsistency between HYPROP samples within a treatment for ψ<100 kPa is that the HYPROP sample volume may be smaller then the representative elementary volume (REV; Bear, 1988) so one core sample did not represent the heterogeneity of soil structure adequately, leading to discrepancies between samples. It is possible that HYPROP sample

volume captured more of the structural variations at 45 cm in the cropping system treatments (CS2 and CS4), as here the development of structure may have been hampered by 25 years of compaction by machinery. At 45 cm in the pasture rotation (CS6), the HYPROP measurements were more varied like the 15 cm measurements. Perhaps this was because the root system in the pasture was deeper and perennial, aiding in the development of structure, and machinery traffic was less. It is interesting that the bulk density measurements at 45 cm were almost identical for the three systems (1.32-1.34 g cm^{-3}), suggesting that either machinery traffic had little impact on bulk density at this depth, or that the reduced machinery traffic in CS6 did not led to changes in bulk density.

The inconsistency across treatments and depths of the continuity between the HYPROP (0-100 kPa) and WP4C (100-10,000 kPa) measurements could potentially be explained by hysteresis occurring in the WP4C measurements. Sometimes the transition from HYPROP to WP4C measurement techniques was smooth, like in CS2 15 cm (Figure 10a). Other times, like in CS4 15 and 45 cm (Figures 10b and 12b), the jump from HYPROP to WP4C measurements was abrupt. The WP4C measurements were conducted by drying the soil and adding water, so the SWCC constructed from these measurements was a wetting curve. Schelle et al. (2013) observed different curves when WP4C samples were prepared by wetting or drying and attributed this difference to hysteresis. This effect was most prominent in finer textured soils. The authors found better agreement between HYPROP data (which always yields a drying curve) and

WP4C data when WP4C samples were prepared as part of the drying curve (Schelle et al., 2013).

The breaks in continuity of the HYPROP data between 0.1-1 kPa was an indicator of air-entry suction. The HYPROP core was completely saturated, and as water evaporated from the top of the soil core, air replaced the evaporating water in small "bursts," creating bounces in soil suction (Diamantopoulos and Durner, 2012). Schelle et al. (2013) observed this across many soil textures when using the evaporation method.

Comparison of Field and Laboratory SWCC

The greater θ reported by laboratory compared to *in situ* measurements was consistent with what previous studies have found, although none of the previous studies used exactly the methods reported here. Pachepsky et al. (2001) compared laboratory (usually undisturbed pressure plates) and field (neutron probes and tensiometers) θ-ψ datasets for 135 soils varying in texture and found that fine-textured soils with sand contents < 50% had substantially lower field θ than laboratory θ for a given suction over the 0.45-0.60 m^3 m^{-3} θ range. Basile et al. (2003) compared SWCC derived using the evaporation method and neutron probes and tensiometers in the field for multiple horizons at two sites with sandy loam and loamy sand textures. The authors found that the SWCC from laboratory data had higher θ then field data from 0-10 kPa, and the SWCCs progressively converged at greater suctions (Basile et al., 2003). A similar pattern was seen in

our results (Figures 10 and 12), however the θ difference between the laboratory and field measured data in this study was greater than in the earlier reports.

The ratio of saturated θ estimated from the field to saturated θ estimated from the lab ($\theta_0^{II}/\theta_0^{I}$), which has been used in the past to quantify field and lab SWCC differences, ranged from 53-64%; this was lower than what has been observed in previous studies, suggesting the difference between field and laboratory measured saturation was greater in this study then what the literature typically reports (Basile et al., 2003). In the field, soil was wet-up from the soil surface during rainfall events, not allowing for all of the air to escape the soil and leading to air entrapment. In many laboratory methods, soil cores are gradually saturated from the bottom of the cores, allowing for the escape of air over time through the top of the sample. Therefore, the laboratory saturated water content is typically greater then the field saturated water content. Hillel (1980) estimated the $\theta_0^{II}/\theta_0^{I}$ ratio to be approximately 90%, and Basile et al. (2003) found similar values of 78-95%, however these ranges were larger than the 53-64% found in this research, suggesting a greater difference between laboratory and field measurements in this work.

Spatial variability, air entrapment, hysteresis, overburden pressure, and nonequilibrium all help explain why laboratory θ estimates were larger than field estimates for a given ψ, and why this discrepancy was greatest near saturation (Pachepsky et al., 2001). The spatial variability of soils, particularly well-aggregated soils with heterogeneous macropores, may not be captured by the

laboratory samples (Schuh et al., 1988), however when fractal scaling is applied to bulk density some of the differences between field and laboratory methods can be explained (Pachepsky et al., 2001). The question of spatial variability arises in field measurements as well; the volume of soil measured for suction by the porous cup of the tensiometer is small (Field et al., 1984). Air entrapment in the field lowers the available pore space for soil water, lowering θ estimations, and the amount of air trapped in the field depends on pore distribution, pore configuration, the history of wetting and drying, and the water supply rate (Basile et al., 2003). Basile et al. (2003) argued that SWCC derived from field (instantaneous profile method) and laboratory (evaporation method) measurements can be explained as two different hysteretic paths that are part of the same hysteresis loop. Nonequilibrium may occur in laboratory measurements, particularly if evaporation from the surface of the HYPROP sample core was too rapid for complete redistribution of water in the sample, resulting in the tensiometer measurements inside the core to not fully reflect the total water loss measured.

SWCC Model Predictions

The CNEAP model and dry-aggregate Nimmo model predicted identical θ values at 0 kPa because the same total porosities (calculated from bulk density) were used in each model. Although the Nimmo model incorporated soil structure into SWCC prediction, it did not account for air entrapment, and neither did the

CNEAP model, resulting in $\theta = \Phi$ at 0 kPa. The wet-aggregate Nimmo model at 15 cm had a lower θ at saturation in the CS4 and CS6 treatments. This was due to the smaller bulk density values used in the wet-aggregate Nimmo model than the dry aggregate model, resulting in a smaller relative Φ (e.g., Figure 10b, c).

The CNEAP consistently predicted greater θ than the Nimmo model for a given ψ (Figures 10-13) because of the different ways the models partitioned the total pore space (see Figure 29 for model partitioning example). The CNEAP model used the total porosity and distributed it across the range of suctions associated with different particle sizes. The Nimmo textural component was the CNEAP model with a cap of 0.3 on the porosity, so it distributed this porosity across the range of suctions, but since there was less to distribute the resulting θ values were lower.

The sensitivity of the Arya-Paris model to the tortuosity parameter α introduced uncertainty that was heightened at the extreme ends of the curve (Haverkamp et al, 1998 in Haverkamp et al., 2002). While this uncertainty may have been somewhat reduced with the adoption of the CNEAP model, the value of α could significantly shift the SWCC curve (Figure 18). Smaller α values suggested less soil pore tortuosity, reducing the pore length estimated by the model, and therefore the amount of water held a given matric suction. As α was an empirically determined parameter, and the original soils used to determine α were of a coarser texture, it has been suggested that a smaller α value should be

used for finer textured soils (Arya and Paris, 1981). However, adjusting α in the CNEAP model was beyond the scope of this analysis.

The sigmoidal shape of the CNEAP model SWCC illustrated the similarity of shape principle with the cumulative particle size distribution (Nimmo et al., 2007). The Nimmo model had a similar sigmoidal shape from high suctions to 10 kPa, but also showed a rapid increase in θ as suctions approached zero, resulting in a second inflection point in the SWCC. The pore space partitioning in the Nimmo model was responsible for this; when the textural and structural components of the Nimmo model were graphed separately, this became clear (Figure 29). The texture component of the SWCC was calculated using the CNEAP model with a lower porosity specified, and the result was a scaled down version of the full CNEAP model because less pore space was available to distribute to the different suctions and particle sizes. The structural component utilized the remaining soil porosity, also in a sigmoidal form that resembled the shape of the cumulative aggregate size distribution.

When the air entry suctions predicted by the CNEAP model (10-20 kPa) and the Nimmo model (0-0.1 kPa) were compared with the typical range of air entry of silt loam soil (2.1-5.0 kPa), it appeared that the CNEAP model overestimates air entry suction, while the Nimmo model underestimated it (Campbell and Norman, 1998; Radcliffe and Rasmussen, 2002). This spoke to the importance of incorporating the structural influence of the soil in SWCC, however

it also illustrated that the Nimmo model may not necessarily capture the structural component completely.

The 5-20 cm wet aggregate data (Jokela et al., 2011) provided the opportunity to compare the sensitivity of the Nimmo model to aggregate size distribution methods and sieve size classes. The wet aggregate Nimmo model predicted higher θ for most of the structural component of the model, likely because of the lower GMR than the dry aggregate data, as discussed in the sensitivity analysis results. The differences in GMR and GSD between wet and dry aggregate data, leading to differences in the Nimmo model predictions, could be due to many reasons, and we cannot know which reasons contribute most within the limits of this study. Different ASD could be determined based on the fact that dry or wet sieving was used. Further, the samples were taken at different times (2009 and 2015), and soil aggregate turnover can happen on time steps varying from 5-27 days, and over years (Six et al., 2004). Hence, although both wet and dry aggregates were sampled after harvest and before fall tillage, seasonal weather patterns and the six years between samplings may have changed the true ASD of the soil. The ASD measurements are sensitive to factors such as sampling time, sampling technique (for example, the diameter of the sample probe), sample storage, and the number and size of sieves used (Dıaz-Zorita et al., 2002). All of these factors could lead to incorrect representations of the true ASD between the wet and dry aggregate measurement techniques. As shown in the results above, adding an additional sieve size into the wet aggregate data altered

the wet aggregate Nimmo model to match more closely with the dry aggregate Nimmo model (Figure 22). While this does not definitively prove that inherent wet vs. dry analysis differences do not matter to the model, it does illustrate the Nimmo model's sensitivity to sieve classes in this instance.

Comparisons of Measured and Modeled SWCCs

The Nimmo model and the HYPROP/WP4C, when available, visually showed the best agreement of the modeled-measured SWCC comparisons. That the Nimmo model provided a closer approximation of the HYPROP/WP4C data than the CNEAP model suggested the importance of incorporating a structural component into SWCC models. The Nimmo model captured the rapid decrease in θ that the HYPROP measured from 0-20 kPa. The Nimmo model did not account for air-entrapment, and the gradual bottom-up wetting of the HYPROP sample cores was intended to minimize air trapped in the samples. The minimal amount of trapped air in the HYPROP samples may therefore explain in part why the Nimmo model, which doesn't account for trapped air, captured the rapid decrease in θ that the HYPROP measured from 0-20 kPa. The Nimmo model's over-prediction of *in situ* SWCC can also in part be explained by trapped air in the field soil that was not accounted for in the model.

The HYPROP/WP4C data laid closer to the Nimmo model than the CNEAP model in the dry end of the SWCC near 1500 kPa (e.g., Figures 10 and 12). This ψ corresponded to the textural component of the Nimmo model, confirming that

the designated textural porosity of 0.3 was appropriate to capture the influences of texture on the SWCC. The CNEAP model predicted greater θ at these high suctions, perhaps suggesting that the CNEAP model assigned too much pore space to the very fine particle range.

In most cases the HYPROP laid more closely with the wet aggregate Nimmo model then the dry aggregate Nimmo model (e.g., Figures 10b, c). The increase in θ from 5 to 0 kPa in the dry aggregate Nimmo model was much more rapid than that measured by the HYPROP data. This was likely an effect of the GMR and GSD. While the wet aggregate Nimmo model resulted in a closer prediction of the laboratory SWCC then the dry aggregate Nimmo model, it was not definitive that wet aggregate data is a more appropriate input to the Nimmo model because, as illustrated above, effects such as the number or size of sieves used can alter this relationship.

DayCent Simulations of θ and N_20 Emissions

In general, DayCent simulations of soil water content with *in situ* derived FC parameters under-predicted the soil water content. The laboratory derived FC parameter simulations resulted in slightly better agreement between predicted and observed soil water contents according to RMSE, *r*, and r^2. The slopes of the observed vs. predicted soil water content relationship are likely distorted by the few days with very high predicted water contents (i.e. DOY 261-262, Figures 24-25). In the *in situ* derived FC simulations, the relationship between observed and

predicted water content appeared to be 1:1 (excluding DOY 261-262), but the relationship is offset to below the 1:1 line (Figures 26-27 a, b). With the laboratory derived FC simulations, however, this relationship crossed the 1:1 line, under predicting at low water contents and over predicting at higher water contents (Figures 27-28 c, d).

The *in situ* and laboratory determined FCs used in this analysis were determined assuming a traditional definition of field capacity, the soil water content at 10 kPa in a sandy soil and 33 kPa in loamy or clayey soils. More recently however, the 10-33 kPa range is being replaced by 5-10 kPa by some soil physicists according to the National Soil Survey Handbook published by the Natural Resources Conservation Service (USDA-NRCS, 2016). If this more modern definition of field capacity is adopted (estimated as the θ at 10 kPa) here, the tested *in situ* FC would be 25 and 27%, and the laboratory FC would be 33 and 35% at 15 cm (Figures 5 and 10a, b). Running this analysis with larger FC values would likely increase the correlation between observed and simulated soil water content. However, this also points to the uncertainty surrounding the definition of FC, and highlights the dependency of simulation models like DayCent on a parameter that is so vague. For decades the definition of FC has been debated; FC can be the water content at a certain matric suction (i.e. what is used in this analysis), after a certain amount of time following saturation, or after a drainage or hydraulic conductivity flux has significantly declined (Assouline and Or, 2014).

The substantial DayCent over-predictions of soil water content on DOY 261-262 (i.e. Figures 24-25) gave insight into potential flow process shortcomings of the DayCent model. These over-predictions corresponded to a two-day rain event of 80 mm (Figure 4). The measured soil water content increased at all depths in response to this rain event, even at 70 cm, and the response was within the same day (Figure 4). This suggested water was flowing through macropores in the soil because the deeper depths increased in water content so quickly.

In the DayCent models water movement through the soil was unidirectional downward, with one soil layer filling to field capacity before water moves into the next soil layer (Parton et al., 1998). This modeling strategy did not account for macropore flow. This likely reduced the accuracy of DayCent predictions of soil water content during large precipitation events, which may have a compounding effect on predicted vs. observed N_2O emissions that depend on the denitrification process that occurs in high moisture soil conditions. Therefore, incorporating macropore flow or a soil structure parameter into the DayCent model may improve its predictions. Recognition of macropore flow in DayCent might have reduced or eliminated the very high simulated values, lowering the slopes of the comparisons between simulated and measured (Table 6).

The fine-scale comparisons of simulated and measured water content made here are also complicated by the details of how the model extracts water

from each layer. The water potential and root biomass in each layer influence how much water is extracted from that layer on a day (Parton et al., 1998). Thus the simulated water content in a layer on a day is a function of previous root growth in it and every other active layer, and the logic by which actual ET is determined and partitioned among layers.

Mean N_2O emissions measured in WICST in 2010 and 2011 ranged from 2.04-3.71 kg N_2O-N ha^{-1} in CS2 and 2.20-2.51 kg N_2O-N ha^{-1} in CS4 (Osterholz et al., 2014). In this 2015 analysis, the majority of the emissions predicted with DayCent simulations for the CS2 treatment were between 2-4.5 kg N_2O-N ha^{-1} (Figure 28), which were within two standard deviations of the largest previously measured emission (i.e. 3.71 ± 0.58*2 kg N_2O-N ha^{-1}, Osterholz et al., 2014). The CS2 FC=32% BD=1.36 g cm^{-3} simulation predicted emissions outside of this range, as did all of the CS4 simulations with FC>23%. Many factors could have contributed to the differences between the Osterholz et al. (2014) 2010 and 2011 measured cumulative emissions and 2015 simulated emissions, including weather patterns, seasonal management, timing of measurements, and growing season length over which emissions were totaled. However it is reassuring that the predicted emissions by the DayCent model in 2015 were of the same magnitude as emissions measured in the same system phases previously. Comparable results were found for DayCent simulated and measured N_2O emissions from a chisel plowed corn field on a loam soil in central Iowa (Jarecki et al., 2008). There, simulated cumulative emissions were 3.29 kg N_2O-N ha^{-1},

lower then the measured cumulative emissions but not significantly so (Jarecki et al., 2008). The authors did not specify how the soil hydraulic parameters (field capacity, wilting point) used in their DayCent simulations were determined.

While the cumulative emissions simulated by DayCent in this study were within the expected order of magnitude of cumulative emissions found in other simulations and field measurements in similar scenarios, it appeared that FC and BD specifications in the model can significantly alter the emission predictions, to as much as doubling them. Further, the emissions predicted with the laboratory-determined FC, which resulted in the best agreement between simulated and observed soil water content, were the greatest, approaching 5 (CS2) and 9 (CS4) kg N_2O-N ha^{-1} (Figures 27-28). While these large emission simulations could be due to other model inaccuracies, the fact that adjusting the FC parameter by the variation found in field vs. laboratory measurements can more than double simulated cumulative N_2O emissions is striking.

At a sub continental scale (i.e. the size of the United States), uncertainties in the DayCent estimates of N_2O emissions from agricultural soils range from -35 to 50% of the emission (Del Grosso et al., 2010). This uncertainty increases at smaller scales, and, at the national scale, uncertainty in model structure (i.e. model processes) accounted for 83% of the total uncertainty (Del Grosso et al., 2010). The range in emissions simulated in this study with varying FC parameter is on par and greater than the uncertainty reported in the literature, suggesting that FC can have a large effect on model outcomes. Recent work investigating the

sensitivity of DayCent model parameters identified DayCent output that is affected by soil water content, but did not test the sensitivity of the hydraulic parameters such as field capacity and wilting point (Necpálová et al., 2015).

CONCLUSION

Few differences were observed among *in situ* SWCCs across the CS2, CS4, and CS6 treatments. Differences in dry down period behavior within a treatment can likely be attributed to hysteresis. Laboratory estimates of the SWCC had greater θ at a given suction then *in situ* estimates at 15 and 45 cm. These differences increase as suctions approach saturation and are larger then what has been observed in previous studies, likely because the pore space in the soil field profile was never fully saturated. This presents an interesting conundrum, as the lower water contents measured in the field and entrapped air represent true conditions, yet the fact that some field soils may never reach full saturation under natural conditions due to air entrapment is not considered in hydraulic property estimates that are used to in soil water simulations.

The CNEAP model, which does not account for soil structure outside of bulk density, predicted greater θ at a given suction then the Nimmo model, which accounts for soil structure. The closer agreement between the laboratory measured SWCC and the Nimmo model over the CNEAP model suggest that incorporating soil structure into SWCC predictions is important. While the Nimmo model was a closer approximation then CNEAP to laboratory data, the *in situ* data was not accurately approximated by either property-transfer model.

This is likely due to hysteresis and air entrapment, and it again raises the issue that models and laboratory estimates of the SWCC may not be capturing the true moisture conditions in the field that affect biological processes.

Using field capacity estimates derived from *in situ* SWCC led to underestimations of soil water content by the DayCent model. Laboratory derived field capacity estimates resulted in slightly better soil water content predictions by DayCent according to commonly used statistical tools, however the differences were not striking. The results are further convoluted by the definition of field capacity, the details of how DayCent extracts water from each soil layer, and DayCent's neglect of macropore flow. This highlights the weakness of using an ill-defined parameter in soil moisture simulations, particularly when soil water content influences other modeled processes. Setting aside this definitional argument, differences in laboratory and *in situ* field capacity estimates were likely due to entrapped air in the field soil, a phenomenon not captured by laboratory measurements and DayCent simulations, potentially contributing to the larger predicted N_2O emissions from increases in simulated denitrification. The range of predicted N_2O emissions when field capacity and bulk density parameters were varied was on par with the uncertainty found in the DayCent-predicted N_2O emissions at larger scales.

Many assumptions are made in systems modeling, and no model can perfectly simulate environmental processes with 100% accuracy. Compromises will always need to be made. However, this investigation suggests that there is

more work to be done in representing true, *in situ* soil water and soil matric suction relationships, in estimating the hydraulic parameters we glean from these relationships, and in how we model processes dependent on complex soil water flow dynamics.

Table 1: Management details of the treatments examined. CS2, corn/soy; CS4, corn/3 years alfalfa; CS6, rotationally grazed pasture

	CS2 Corn 2015	CS4 Corn 2015	CS6 Pasture 2015
Primary tillage	Strip-tilled 11/12/14	Disk chisel 8" (Agco 7400) 11/12/14	
Secondary tillage		Field cultivated 6" (Case IH 200) 4/30/15	
Planting date	4/30/15	4/30/15	4/22/13
Variety	Pioneer PO157 AMX	Pioneer PO157 AMX	Freedom Red Clover, Kopu II White clover
Rate	34,000 seeds/ac	34,000 seeds/ac	11 lbs/ac
Starter fertilizer	5-14-42 (100 lbs/ac) 4/30/15	5-14-42 (100 lbs/ac) 4/30/15	
Nitrogen fertilizer	28% UAN sidedress, (135 lbs N/ac) 6/16/15,		50 lbs N/ac 6/5/15
Manure	12,000 GPA liquid manure (Blaine Dairy) 11/20/2013	12,000 GPA manure (Blaine Dairy) 11/12/2014	
Pre-emergence Pesticide/ Herbicide	RoundUp (44 oz/ac) Dual II Magnum (32 oz/ac) 2,4D (16 oz/ac) 4/30/2015		
Post-emergence Pesticide/ Herbicide	Round Up Power Max (32 oz/ac) 6/1/2015	Round Up Power Max (32 oz/ac) 6/1/2015	
Harvest date	10/22/15	10/22/15	Whole pasture cut for dry hay on 6/1/15 Exclosure harvested 7/17, 8/24, 10/1
Yield	215 bu/ac	249 bu/ac	in T/ac: 1.36, 0.89, 0.56; 2nd, 3rd, 4th harvests

Table 2: Bulk density and field capacity specifications in the DayCent simulations. The DayCent model was run with each of the field capacity pairs (15 + 45 cm) specified for each of the bulk densities listed for 15 cm.

Layers (cm)	Bulk Density ($g\ cm^{-3}$)	Field Capacity			
0-2, 2-5, 5-10, 10-20, 20-30 (i.e. 15 cm)	1.17 1.26 1.36	0.23	0.24	0.28	0.32
30-45, 45-60, 60-75, 75-90, 90-105, 105-120, 120-150, 150-180, 180-120 (i.e. 45 cm)	1.33	0.23	0.26	0.32	0.34

Table 3: RMSE of DayCent simulated vs. observed soil water content.

Bulk Density, $g\ cm^{-3}$		1.17	1.26	1.36
			RMSE	
System	Field Capacity, %θ			
CS2	23	0.046	0.044	0.041
	24	0.045	0.042	0.039
	28	0.043	0.042	0.040
	32	0.043	0.041	0.039
CS4	23	0.046	0.043	0.040
	24	0.045	0.043	0.041
	28	0.042	0.041	0.040
	32	0.042	0.040	0.038

Table 4: r of DayCent simulated vs .observed soil water content

Bulk Density, g cm-3		1.17	1.26	1.36
			r	
System	Field Capacity, %			
CS2	23	0.695	0.713	0.734
	24	0.646	0.667	0.690
	28	0.694	0.706	0.725
	32	0.745	0.765	0.784
CS4	23	0.680	0.700	0.721
	24	0.582	0.605	0.625
	28	0.700	0.713	0.730
	32	0.761	0.780	0.801

Table 5: R^2 of DayCent simulated vs. observed soil water content

	Bulk Density, g cm-3	1.17	1.26	1.36
			r^2	
System	Field Capacity, %			
CS2	23	0.483	0.509	0.538
	24	0.417	0.444	0.476
	28	0.482	0.499	0.526
	32	0.556	0.585	0.614
CS4	23	0.463	0.490	0.520
	24	0.339	0.367	0.390
	28	0.490	0.508	0.533
	32	0.578	0.608	0.642

Table 6: Slope of DayCent simulated vs. observed soil water content.

	Bulk Density, g cm^{-3}	1.17	1.26	1.36
			Slope	
System	Field Capacity, %			
CS2	23	2.48	2.45	2.43
	24	2.10	2.08	2.08
	28	2.29	2.30	2.32
	32	2.68	2.70	2.70
CS4	23	1.96	1.94	1.93
	24	1.50	1.50	1.51
	28	1.92	1.94	1.96
	32	2.29	2.30	2.32

Table 7: Y-Intercept of DayCent simulated vs. observed soil water content.

	Bulk Density, g cm-3	1.17	1.26	1.36
			Y-Intercept	
System	Field Capacity, %			
CS2	23	-0.430	-0.424	-0.418
	24	-0.316	-0.311	-0.310
	28	-0.321	-0.322	-0.327
	32	-0.383	-0.387	-0.388
CS4	23	-0.294	-0.290	-0.286
	24	-0.160	-0.160	-0.161
	28	-0.225	-0.227	-0.231
	32	-0.279	-0.282	-0.286

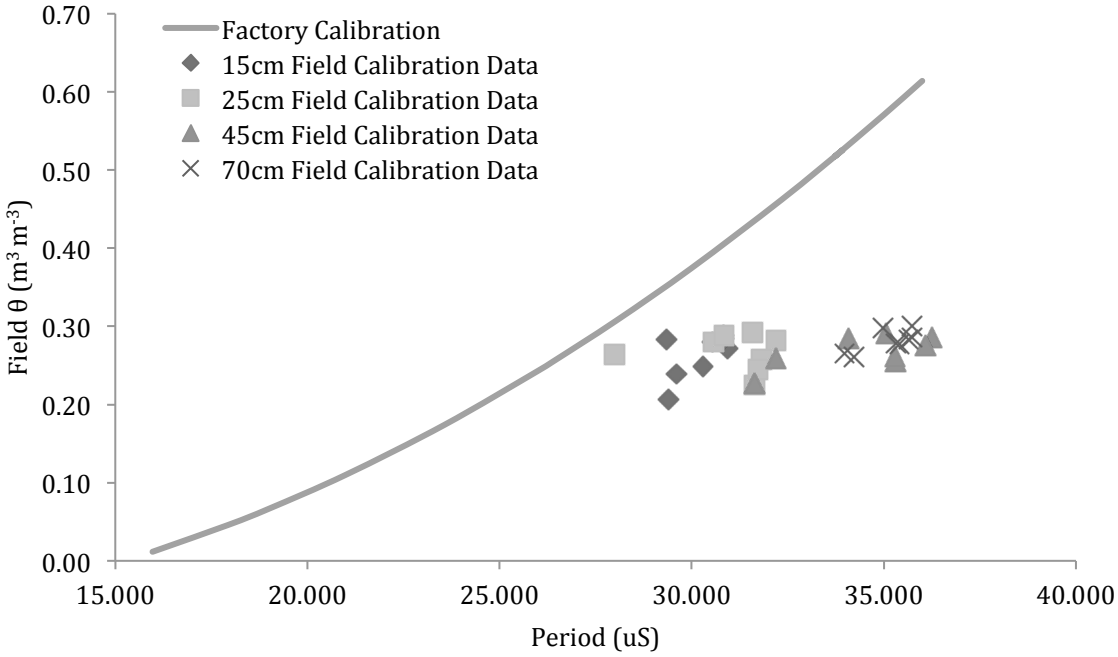

Figure 1: Field-collected θ measurements at each depth and the factory-supplied default calibration from Campbell Scientific.

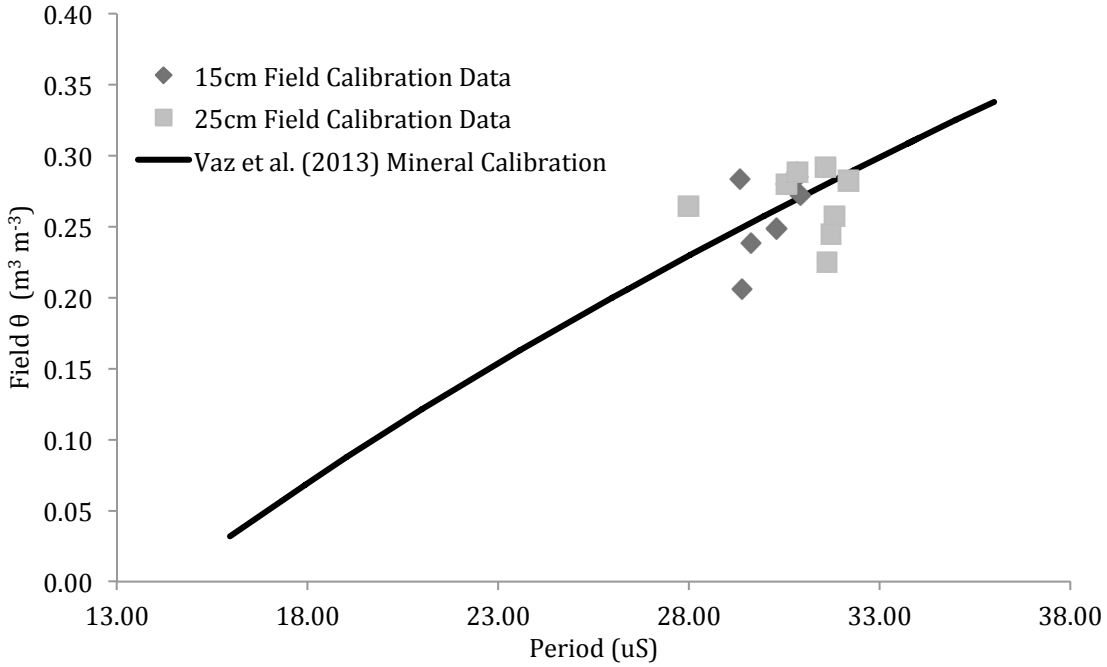

Figure 2: Field-collected θ measurements and the Vaz et al. (2013) calibration. This is the calibration applied to the 15 and 25 cm probes in this experiment.

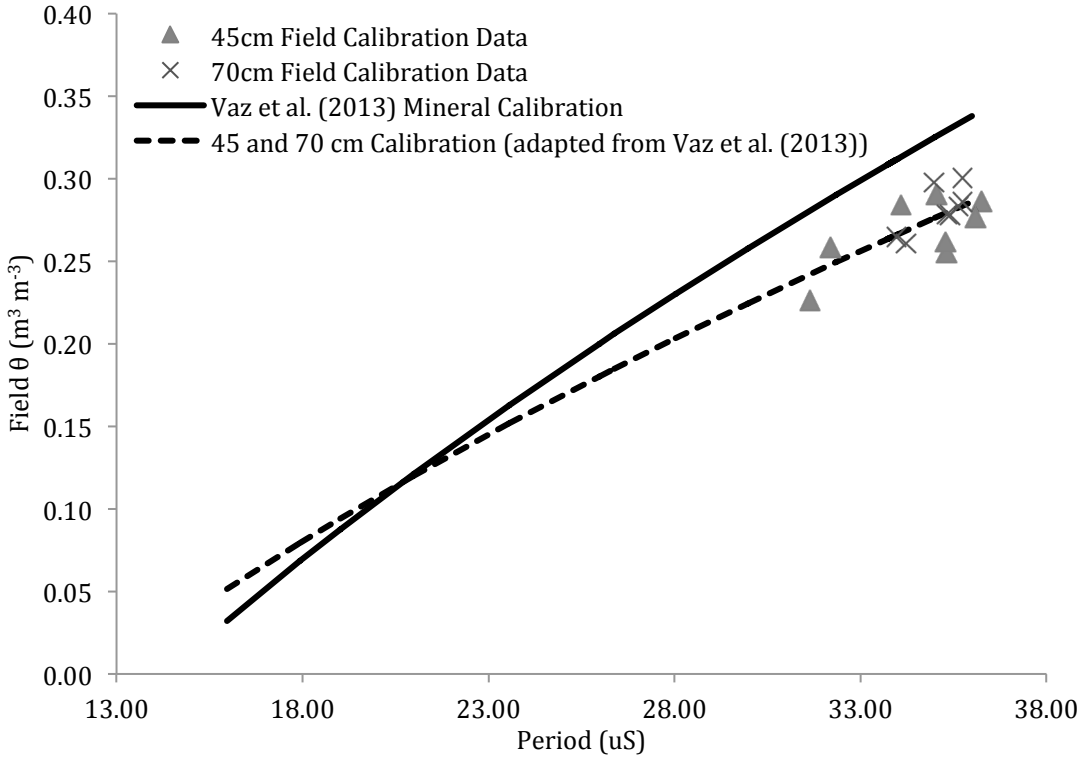

Figure 3: Field-collected θ measurements, the Vaz et al. (2013) calibration, and the adapted Vaz et al. (2013) calibration. The adapted calibration is applied to the 45 and 70 cm probes in this experiment.

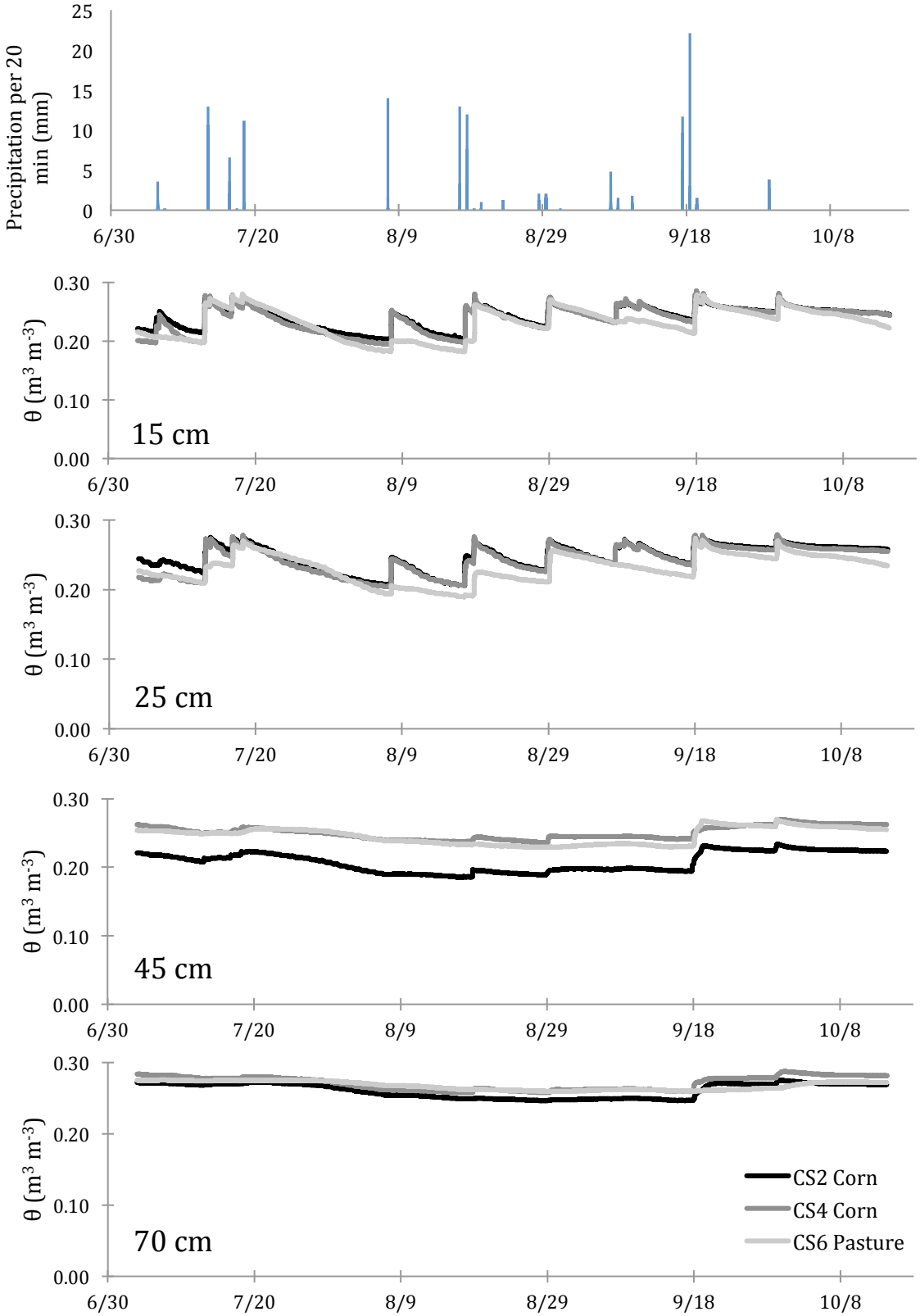

Figure 4: Soil water content θ at the four depths measured and rainfall over the growing season.

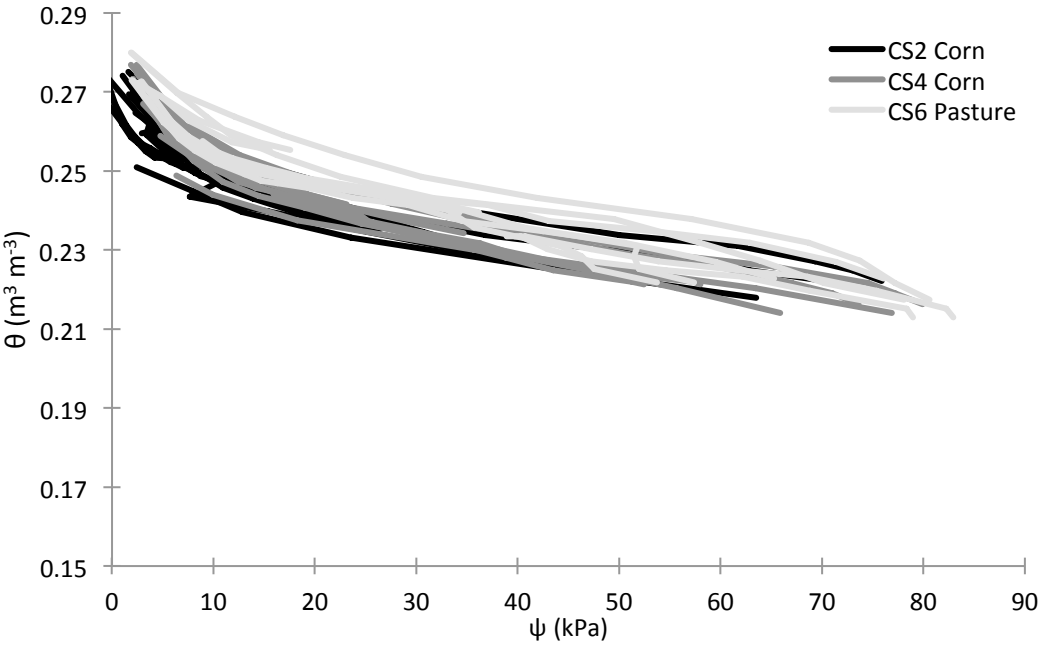

Figure 5: Soil water characteristic curves derived from *in situ* data at 15 cm in the three treatments.

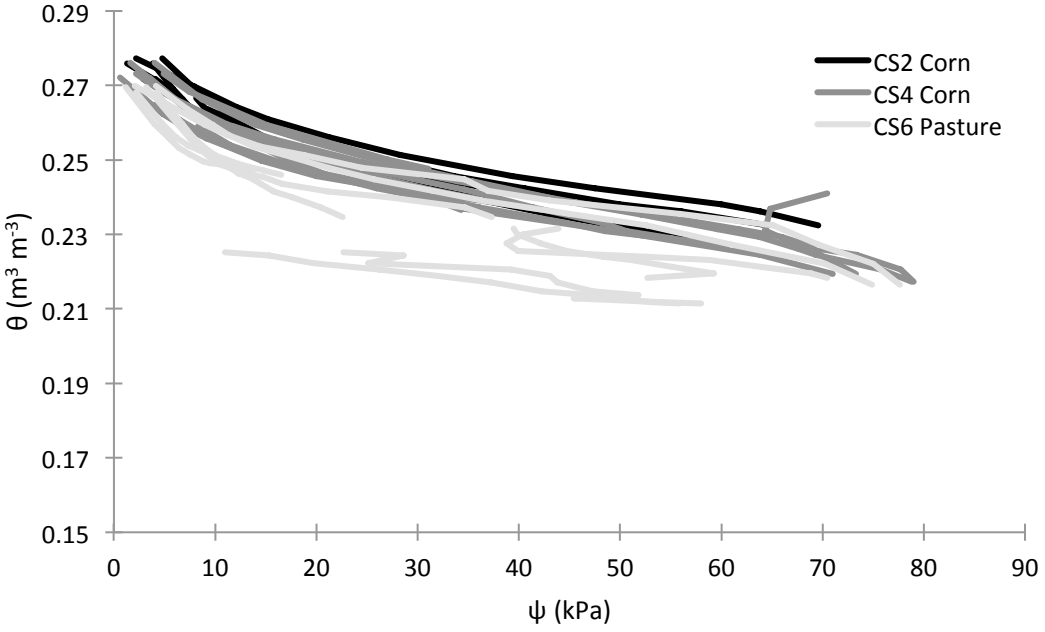

Figure 6: Soil water characteristic curves derived from *in situ* data at 25 cm in the three treatments.

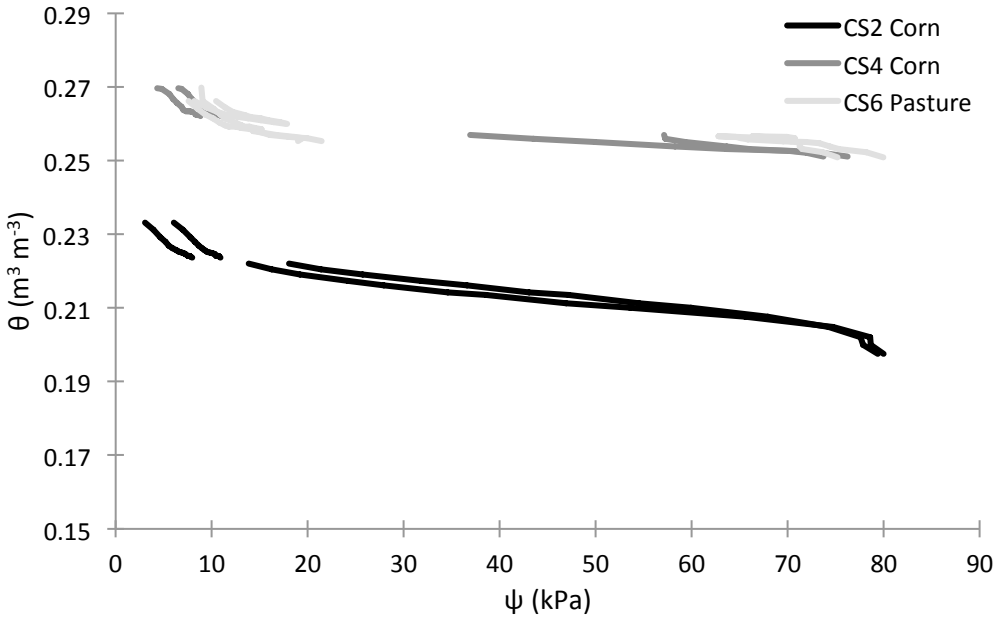

Figure 7: Soil water characteristic curves derived from *in situ* data at 45 cm in the three treatments.

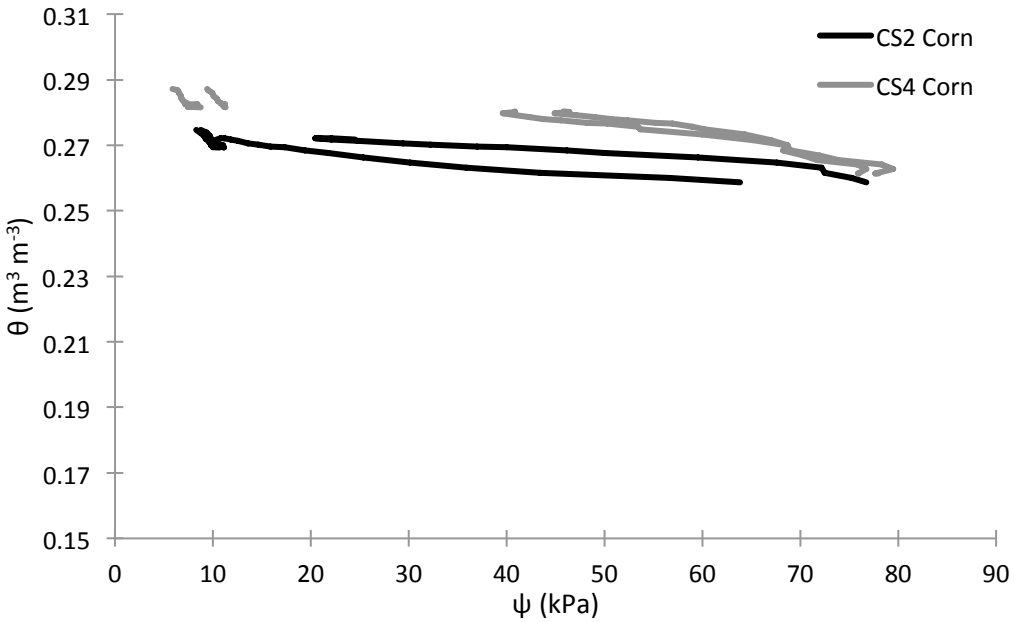

Figure 8: Soil water characteristic curves derived from *in situ* data at 70 cm in the three treatments.

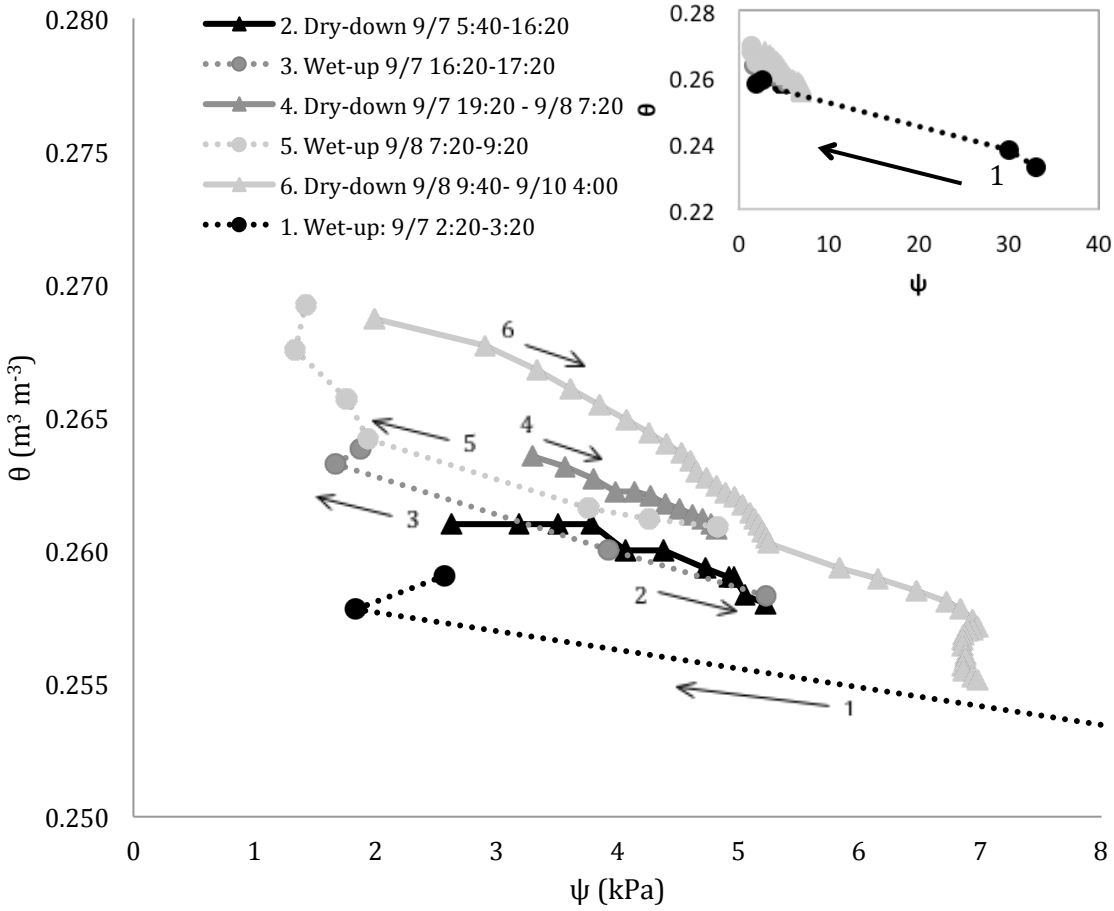

Figure 9: Example of the hysteretic behavior seen in the measurements, taken from CS2-15 cm Sept. 7-10. Drying and wetting events are numbered in the sequential order they occurred. Hourly averages are used for drying periods, 20-minute averages for wetting periods. Top graph includes the first wetting event; bottom graph zooms in on the remaining events. Triangles and solid lines indicate drying, circles and dashed lines indicate wetting. Events are shaded in the order they occurred- dark (first) to light (last).

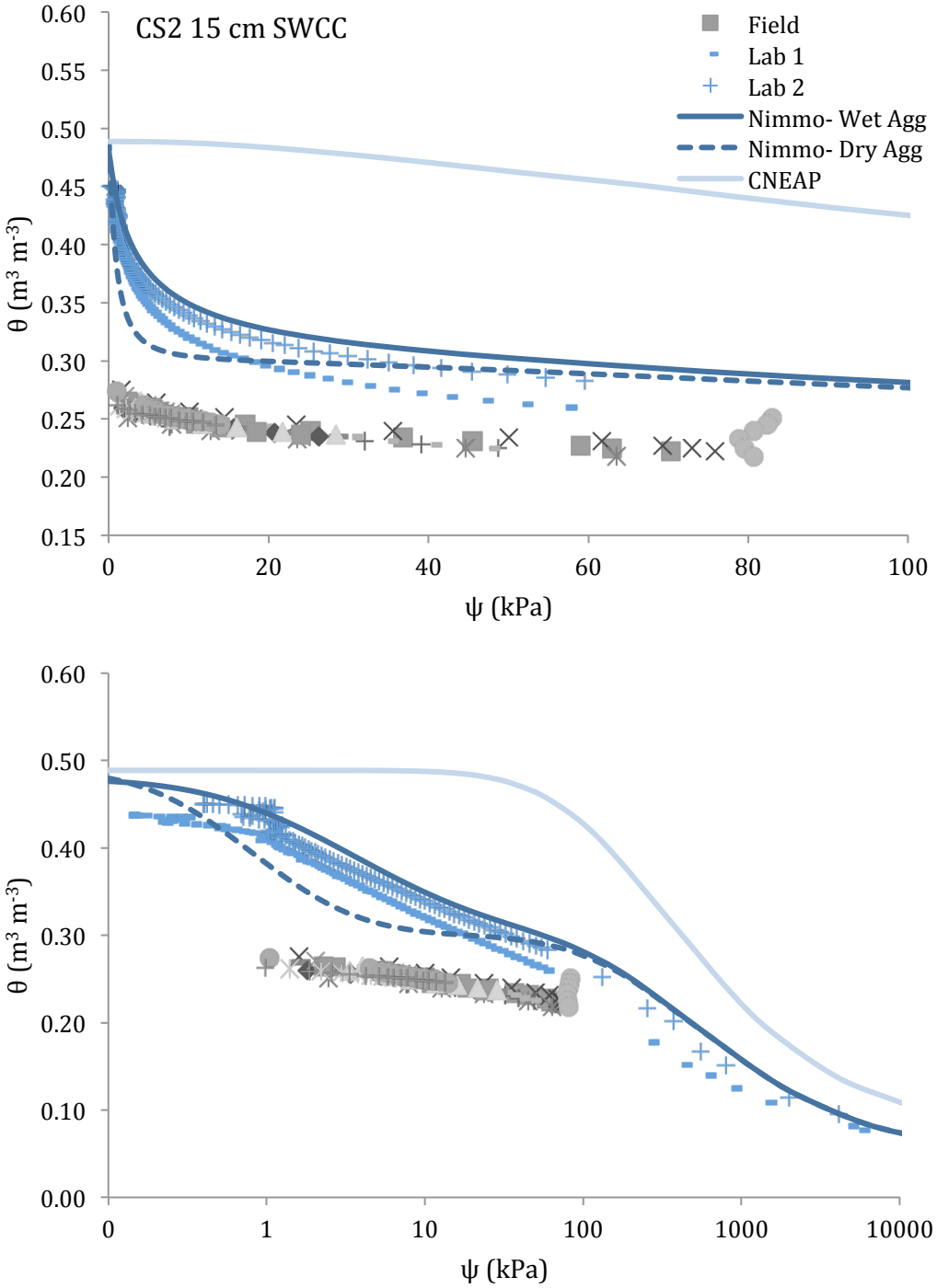

Figure 10a: Measured and modeled SWCC for the CS2 treatment at 15 cm depth. The top panel covers a smaller range of matric suctions, and the bottom panel is the entire suction range (log scale). Measured data is shown as points and property-transfer models are shown as lines.

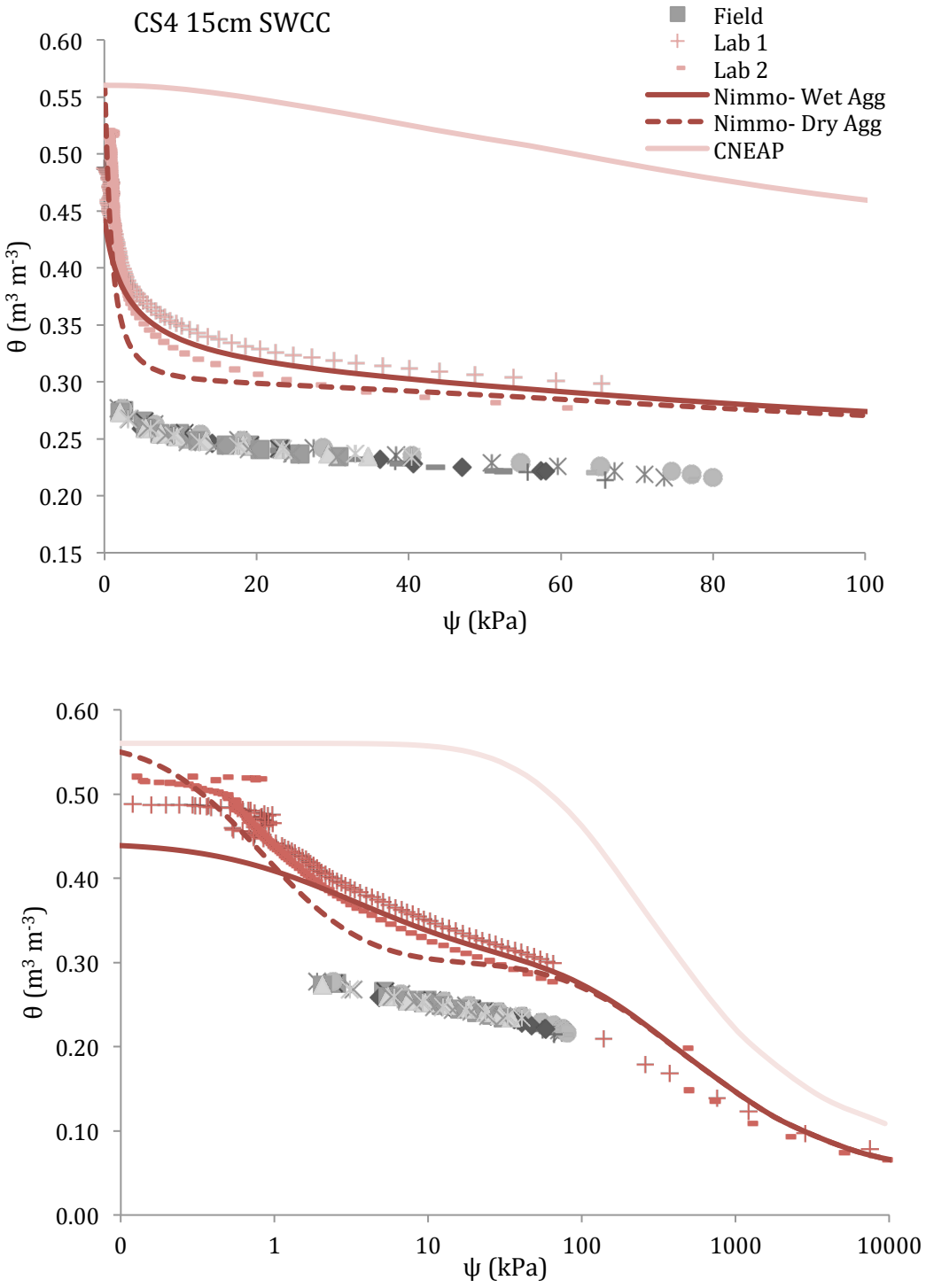

Figure 10b: Measured and modeled SWCC for the CS4 treatment at 15 cm depth. The top panel covers a smaller range of matric suctions, and the bottom panel is the entire suction range (log scale). Measured data is shown as points and property-transfer models are shown as lines.

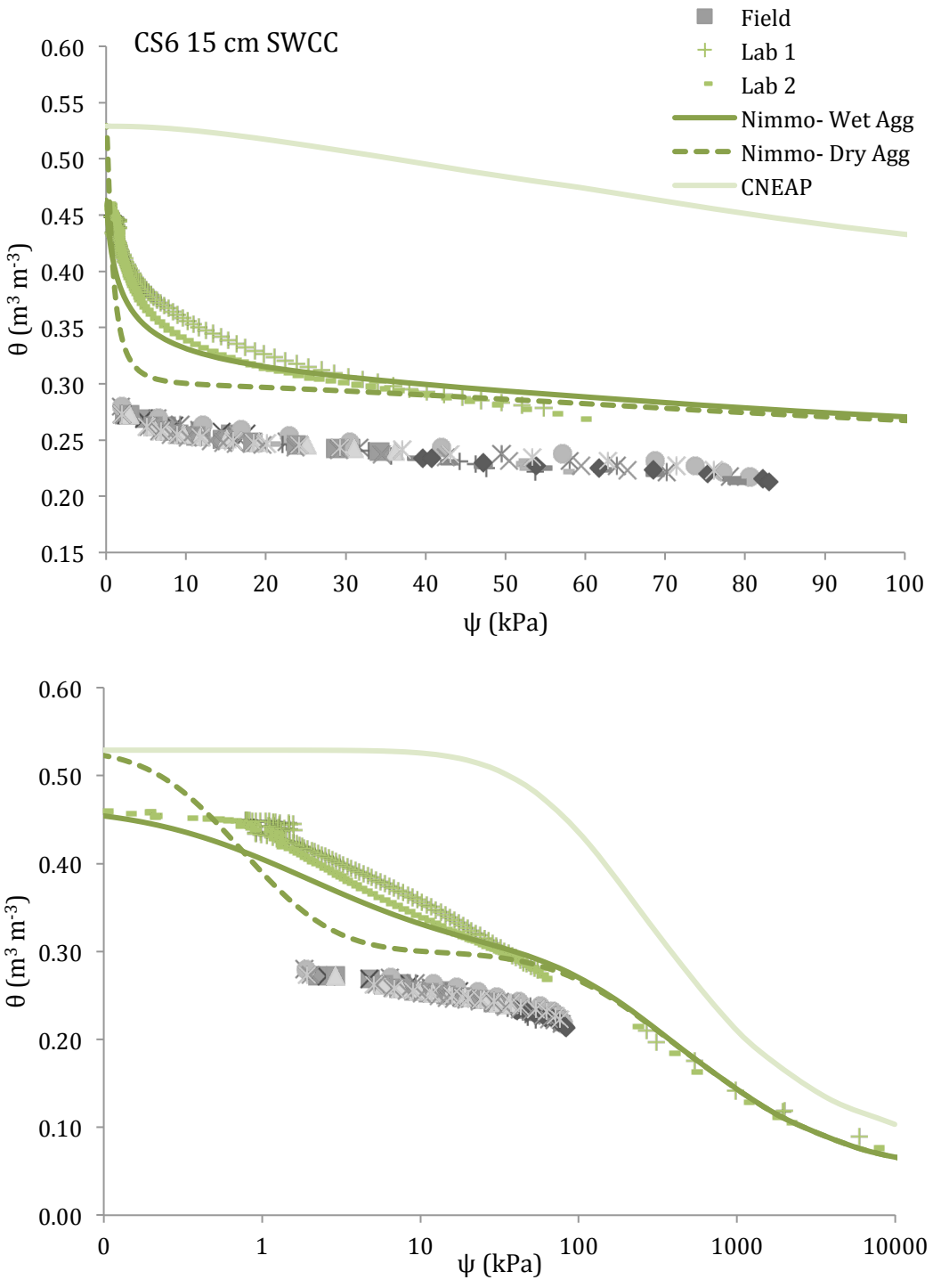

Figure 10c: Measured and modeled SWCC for the CS6 treatment at 15 cm depth. The top panel covers a smaller range of matric suctions, and the bottom panel is the entire suction range (log scale). Measured data is shown as points and property-transfer models are shown as lines.

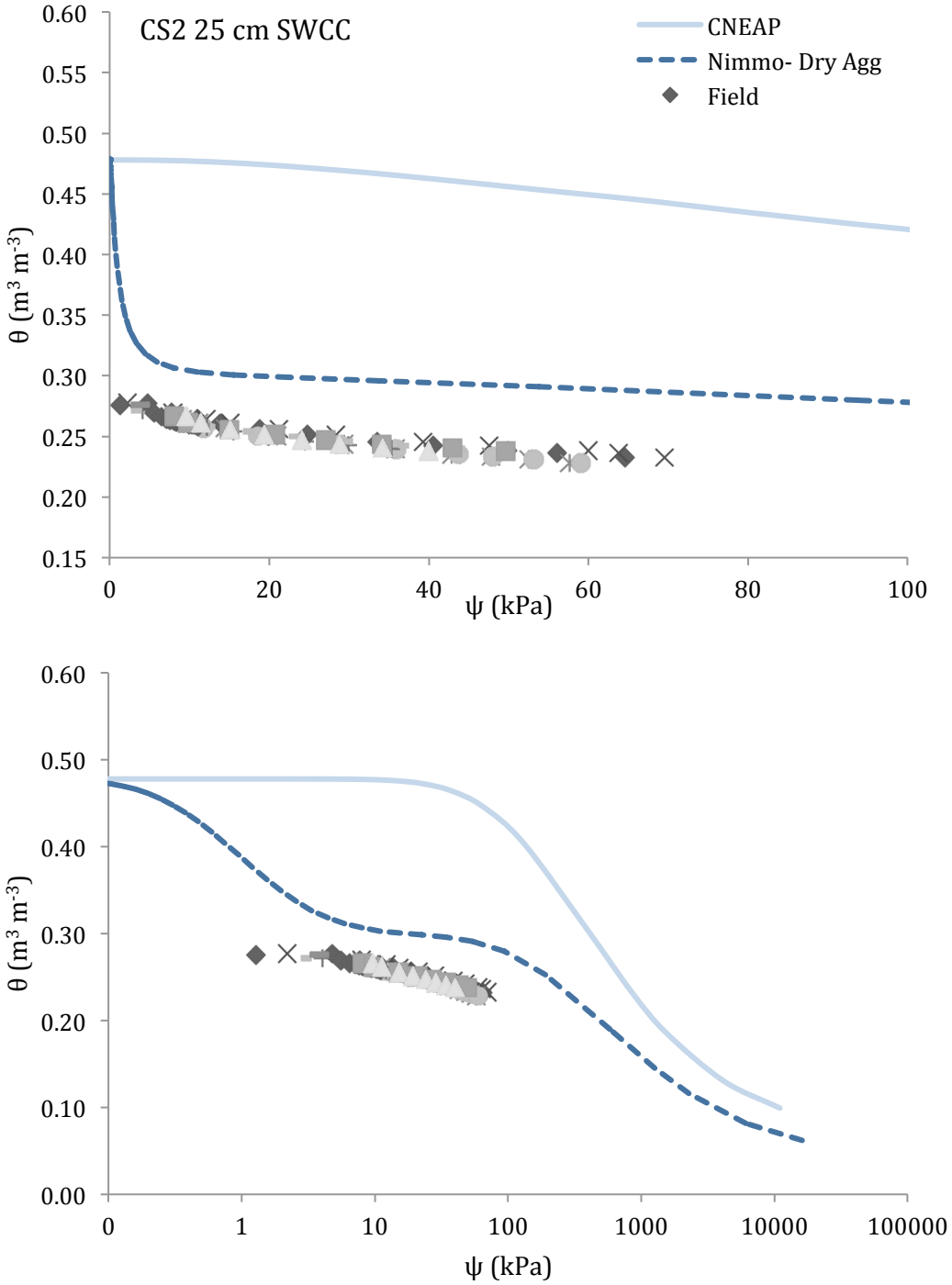

Figure 11a: Measured and modeled SWCC for the CS2 treatment at 25 cm depth. The top panel covers a smaller range of matric suctions, and the bottom panel is the entire suction range (log scale). Measured data is shown as points and property-transfer models are shown as lines.

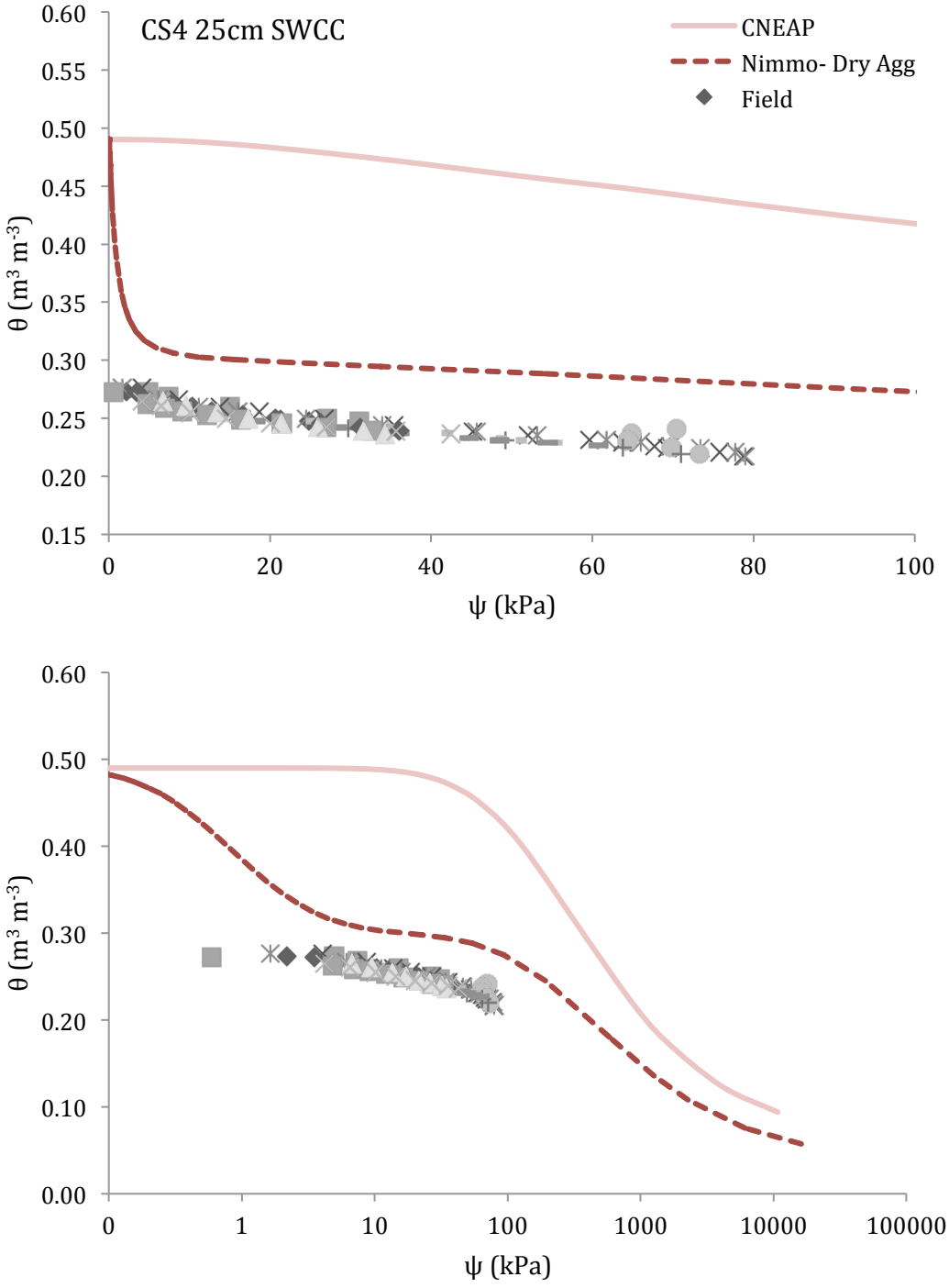

Figure 11b: Measured and modeled SWCC for the CS4 treatment at 25 cm depth. The top panel covers a smaller range of matric suctions, and the bottom panel is the entire suction range (log scale). Measured data is shown as points and property-transfer models are shown as lines.

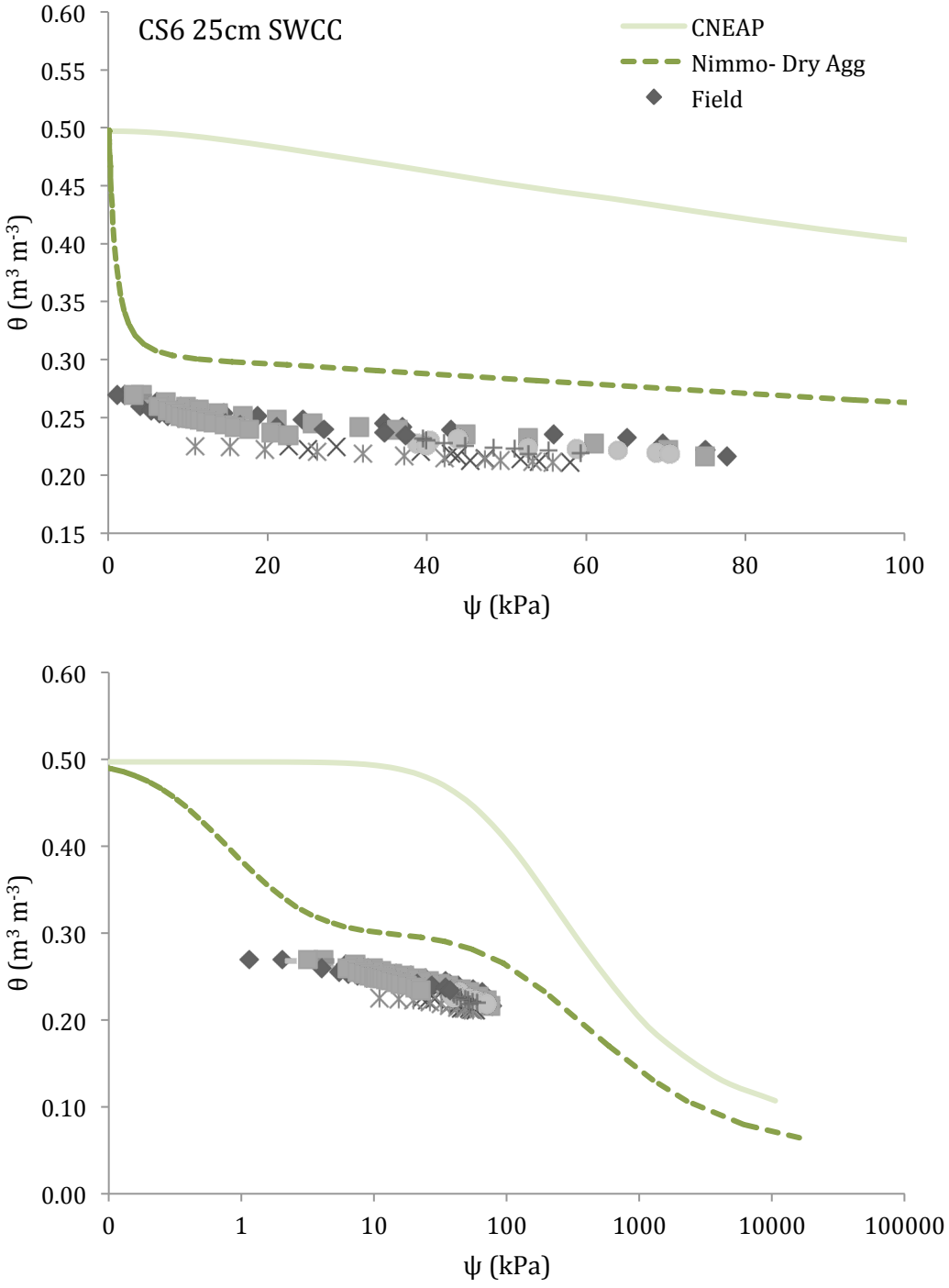

Figure 11c: Measured and modeled SWCC for the CS6 treatment at 25 cm depth. The top panel covers a smaller range of matric suctions, and the bottom panel is the entire suction range (log scale). Measured data is shown as points and property-transfer models are shown as lines.

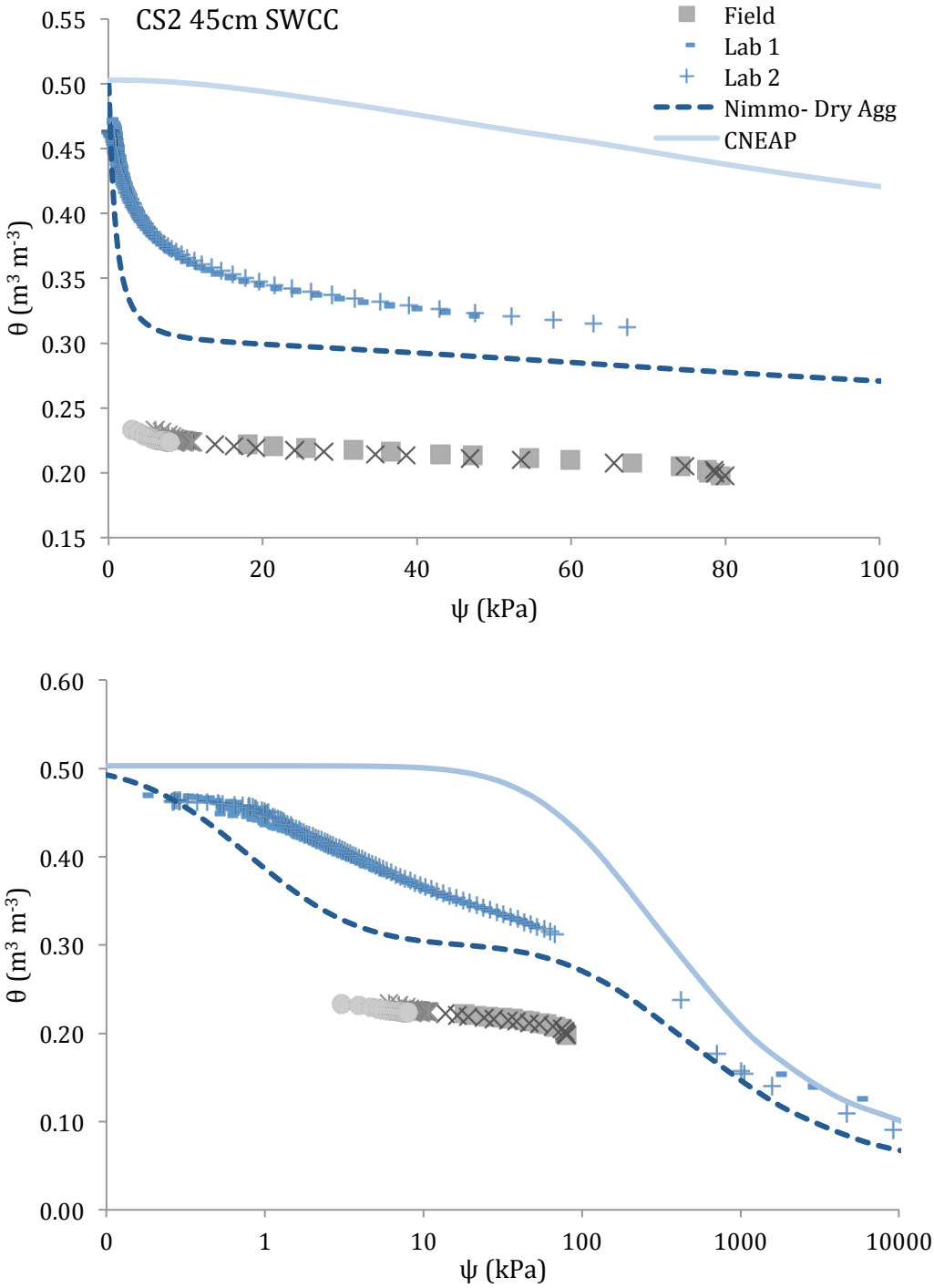

Figure 12a: Measured and modeled SWCC for the CS2 treatment at 45 cm depth. The top panel covers a smaller range of matric suctions, and the bottom panel is the entire suction range (log scale). Measured data is shown as points and property-transfer models are shown as lines

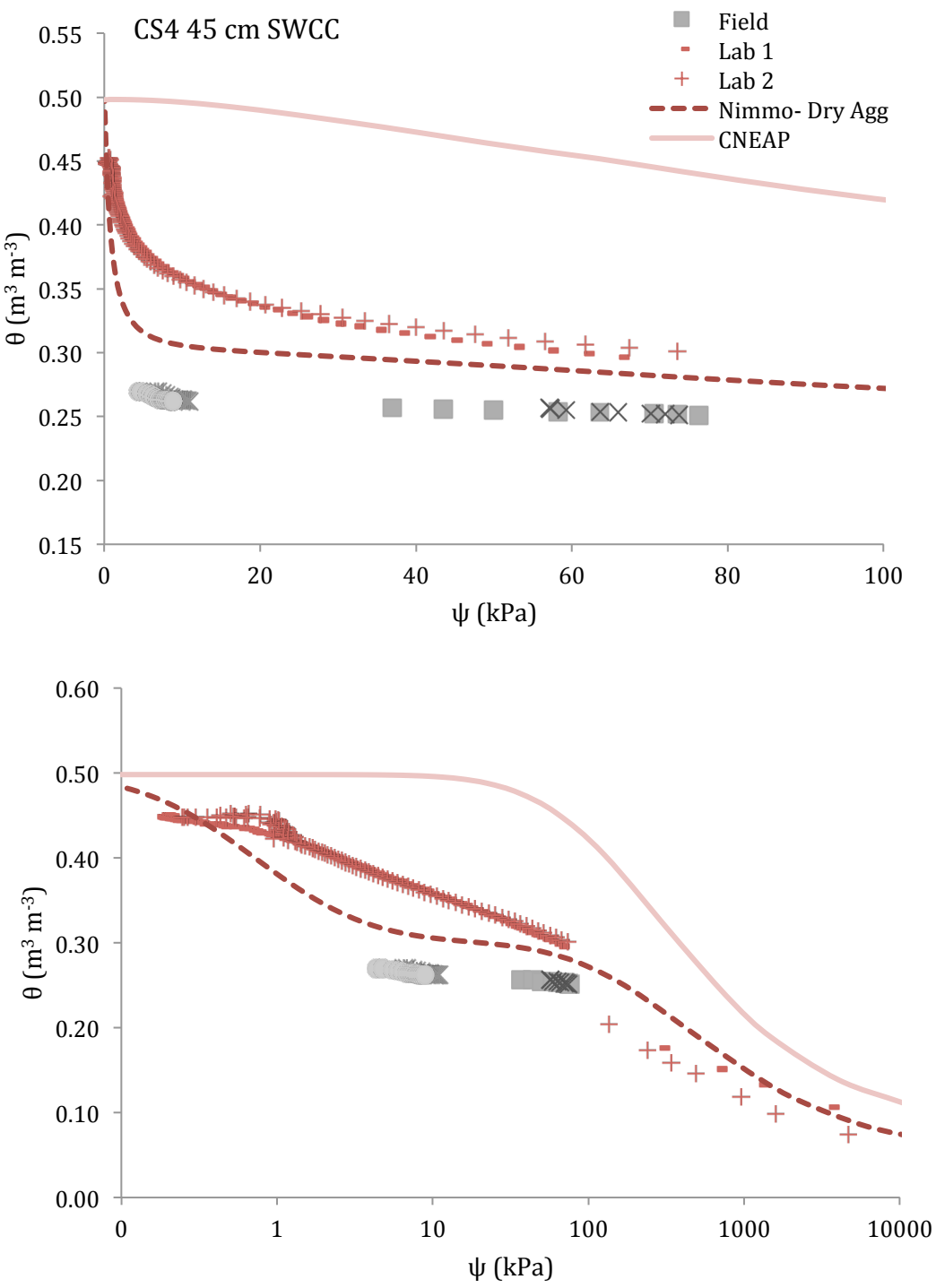

Figure 12b: Measured and modeled SWCC for the CS4 treatment at 45 cm depth. The top panel covers a smaller range of matric suctions, and the bottom panel is the entire suction range (log scale). Measured data is shown as points and property-transfer models are shown as lines.

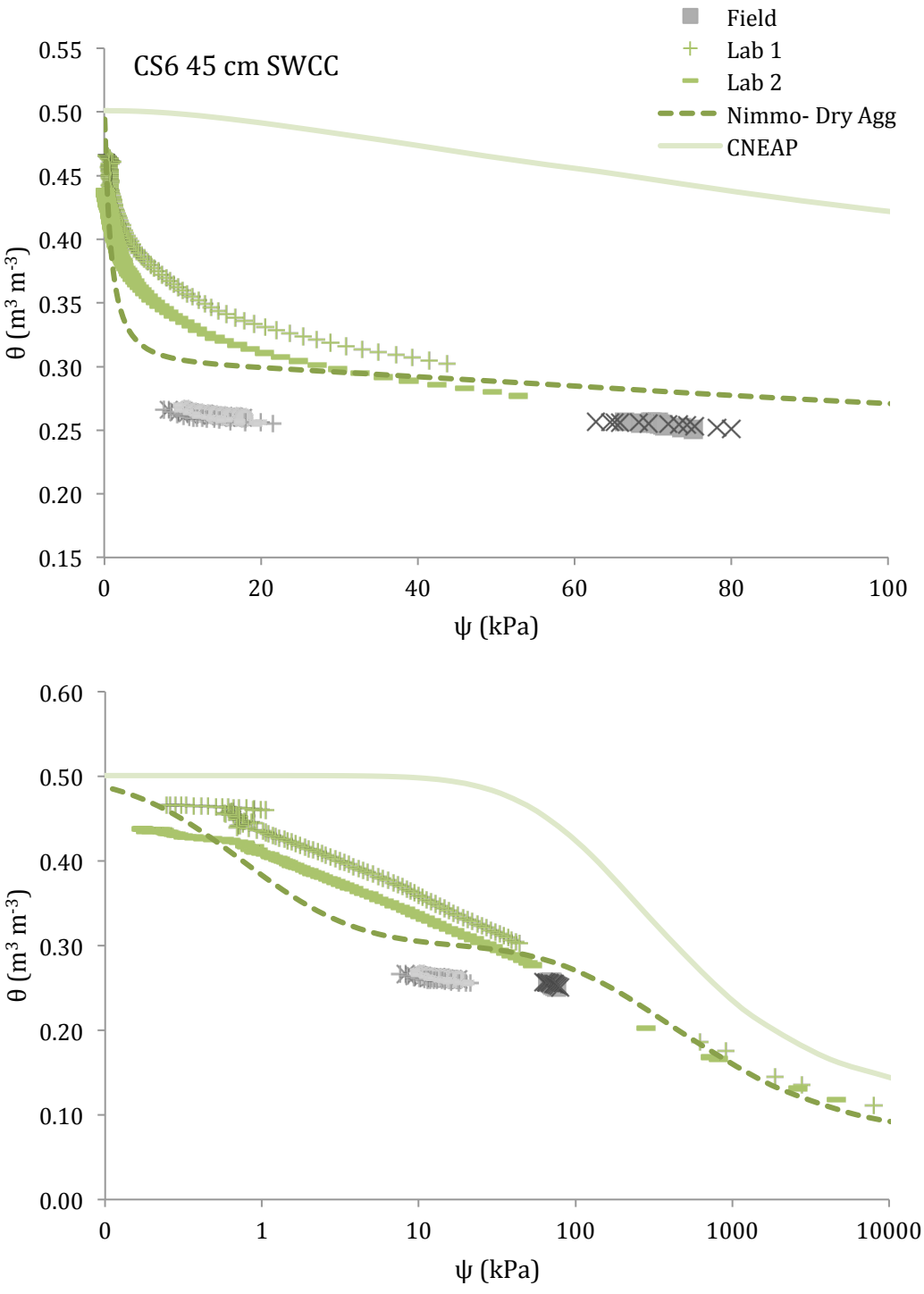

Figure 12c: Measured and modeled SWCC for the CS6 treatment at 45 cm depth. The top panel covers a smaller range of matric suctions, and the bottom panel is the entire suction range (log scale). Measured data is shown as points and property-transfer models are shown as lines.

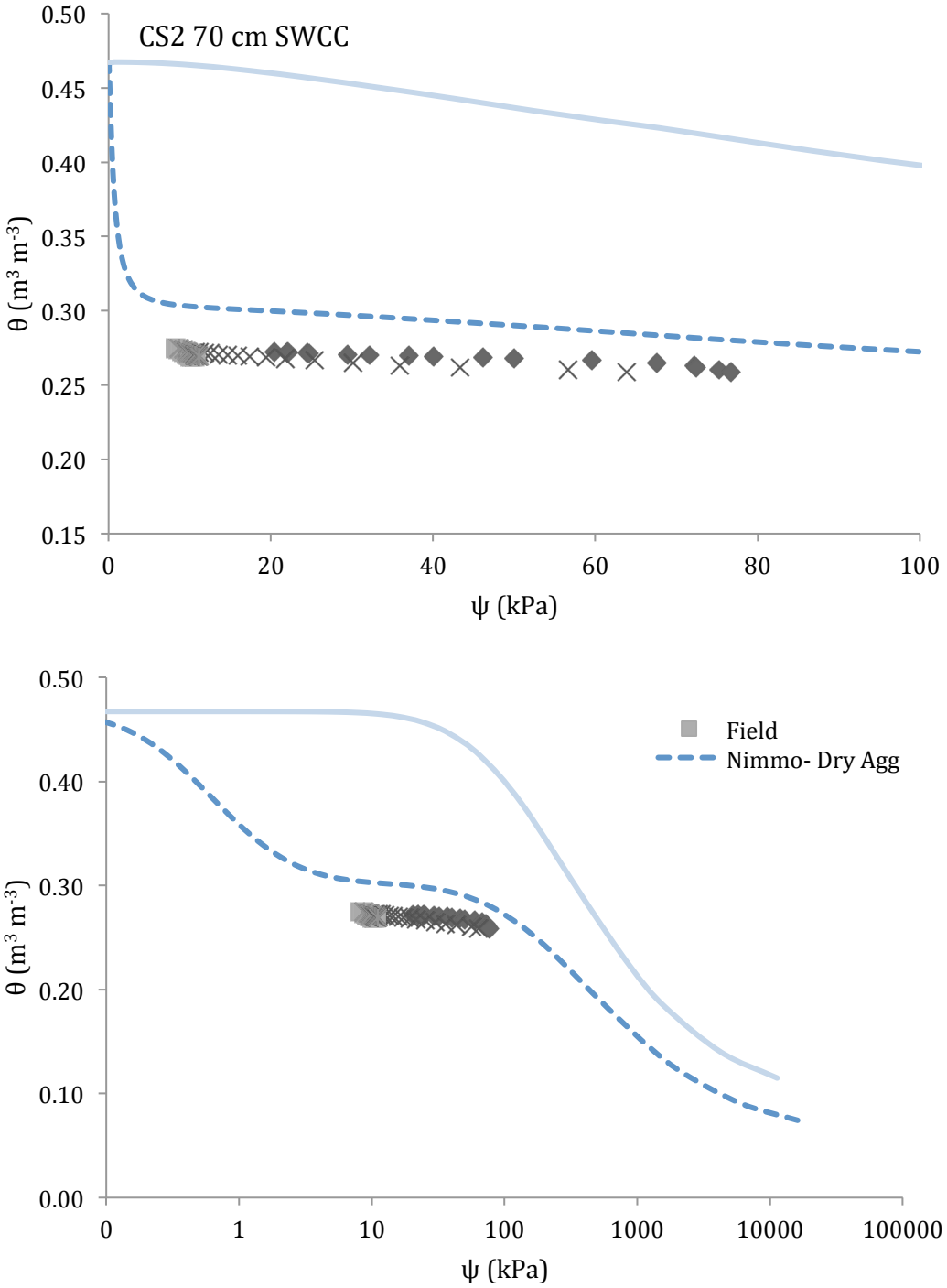

Figure 13a: Measured and modeled SWCC for the CS2 treatment at 70 cm depth. The top panel covers a smaller range of matric suctions, and the bottom panel is the entire suction range (log scale). Measured data is shown as points and property-transfer models are shown as lines.

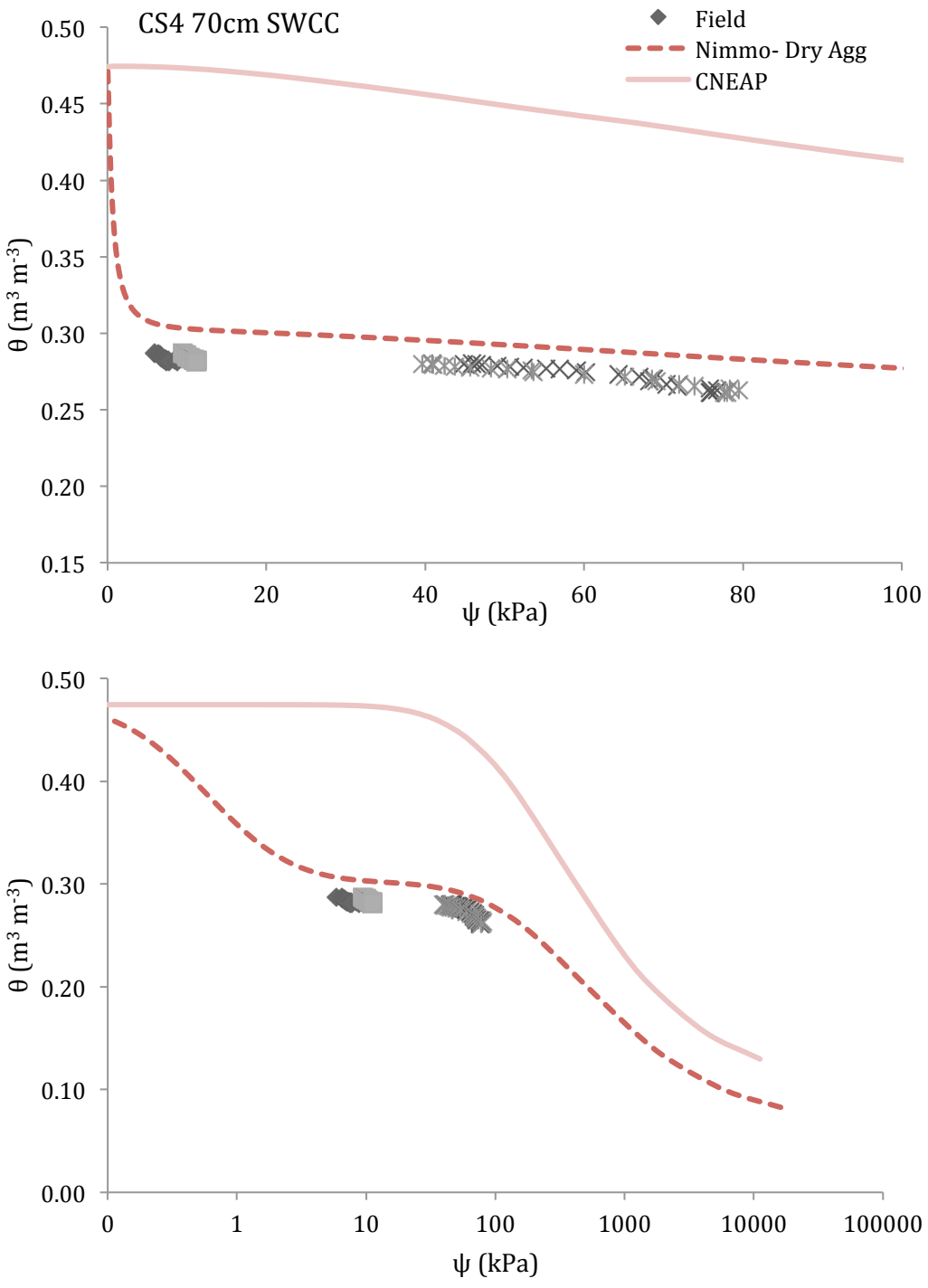

Figure 13b: Measured and modeled SWCC for the CS4 treatment at 70 cm depth. The top panel covers a smaller range of matric suctions, and the bottom panel is the entire suction range (log scale). Measured data is shown as points and property-transfer models are shown as lines.

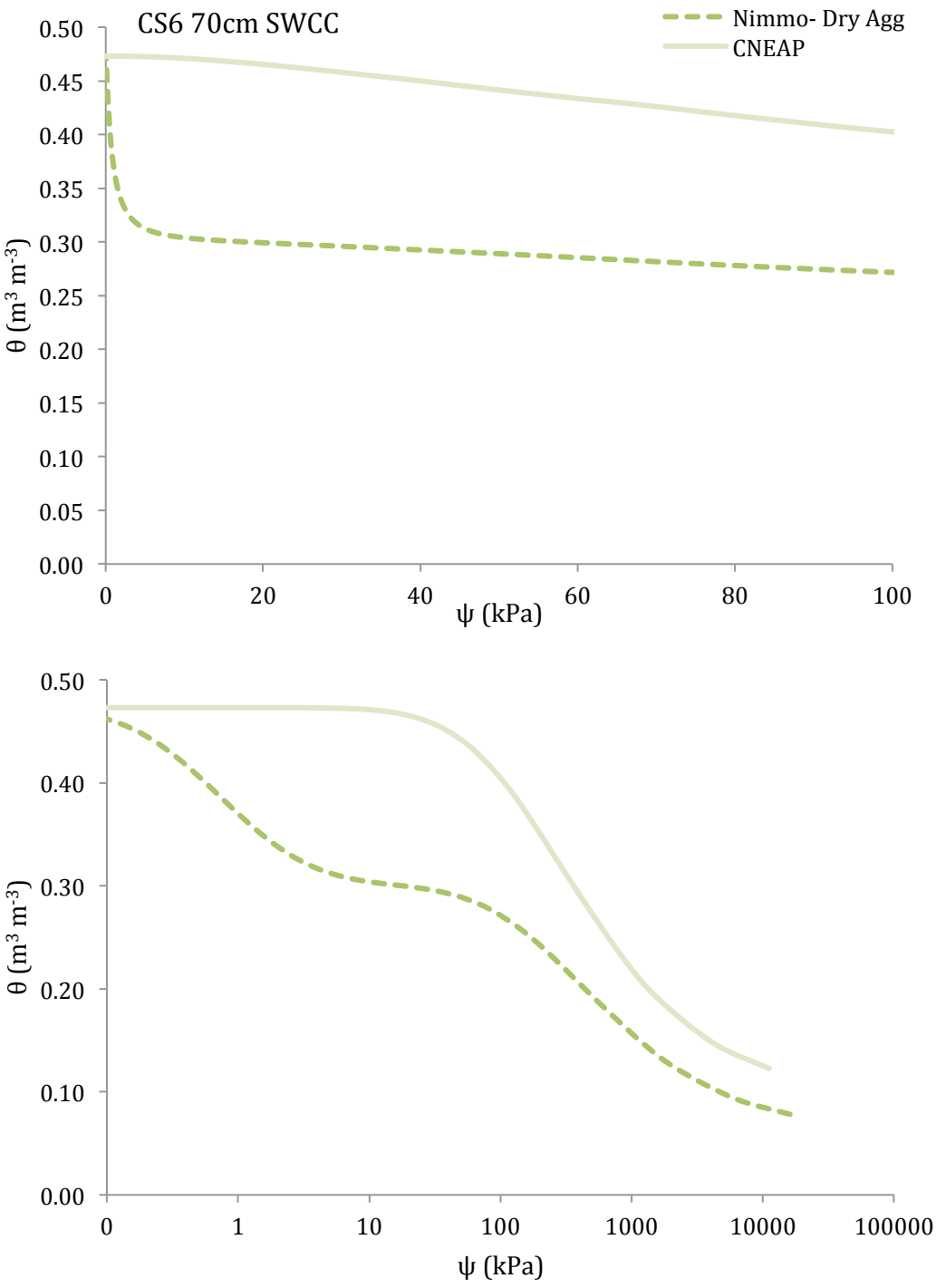

Figure 13c: Measured and modeled SWCC for the CS6 treatment at 70 cm depth. The top panel covers a smaller range of matric suctions, and the bottom panel is the entire suction range (log scale). Property-transfer models are shown as lines. No SWCC could be constructed from measured data at this depth in CS6.

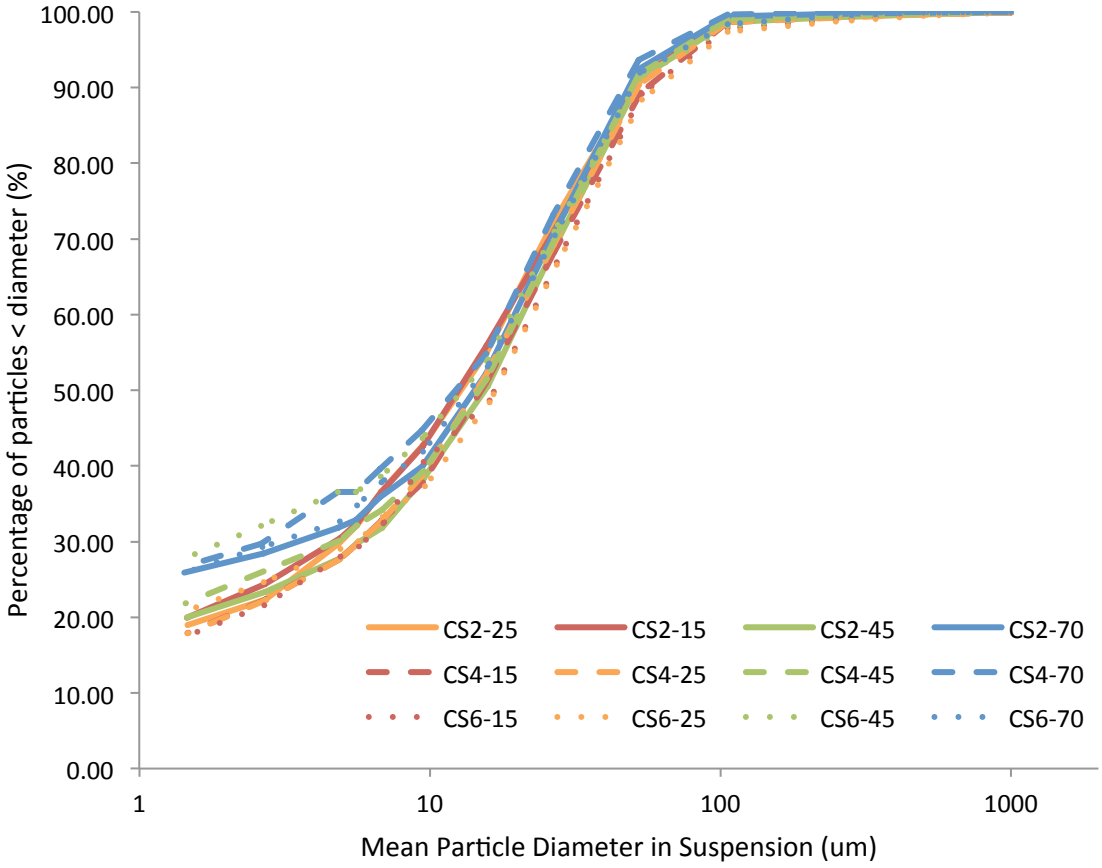

Figure 14: Particle size distribution across all depths and treatments.

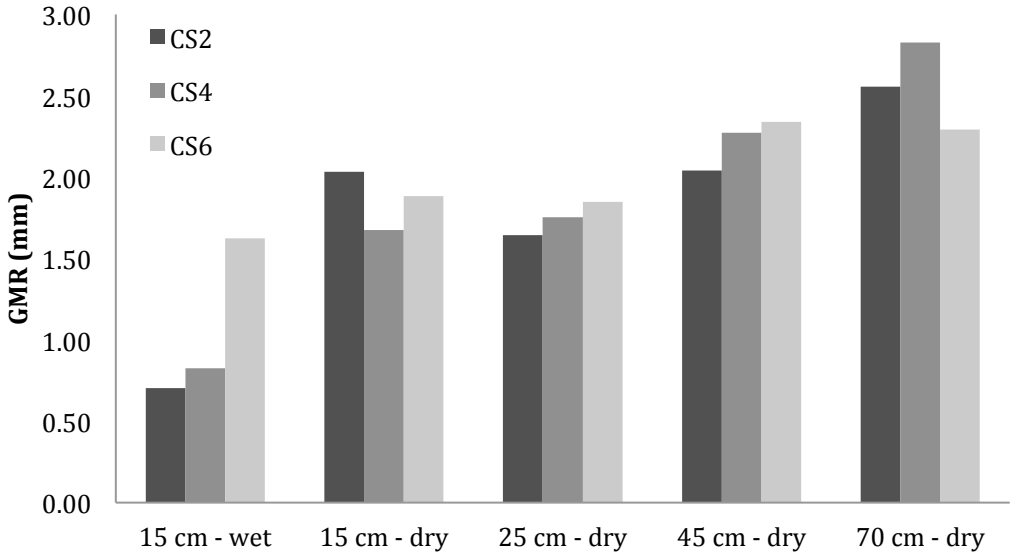

Figure 15: Average GMR determined by wet and dry aggregate distribution analysis.

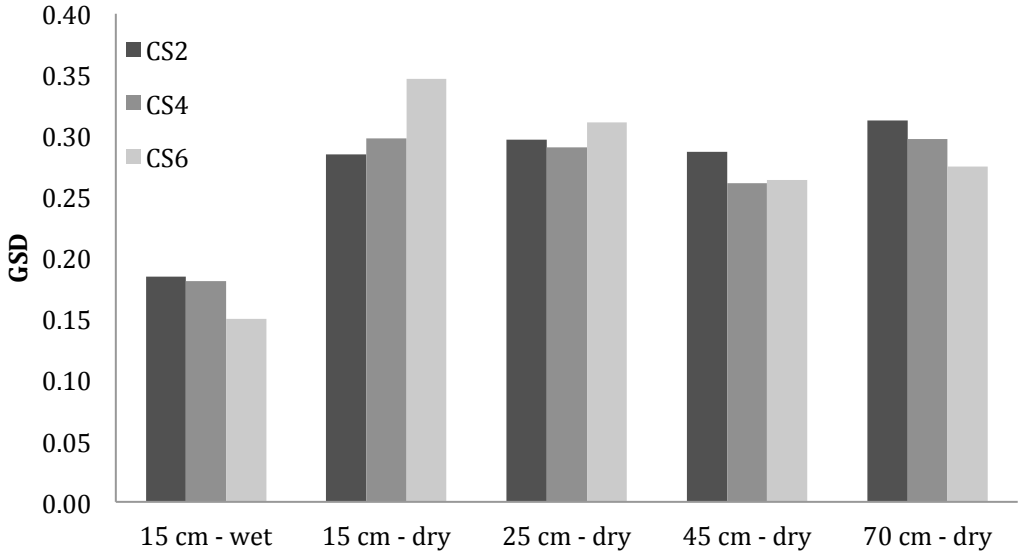

Figure 16: Average GSD determined by wet and dry aggregate distribution analysis.

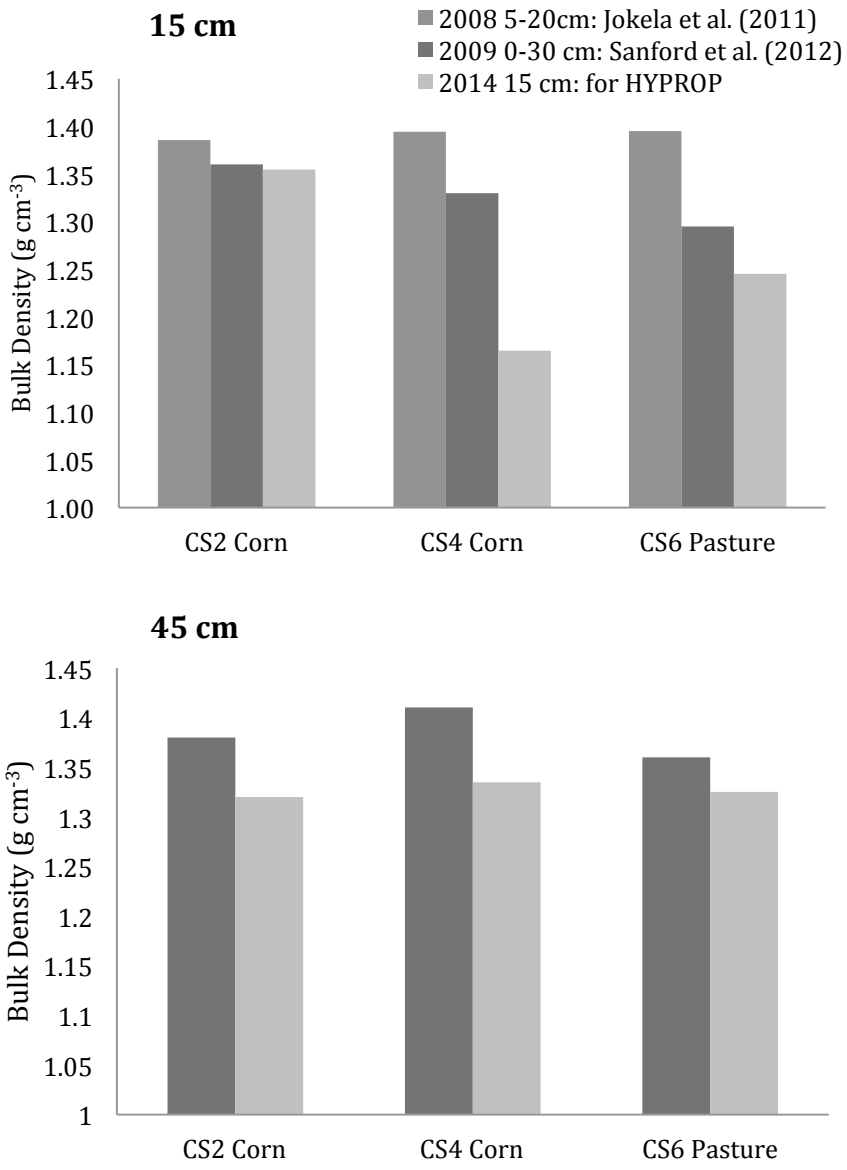

Figure 17: The various bulk density measurements made at WICST used in this study to approximate bulk density at 15 (top) and 45 cm (bottom) depths.

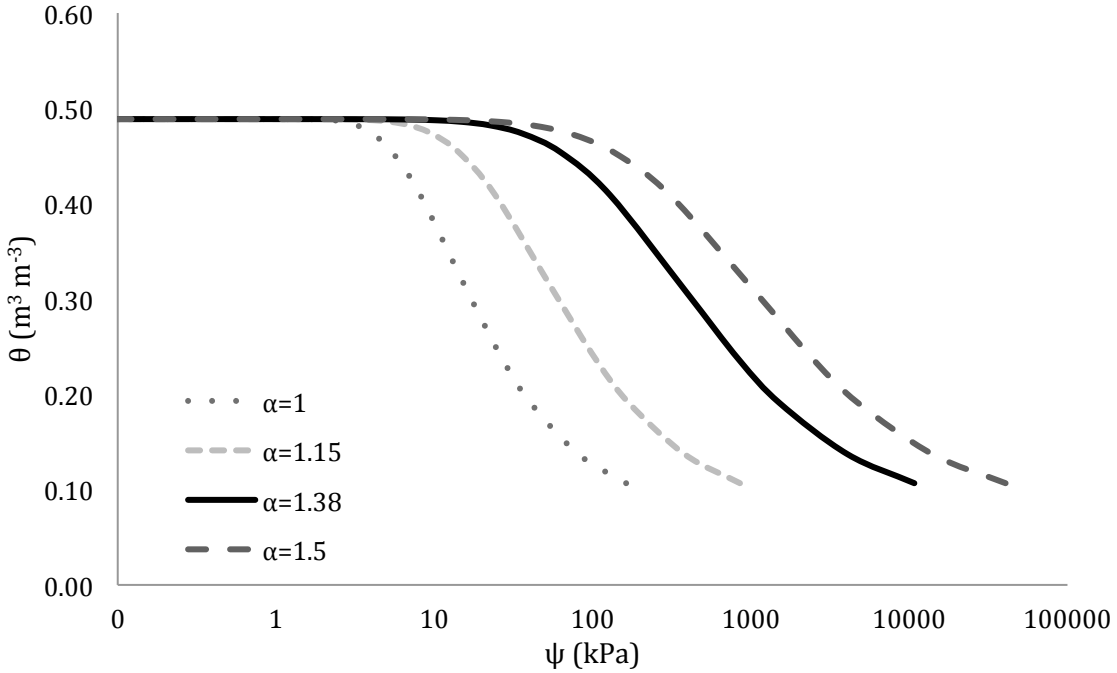

Figure 18: The sensitivity of the CNEAP model to changes the empirical α parameter.

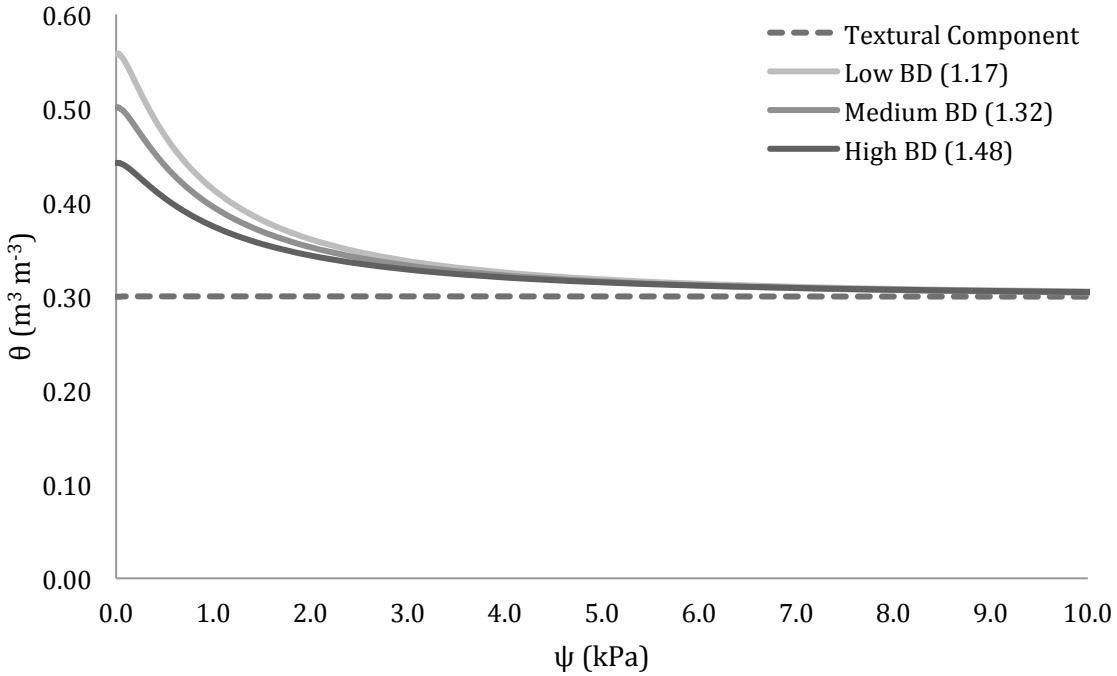

Figure 19: The sensitivity of the Nimmo model to changes in bulk density (BD). Only the structural component of the model changes, and differences are limited to 0-10 kPa.

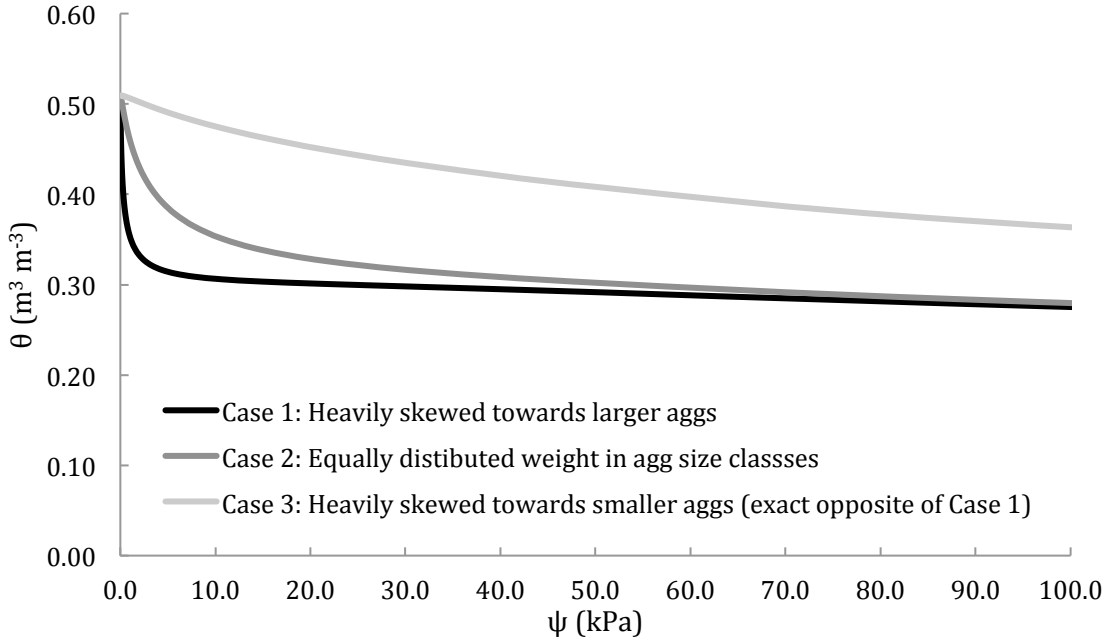

Figure 20: Nimmo model sensitivity to variations in GMR. Case 1 and 3 have the same GSD and show the effect of increasing GMR. Bulk density is held constant.

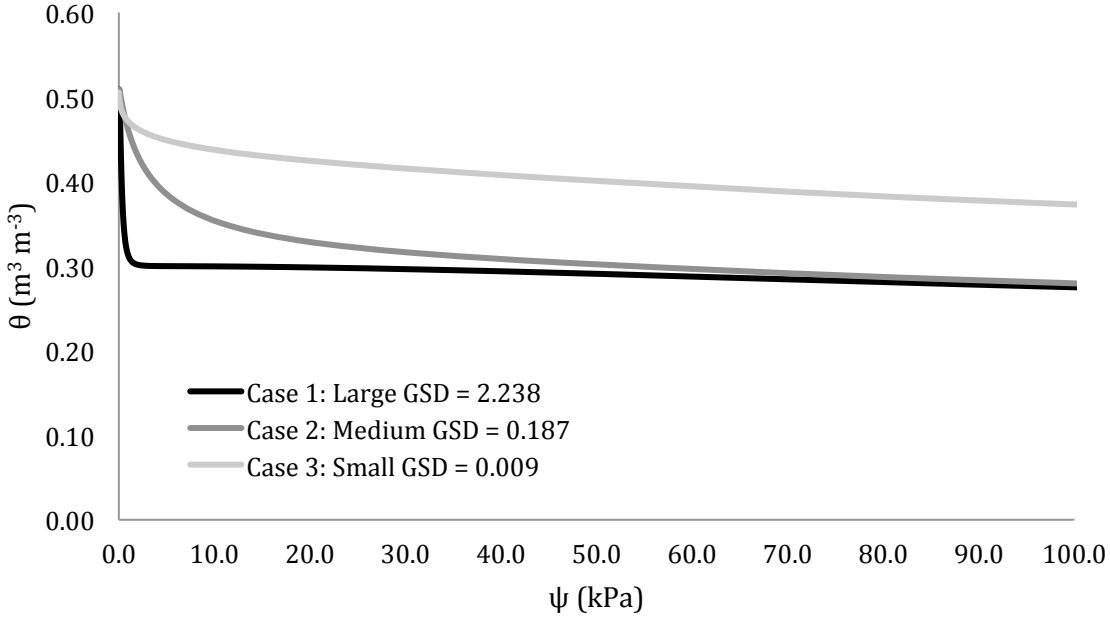

Figure 21: Nimmo model sensitivity to variations in GSD. GMR and bulk density are held constant.

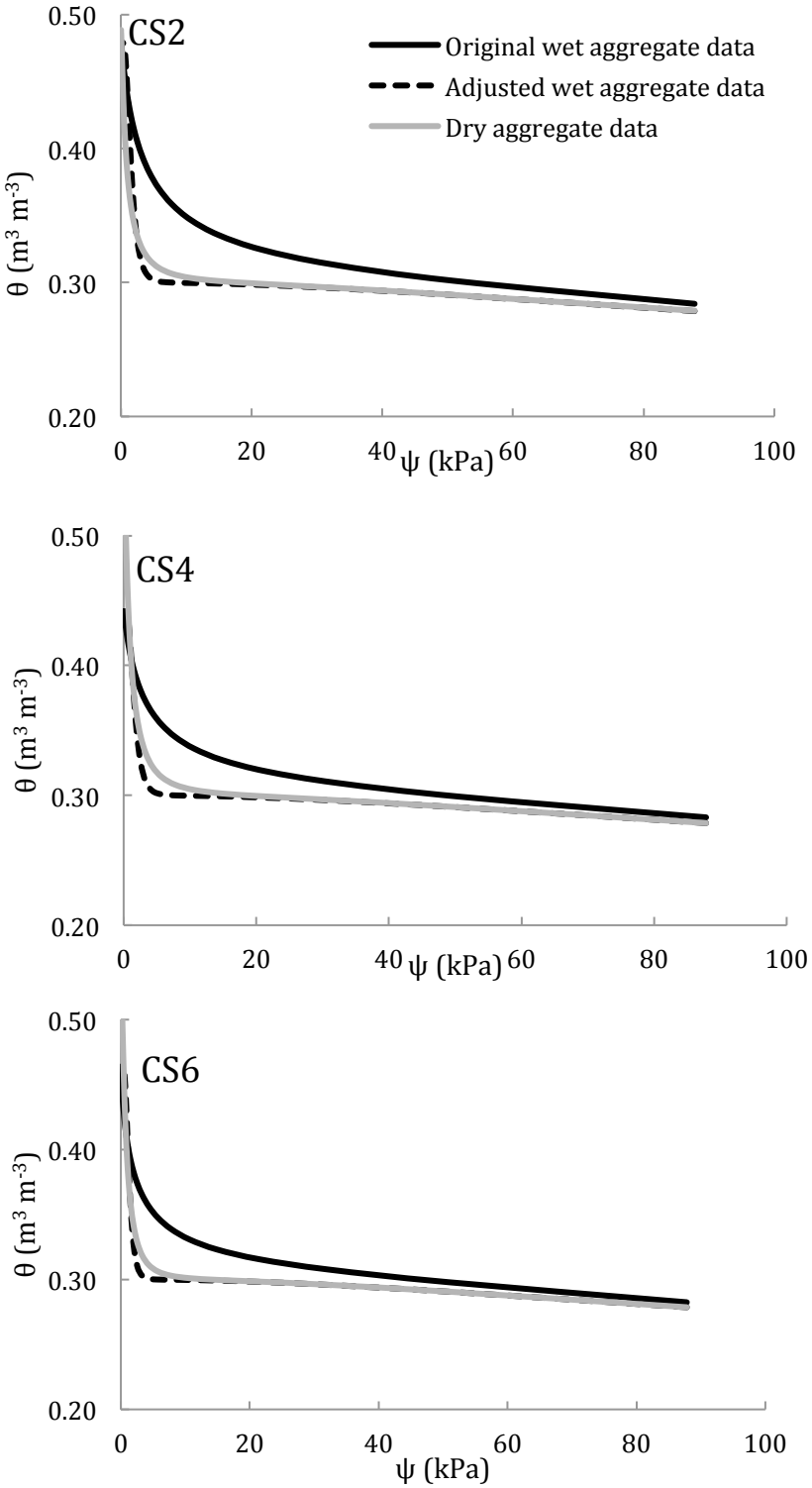

Figure 22: Nimmo model sensitivity to sieve sizes. Adjusted wet aggregate data is the wet aggregate data with an additional sieve included in the analysis to match the dry aggregate sieve sizes.

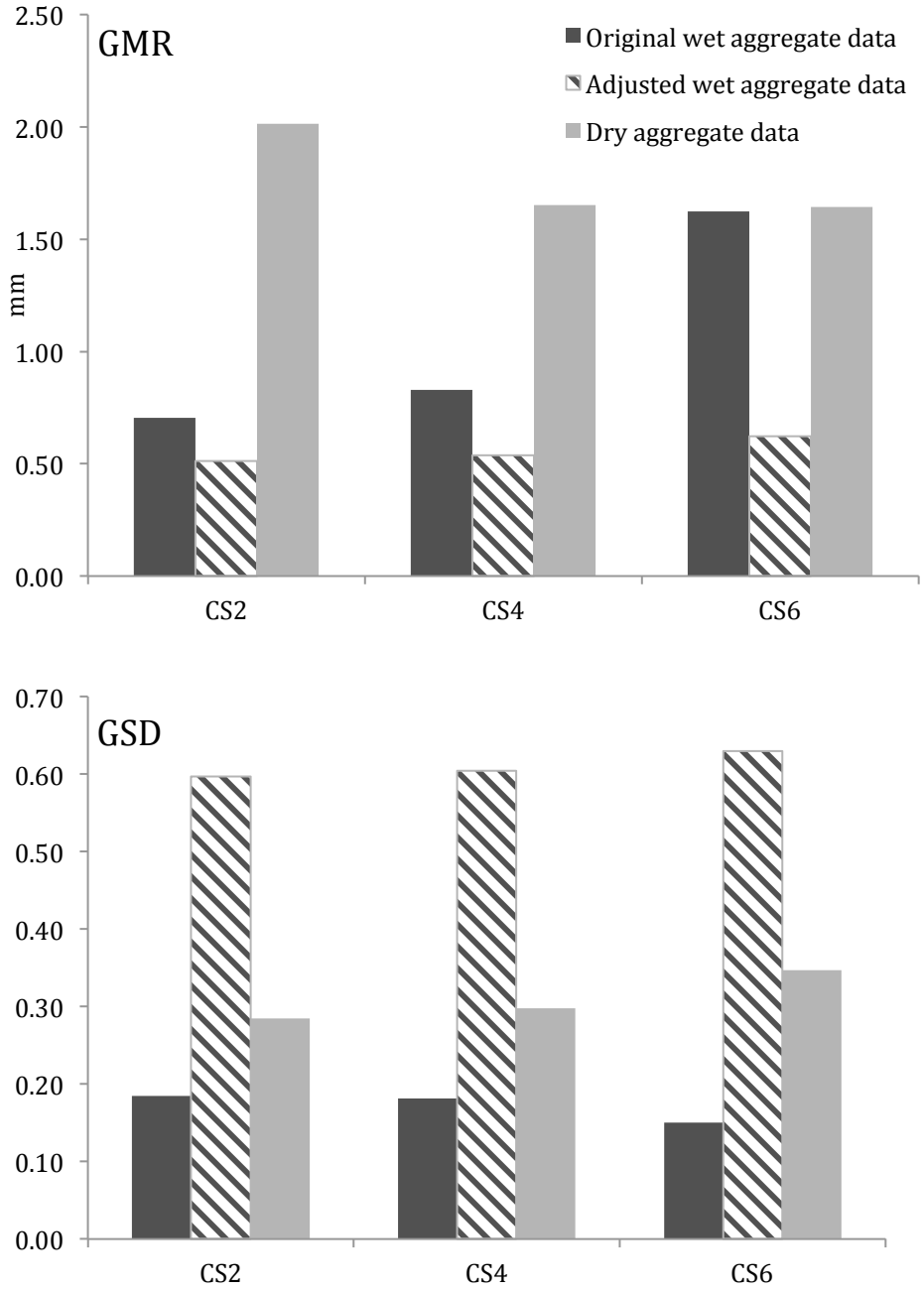

Figure 23: GMR and GSD comparison of dry, wet, and adjusted wet aggregate data in Nimmo sieve sensitivity test.

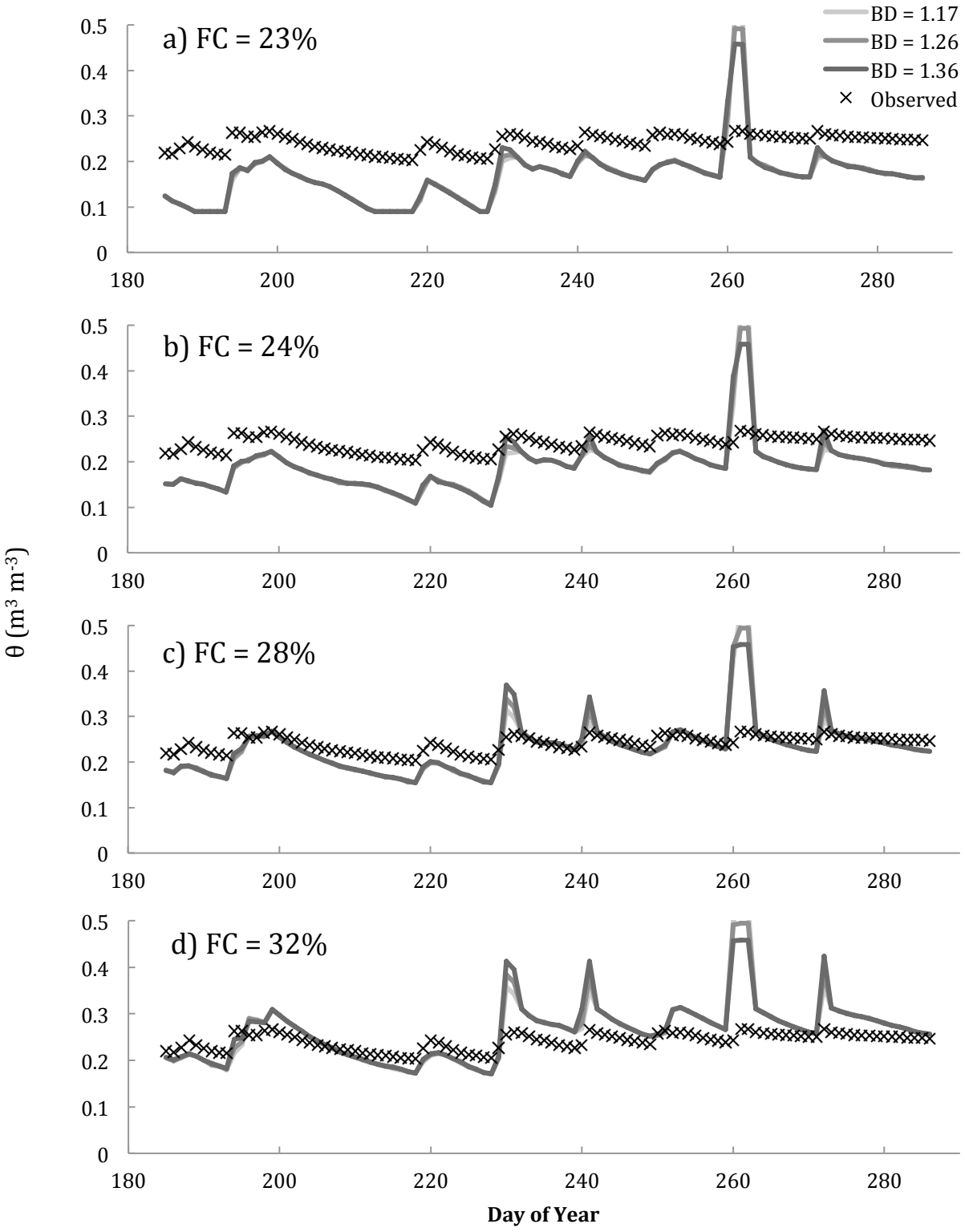

Figure 24: CS2 DayCent simulated soil water content at 15 cm depth using *in situ* (a, b) derived field capacity (FC) parameters and laboratory (c, d) derived FC parameters. Bulk density (BD) was also varied in the simulations.

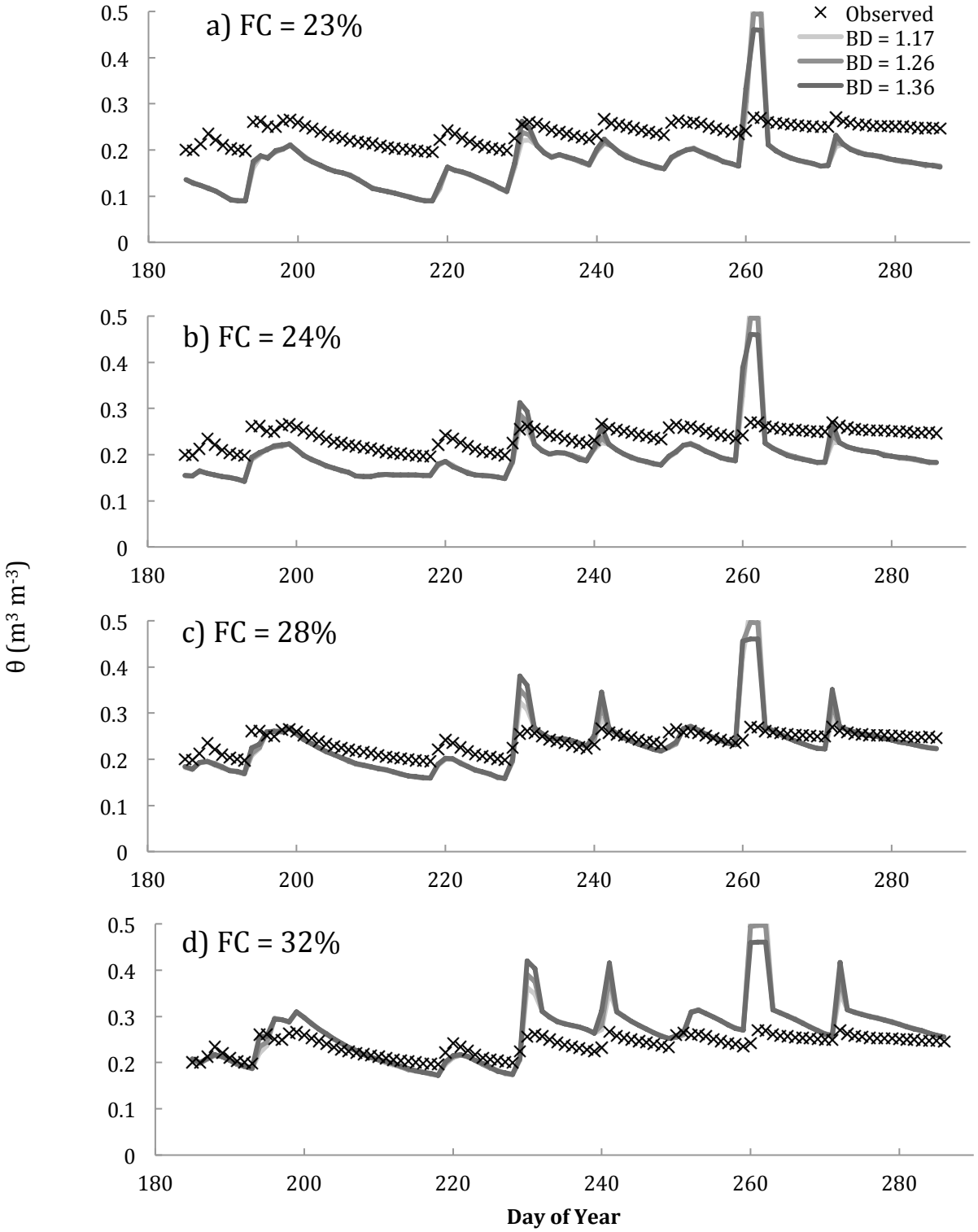

Figure 25: CS4 DayCent simulated soil water content at 15 cm depth using *in situ* (a, b) derived field capacity (FC) parameters and laboratory (c, d) derived FC parameters. Bulk density (BD) was also varied in the simulations.

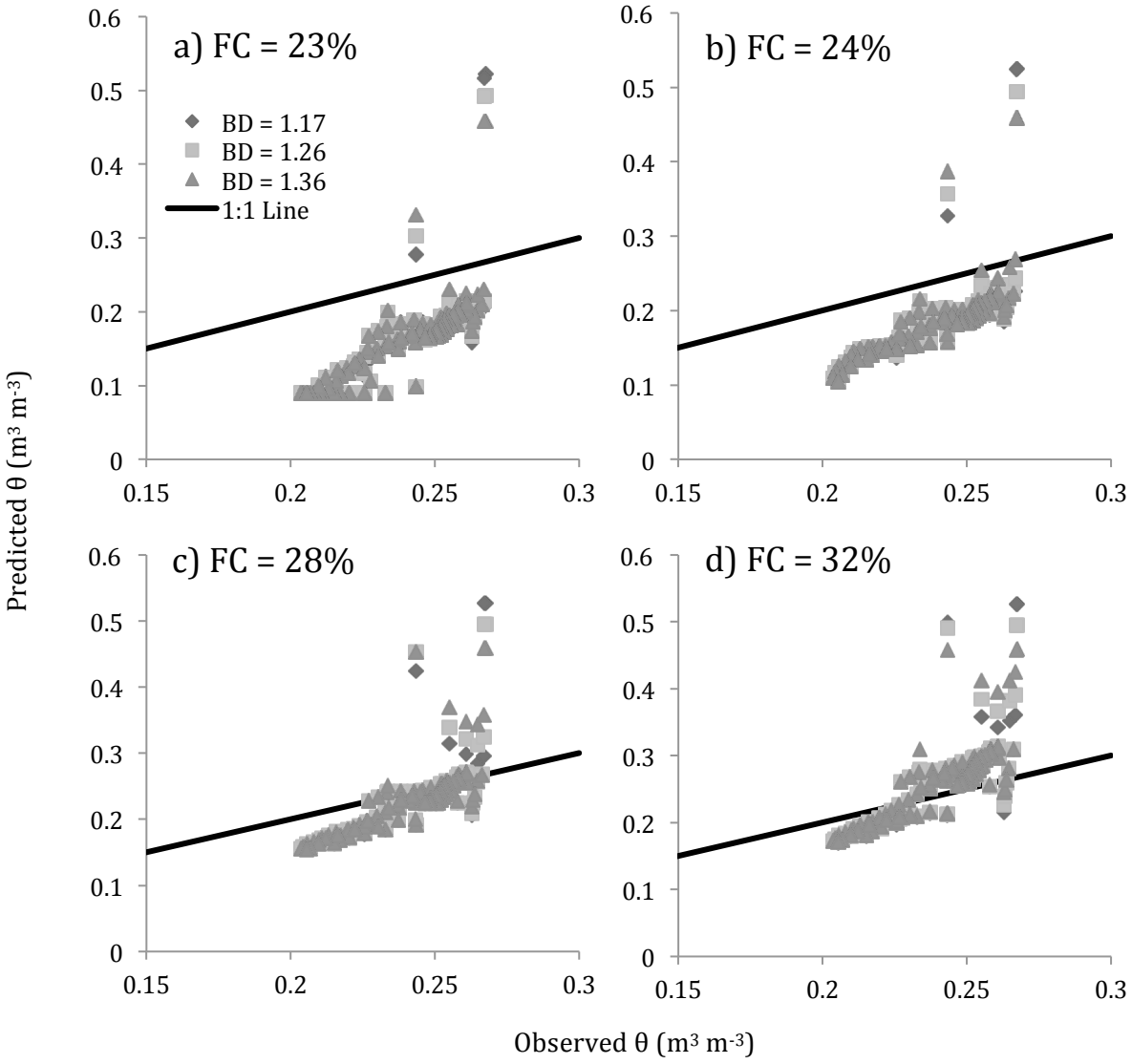

Figure 26: CS2 DayCent simulated vs. observed soil water contents at 15 cm depth using *in situ* (a, b) derived field capacity (FC) parameters and laboratory (c, d) derived FC parameters. Bulk density (BD) was also varied in the simulations.

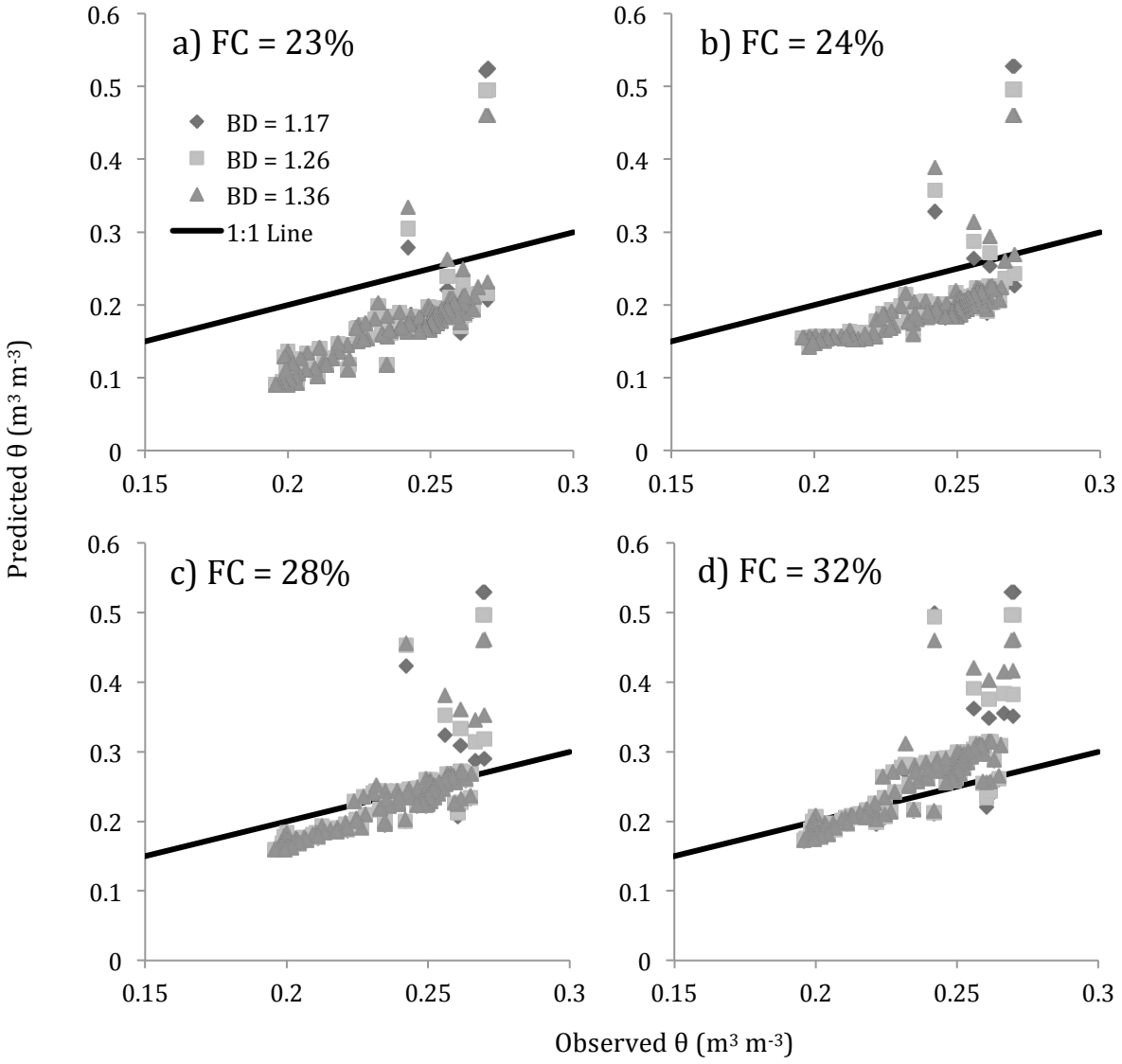

Figure 27: CS4 DayCent simulated vs. observed soil water contents at 15 cm depth using *in situ* (a, b) derived field capacity (FC) parameters and laboratory (c, d) derived FC parameters. Bulk density (BD) was also varied in the simulations.

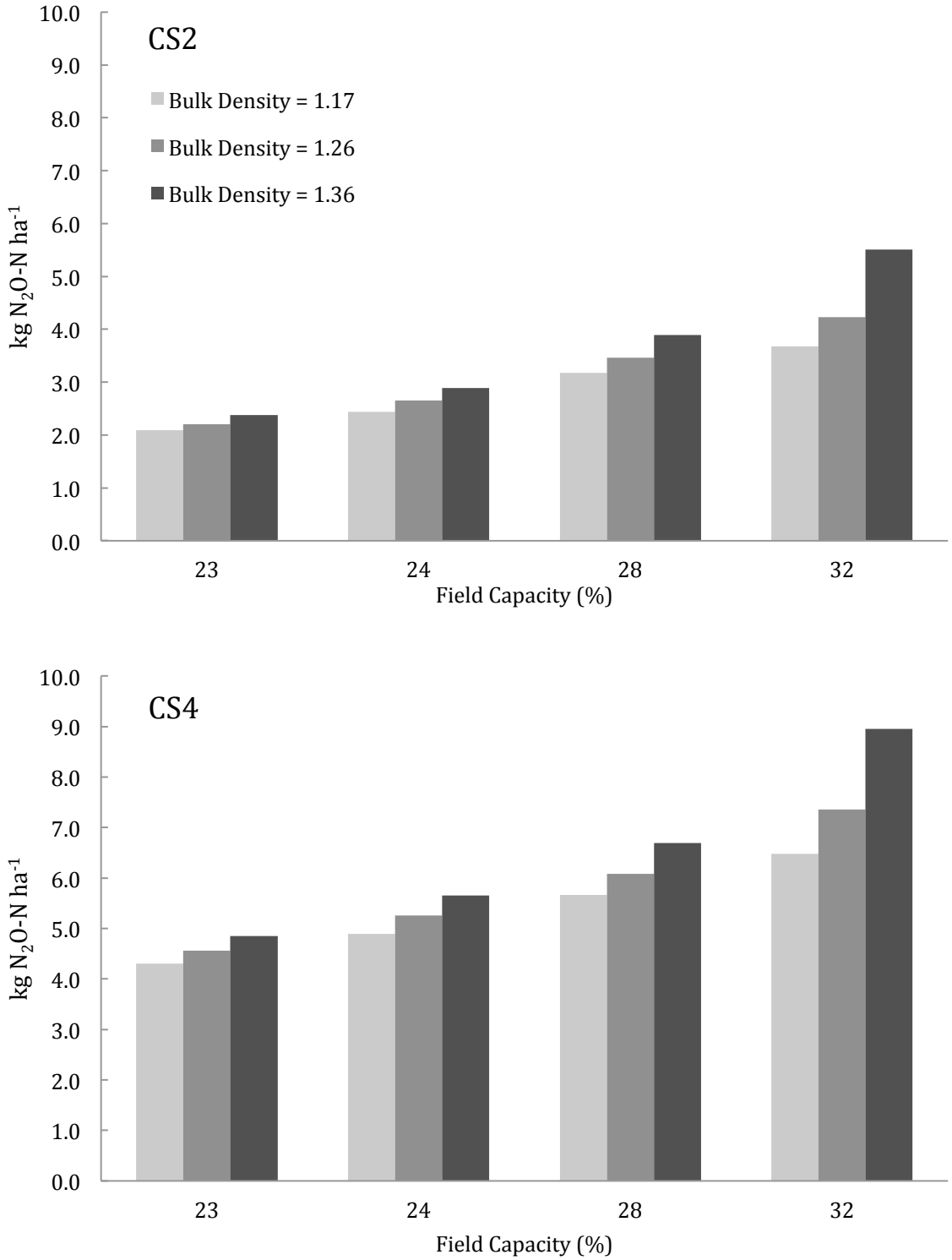

Figure 28: Variation in DayCent simulated cumulative N_2O emissions under different field capacity and bulk density input parameters in CS2 (top) and CS4 (bottom). Cumulative emissions were calculated as the sum of emissions April 1-Nov 30 2015.

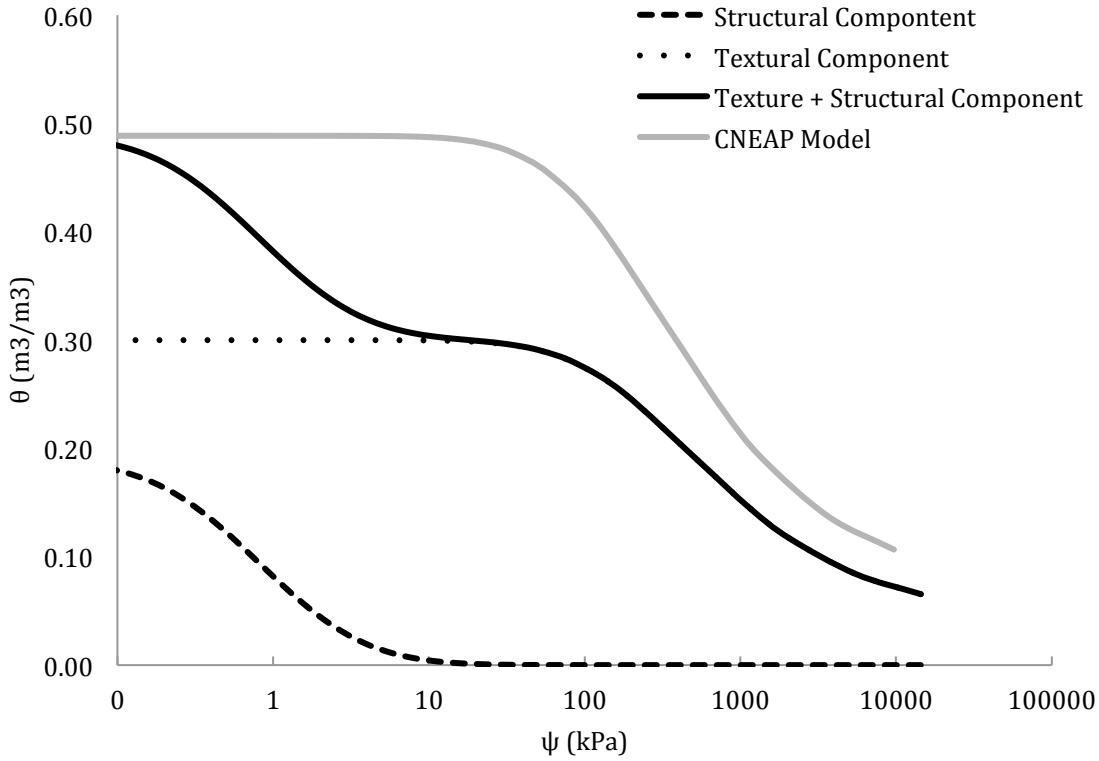

Figure 29: CNEAP model and the Nimmo model divided into its textural, structural, and combined components.

REFERENCES

Arya, L.M., and J.F. Paris. 1981. A Physicoempirical Model to Predict the Soil Moisture Characteristic from Particle-Size Distribution and Bulk Density Data. Soil Sci. Soc. Am. J. 45: 1023–1030.

Assouline, S., and D. Or. 2013. Conceptual and Parametric Representation of Soil Hydraulic Properties: A Review. Vadose Zone J. 12(4): 0.

Assouline, S., and D. Or. 2014. The concept of field capacity revisited: Defining intrinsic static and dynamic criteria for soil internal drainage dynamics. Water Resour. Res. 50(6): 4787–4802.

Basile, A., G. Ciollaro, and A. Coppola. 2003. Hysteresis in soil water characteristics as a key to interpreting comparisons of laboratory and field measured hydraulic properties. Water Resour. Res. 39(12): 1–13.

Bear, J. 1988. Dynamics of Fluids in Porous Media. Revised ed. Dover Publications.

Brooks, R.H., and A.T. Corey. 1964. Hydraulic Properties of Porous Media. Colorado State University.

Cambardella, C.A., and E.T. Elliott. 1993. Carbon and nitrogen distribution in aggregates from cultivated and native grassland soils. Soil Sci. Soc. Am. J. 57: 1071–1076.

Campbell, G.S., and J.M. Norman. 1998. An Introduction to Environmental Biophysics. 2nd ed. Springer-Verlag New York, Inc., New York.

Campbell Scientific, Inc. 2016. CS616 and CS625 Water Content Reflectometers Instruction Manual.

Dane, J.H., and J.W. Hopmans. 2002. Water Retention and Storage. p. 675–703. *In* Dane, J.H., Topp, G.C. (eds.), Methods of Soil Analysis Part 4- Physical Methods. Soil Science of Society of America. Soil Science Society of America, Inc., Madison, WI.

Decagon Devices, Inc. 2015. WP4C Dew Point PotentiaMeter Operator's Manual.

Del Grosso, S.J., S.M. Ogle, W.J. Parton, and F.J. Breidt. 2010. Estimating uncertainty in N2O emissions from U.S. cropland soils. Glob. Biogeochem. Cycles 24(1): 1–12.

Del Grosso, S.J., W.J. Parton, C.A. Keough, and M. Reyes-Fox. 2011. Special features of the DayCent modeling package and additional procedures for parameterization, calibration, validation, and applications. Methods Introd. Syst. Models Agric. Res. (methodsofintrod): 155–176.

Diamantopoulos, E., and W. Durner. 2012. Dynamic Nonequilibrium of Water Flow in Porous Media: A Review. Vadose Zone J. 11(3): 0.

Dıaz-Zorita, M., E. Perfect, and J.H. Grove. 2002. Disruptive methods for assessing soil structure. Soil Tillage Res. 64: 3–22.

Field, J.A., J.C. Parker, and N.L. Powell. 1984. Comparison of field- and laboratory-measured and predicted hydraulic properties of a soil with macropores.pdf. Soil Sci. 138(6): 385–396.

Gardner, W.R. 1956. Representation of Soil Aggregate-Size Distribution by a Logarithmic-Normal Distribution1, 2. Soil Sci. Soc. Am. J. 20(2): 151–153.

Gardner, W.R. 1958. Some steady state solutions of unsaturated moisture flow equations with application to evaporation from a water table. Soil Sci. 85: 228–232.

Gee, G.W., and D. Or. 2002. Particle-Size Analysis. p. 255–294. *In* Dane, J.H., Topp, G.C. (eds.), Methods of Soil Analysis Part 4- Physical Methods. Soil Sciene of Society of America. Soil Science Society of America, Inc., Madison, WI.

van Genuchten, M.T. 1980. A closed-form equation for predicting the hydraulic conductivity of unsaturated soils. Soil Sci. Soc. Am. J. 44(5): 892–898.

Haverkamp, R., and J.Y. Parlange. 1986. Predicting the water retention curve from particle-size distribution: I. Sandy soils wtihout organic matter. Soil Sci. 142: 325–339.

Haverkamp, R., P. Reggiani, and J.R. Nimmo. 2002. Property-Transfer Models. p. 759–761. *In* Dane, J.H., Topp, G.C. (eds.), Methods of Soil Analysis Part 4-Physical Methods. Soil Sciene of Society of America. Soil Science Society of America, Inc., Madison, WI.

Hillel, D. 1998. Introduction to Environmental Soil Physics. 1st ed. Elsevier Academic Press.

Hillel, D. 2004. Introduction to Environmental Soil Physics. Elsevier Academic Press.

Jarecki, M.K., T.B. Parkin, A.S.K. Chan, J.L. Hatfield, and R. Jones. 2008. Comparison of DAYCENT-Simulated and Measured Nitrous Oxide Emissions from a Corn Field. J. Environ. Qual. 37(5): 1685.

Jokela, W., J. Posner, J. Hedtcke, T. Balser, and H. Read. 2011. Midwest Cropping System Effects on Soil Properties and on a Soil Quality Index. Agron. J. 103(5): 1552–1562.

Kosugi, K., J.W. Hopmans, and J.H. Dane. 2002. Parametric Models. p. 739–757. *In* Dane, J.H., Topp, G.C. (eds.), Methods of Soil Analysis Part 4- Physical Methods. Soil Science of Society of America Book Series. Soil Science Society of America, Inc., Madison, WI.

Larney, F. 2008. Dry-Aggregate Size Distribution. *In* Carter, M.R., Gregorich, E.G. (eds.), Soil Sampling and Methods of Analysis, Second Edition. CRC Press.

Leong, E.C., and H. Rahardjo. 1997. Review of Soil-Water Characteristic Curve Equations. J. Geotech. Geoenvironmental Eng. 123: 1106–1117.

National Cooperative Soil Survey. 1996. National Cooperative Soil Survey. Natl. Coop. Soil Surv. Charact. DatabaseAvailable at http://ncsslabdatamart.sc.egov.usda.gov/.

National Weather Service. 2016. NOAA Online Weather Data for Arlington University Farm, WI. NOWData- NOAA Online Weather Data Available at http://w2.weather.gov/climate/xmacis.php?wfo=mkx (verified 3 March 2016).

Necpálová, M., R.P. Anex, M.N. Fienen, S.J. Del Grosso, M.J. Castellano, J.E. Sawyer, J. Iqbal, J.L. Pantoja, and D.W. Barker. 2015. Understanding the DayCent model: Calibration, sensitivity, and identifiability through inverse modeling. Environ. Model. Softw. 66: 110–130.

Nimmo, J.R. 1997. Modeling structural influences on soil water retention. Soil Sci. Soc. Am. J. 61(3): 712–719.

Nimmo, J.R. 2002. Property Transfer from Particle and Aggregate Size to Water Retention. p. 777–782. *In* Dane, J.H., Topp, G.C. (eds.), Methods of Soil Analysis Part 4- Physical Methods. Soil Science of Society of America. Soil Science Society of America, Inc., Madison, WI.

Nimmo, J.R., W.N. Herkelrath, and A.M. Laguna Luna. 2007. Physically Based Estimation of Soil Water Retention from Textural Data: General Framework, New Models, and Streamlined Existing Models. Vadose Zone J. 6(4): 766.

Nimmo, J.R., and K.S. Perkins. 2002. Aggregate Stability and Size Distribution. p. 317–328. *In* Dane, J.H., Topp, G.C. (eds.), Methods of Soil Analysis Part 4-Physical Methods. Soil Science of Society of America.

Or, D., and J.M. Wraith. 2002. Soil Water Content and Water Potential Relationships. p. 49–84. *In* Warrick, A.W. (ed.), Soil Physics Companion. CRC Press LLC, New York.

Osterholz, W.R., C.J. Kucharik, J.L. Hedtcke, and J.L. Posner. 2014. Seasonal Nitrous Oxide and Methane Fluxes from Grain- and Forage-Based Production Systems in Wisconsin, USA. J. Environ. Qual. 43(6): 1833.

Pachepsky, Y., W.J. Rawls, and D. Giménez. 2001. Comparison of soil water retention at field and laboratory scales. Soil Sci. Soc. Am. J. 65(2): 460–462.

Parton, W.J., M. Hartman, D. Ojima, and D. Schimel. 1998. DAYCENT and its land surface submodel: description and testing. Glob. Planet. Change 19(1): 35–48.

Parton, W.J., E.A. Holland, S.J. Del Grosso, M.D. Hartman, R.E. Martin, A.R. Mosier, D.S. Ojima, and D.S. Schimel. 2001. Generalized model for NOx and N2O emissions from soils. J. Geophys. Res. 106(D15): 17,403–17,419.

Pertassek, T., A. Peters, and W. Durner. 2015. HYPROP-FIT Software User's Manual, V.3.0. UMS GmbH, Munich, Germany.

Posner, J.L., J.O. Baldock, and J.L. Hedtcke. 2008. Organic and conventional production systems in the Wisconsin integrated cropping systems trials: I. Productivity 1990–2002. Agron. J. 100(2): 253–260.

Radcliffe, D.E., and T.C. Rasmussen. 2002. Soil Water Content and Water Potential Relationships. p. 85–126. *In* Warrick, A.W. (ed.), Soil Physics Companion. CRC Press LLC, New York.

Sanford, G.R., J.L. Posner, R.D. Jackson, C.J. Kucharik, J.L. Hedtcke, and T.-L. Lin. 2012. Soil carbon lost from Mollisols of the North Central U.S.A. with 20 years of agricultural best management practices. Agric. Ecosyst. Environ. 162: 68–76.

Saxton, K.E., and W.J. Rawls. 2006. Soil Water Characteristic Estimates by Texture and Organic Matter for Hydrologic Solutions. Soil Sci. Soc. Am. J. 70(5): 1569.

Scanlon, B.R., B.J. Andraski, and J. Bilskie. 2002. Miscellaneous Methods for Measuring Matric or Water Potential. p. 643–673. *In* Dane, J.H., Topp, G.C.

(eds.), Methods of Soil Analysis Part 4- Physical Methods. Soil Sciene of Society of America. Soil Science Society of America, Inc., Madison, WI.

Schelle, H., L. Heise, K. Jänicke, and W. Durner. 2013. Water retention characteristics of soils over the whole moisture range: a comparison of laboratory methods: Water retention characteristics. Eur. J. Soil Sci. 64(6): 814–821.

Schindler, U., W. Durner, G. von Unold, L. Mueller, and R. Wieland. 2010a. The evaporation method: Extending the measurement range of soil hydraulic properties using the air-entry pressure of the ceramic cup. J. Plant Nutr. Soil Sci. 173(4): 563–572.

Schindler, U., W. Durner, G. von Unold, and L. Müller. 2010b. Evaporation Method for Measuring Unsaturated Hydraulic Properties of Soils: Extending the Measurement Range. Soil Sci. Soc. Am. J. 74(4): 1071.

Schindler, U., G. von Unold, and L. Muller. 2015. Laboratory Measurement of Soil Hydraulic Functions in a Cycle of Drying and Rewetting.

Schuh, W.M., R.L. Cline, and M.D. Sweeney. 1988. Comparison of a Laboratory Procedure with a Textural Model for Predicting In Situ Soil Water Retention. Soil Sci. Soc. Am. J. 52: 1218–1227.

Six, J., H. Bossuyt, S. Degryze, and K. Denef. 2004. A history of research on the link between (micro)aggregates, soil biota, and soil organic matter dynamics. Soil Tillage Res. 79(1): 7–31.

UMS. 2012. User Manual HYPROP. UMS GmbH, Munich, Germany.

USDA-NRCS. 2016. National Soil Survey Handbook, title 430-VI.

U.S. Environmental Protection Agency. 2016. DRAFT Inventroy of U.S. Greenhouse Gas Emissions and Sinks: 1990-2014. Washington, D.C.

UW Extension. 2016. Weather Station Status and Data. UW Ext. Ag WeatherAvailable at http://agwx.soils.wisc.edu/uwex_agwx/awon.

Vaz, C.M.P., S. Jones, M. Meding, and M. Tuller. 2013. Evaluation of Standard Calibration Functions for Eight Electromagnetic Soil Moisture Sensors. Vadose Zone J. 12(2).